A New Algorithm for Minutiae Extraction and Matching in Fingerprint

by

Azad Noor

Dissertation submitted to the
School of Engineering and Design
at Brunel University, UK
in partial fulfilment of the requirements
for the degree of

Doctor of Philosophy
in
Electronic & Computer Engineering

Uxbridge, London

July 2012

Abstract

A novel algorithm for fingerprint template formation and matching in automatic fingerprint recognition has been developed.

At present, fingerprint is being considered as the dominant biometric trait among all other biometrics due to its wide range of applications in security and access control. Most of the commercially established systems use singularity point (*SP*) or '*core'* point for fingerprint indexing and template formation. The efficiency of these systems heavily relies on the detection of the core and the quality of the image itself. The number of multiple *SPs* or absence of '*core'* on the image can cause some anomalies in the formation of the template and may result in high False Acceptance Rate (FAR) or False Rejection Rate (FRR). Also the loss of actual minutiae or appearance of new or spurious minutiae in the scanned image can contribute to the error in the matching process. A more sophisticated algorithm is therefore necessary in the formation and matching of templates in order to achieve low FAR and FRR and to make the identification more accurate.

The novel algorithm presented here does not rely on any 'core' or SP thus makes the structure invariant with respect to global rotation and translation. Moreover, it does not need orientation of the minutiae points on which most of the established algorithm are based. The matching methodology is based on the local features of each minutiae point such as distances to its nearest neighbours and their internal angle.

Using a publicly available fingerprint database, the algorithm has been evaluated and compared with other benchmark algorithms. It has been found that the algorithm has performed better compared to others and has been able to achieve an error equal rate of 3.5%.

Acknowledgements

First of all, I would like to thank my supervisor Professor Wamadeva Balachandran for his enormous support, invaluable advice and positive encouragement throughout the course of my research. I am grateful to Dr Nadarajan Manivanan for his kind assistance, advice and friendly support during my hard work. Also, I would like to thank everyone in the Centre for Electronic Systems Research lab for keeping the lab lively and making my time enjoyable. Finally, a special thanks to my wife Nafiza for inspiring me all the time and being with me with her love.

Table of contents

List of figures

List of tables

Acronyms

ANSI	American National Standard for Information System
AFIS	Automatic fingerprint identification systems
AFRS	Automatic fingerprint recognition systems
ATM	Automatic Teller Machine
CN	Crossing Number
FTA	Failure to Acquire
FTE	Failure to Enrol
FAR	False Acceptance Rate
FRR	False Rejection rate
FVC	Fingerprint Verification Competition
MINEX	Minutiae Exchange
NIST	National Institute of Standards and Technology
PM	Percentage Match
PIN	Personal Identification Number
RF	Radio frequency
SP	Singularity Point
SVM	Support Vector Machine
TH	Threshold
TIAAFR	Transformation Invariant Algorithm for Automatic Fingerprint Recognition

Introduction

In recent years, biometrics has become a potential authentication tool which can address the inherent weaknesses of the traditional knowledge-based (e.g., password) and possession based (e.g., key or token) recognition systems in terms of authenticating genuine users. The uniqueness and permanence of biometric features such as ridge and valley structure on fingerprint, geometry of hand, facial thermogram or iris structure have made it possible to replace the traditional knowledge and token based authentication system by more reliable, robust and effective biometric system. Each biometric attribute has its strengths and weaknesses and the choice typically depends on the feasibility of its use, characteristics of the application and cost. In some applications, the biometric works as a deterrent; in others, it is central to system operation. Whatever the application, the common elements of any biometric system are [1]

- The biometric can offer a high degree of certainty regarding an individual's identity.
- The benefits lead directly or indirectly to cost savings, enhanced security or to reduced risk of financial losses for an individual or institution.

1.1 Benefits of biometrics

There are many benefits of using biometrics as an authentication tool over traditional knowledge-based or token-based tools that includes increased security, increased convenience, reduced fraud or delivery of enhanced services. Access to personal computers, networks and applications, access to secured areas of a building, authorisation at automatic teller machine (ATM) and transaction in online banking are some common applications of knowledge-based autehtication systems. Handheld tokens such as cards and key fobs are used mainly for building access but they have replaced passwords in some high security applications. The generation of personal identification number (PIN)s using key generator for online banking is an example of this. However, passwords, PINs, tokens or cards have a number of weaknesses that may raise concern about their suitability in modern applications, especially high-security applications such as acess to online financial accounts or medical data.

The authentication mechanism can be implemented by any of the followings or combination of these

- Something you know such as passwords and PINs.
- Something you have such as smart cards, keys or tokens.
- Soemthing you are, which refers to biometrics- the measurement of physical characteristics or personal traits.

The knowledge based system which is based on passwords and PINs is still most widely used authentication system but the shortcomings of the knowledge-based or token based authentication can be overcome by the introduction of biometrics and the benefits it can bring are

a) *Increased Security:* Biometrcis can provide an enhanced level of security to the traditional authentication methods by allowing access only to authorised users and restrict access or protect data from unautorised users. Although password is meant to be confidential, should be hard to guess and should not be written down; in practice, people often forgot their passwords, sometimes share it with their friends and colleagues. Many users use obvious words or numbers to make passwords and PINs that can be easily guessed so unauthorised users can break into account with little effort. “ Good passwords” , i.e. long passwords with numbers and symbols, are difficult to remembr for most users and rarely enforced.

On the other hand, biometric data cannot be guessed or stolen in the same way as password or token. Although some biometric systems can be broken under certain conditions, todays biometric systems are highly unlikely to be fooled by a picture of a face, an impression of a fingerprint or recording of a voice. This assumes, of course, that the imposter has been able to gather these physiological characteristic- which is unlikely in most cases.

b) Increased convenience: Most of the time, ordinary users choose simple words as their passwords so they are not forgotten. As computer users are forced to manage a number of passwords, the likelyhood of passwords being forgotten increases unless the user choose to use a universal password for every login, which in effect reduces the security. Tokens and cards can sometimes be forgotten or lost.

Because biometrics are always attached with the person and so there is nothing to forgot. It offers a greater convenience than systems based on remembering multiple passwords or on keeping possession of an authentication token. For PC applications, where users can have access to multiple resources, biometric can simplify the authentication process by replacing multiple passwords and thus reduce the burden on both the user and the system administrator. Applications such as point of sale transactions have also begun to see the use of biometrics to authorise purchases from prefunded accounts, eliminating the need for cards.

Biometric authentication can also be used to allow users to access higher level of rights and privileges. Highly sensitive and critical information can be readily available on a biometrically protected network than on one protected by passwords. This can increase user and enterprise conveniences, as users can access otherwise protected information without the need for human intervention.

c) Increased accountability: The increased awareness of security in the enterprise and service industry has put a huge demand on auditing and reporting capabilities. Biometrics can be a very useful tool to secure computers and facilities and offer a high degree of certainity as to what an user has accessed in which computer at what time. Although the auditing and reporting capability of a computer system is rarely used, the presence of such system can be an effective deterrent for fraudstars.

Until now, a number of biometric technologies has been developed and deployed in different industries and some are still in the development process. Each biometric technology has its own advantages and disadvantages but they should be considered and evaluated giving full consideration to the following characteristics [2]:

Universality: Every person should have the characteristic. People who are mute or does not have a fingerprint will need to be accommodated in some way.

Uniqueness: Generally, no two people have identical characteristics. However, identical twins are hard to distinguish.

Permanence: The characteristics should not vary with time. A person's face, for example, may change with age.

Collectibility: The characteristics must be easily collectible and measurable.

Performance: The method must deliver accurate results under varied environmental circumstances.

Acceptability: The general public must accept the sample collection routines. Nonintrusive methods are more acceptable.

Circumvention: The technology should be difficult to deceive.

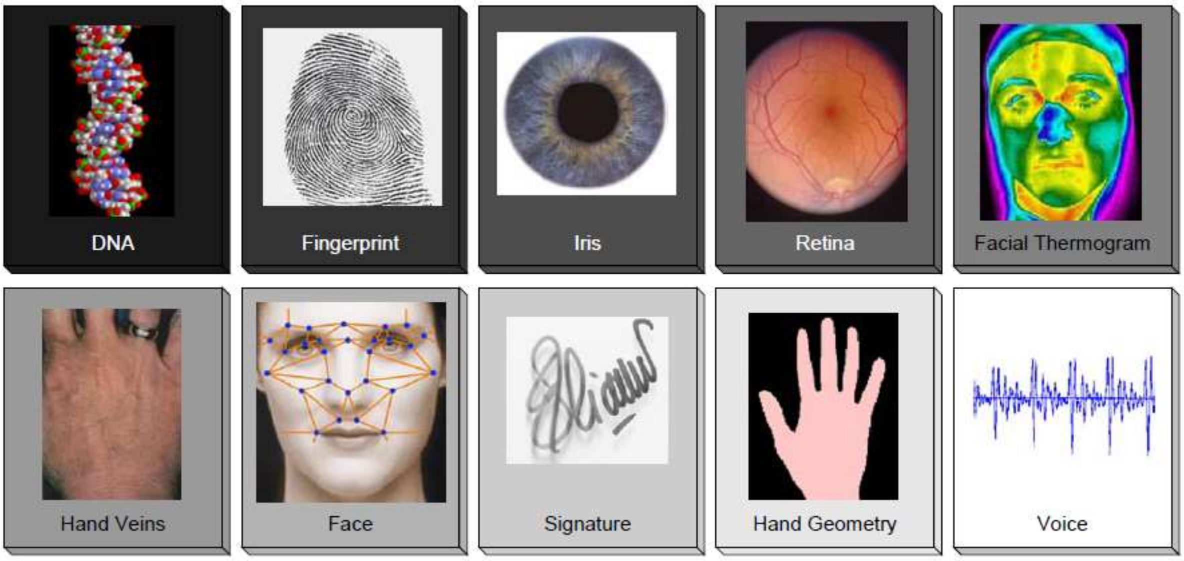

Figure1.1: Different Biometric features that can be used to generate uniqueness [3].

Some biometric features that can be used to generate uniqueness for a person are shown in Figure 1.1. Not all of them have gained the same level of acceptance in the industry due to their cost and viability in deployment. Table 1.1 has summarised some of the existing biometric technologies and their advantages and disadvantages [4].

Technology	***Advantages***	***Disadvantages***

Fingerprint	• Very high accuracy • Is the most economical biometric PC user authentication technique • It is one of the most developed biometrics • Easy to use. • Small storage space required for the biometric template, reducing the size of the database memory required • It is standardized.	• For some people it is very intrusive, because is still related to criminal identification • It can make mistakes with the dryness or dirty of the finger's skin, as well as with the age (is not appropriate with children, because the size of their fingerprint changes quickly) • Image captured at 500 dots per inch (dpi). Resolution: 8 bits per pixel. A 500 dpi fingerprint image at 8 bits per pixel demands a large memory space, 240 Kbytes approximately → Compression required (a factor of 10 approximately).
Facial recognition	• Non intrusive or no contact required • Commonly available sensors • Large amounts of existing data to allow background and/or watch list checks • Easy for humans to verify results	• Face can be obstructed by hair, glasses, hats, scarves etc • Sensitive to changes in lighting, expression and pose • Faces change over time • Propensity for users to provide poor-quality video images yet to expect accurate results
Hand geometry	• Easy to capture • Believed to be a highly stable pattern over the adult lifespan	• User requires some training • Not sufficiently distinctive for identification over large databases; usually used for verification of a claimed enrolment identity • System requires a large amount of physical space
Voice recognition	• Public acceptance • No contact required	• Difficult to control sensor and channel variances that

	• Commonly available sensors (telephones, microphones) • Cheap technology	significantly impact capabilities • Not sufficiently distinctive over large database
Retinal scanning	• Very high accuracy. • There is no known way to replicate a retina. • The eye from a dead person would deteriorate too fast to be useful, so no extra precautions have to been taken with retinal scans to be sure the user is a living human being.	• Very intrusive. • It has the stigma of consumer's thinking it is potentially harmful to the eye • Comparisons of template records can take upwards of 10 seconds, depending on the size of the database. • Very expensive.
Iris Recognition	• Very high accuracy. • Verification time is generally less than 5 seconds. • The eye from a dead person would deteriorate too fast to be useful, so no extra precautions have to been taken with retinal scans to be sure the user is a living human being.	• Intrusive. • A lot of memory for the data to be stored. • Very expensive
Signature Recognition	• Non intrusive • Little time of verification (about five seconds) • Cheap technology	• Signature verification is designed to verify subjects based on the traits of their unique signature. As a result, individuals who do not sign their names in a consistent manner may have difficulty enrolling and verifying in signature verification • Error rate: 1 in 50
DNA	• Very high accuracy • It impossible that the system made mistakes	• Extremely intrusive. • Very expensive

	- It is standardized.	

Table 1.1: Advantages and disadvantages of different biometric technologies.

1.2 Advantages of fingerprint biometrics

Among all biometrics, fingerprint biometrics has proved itself the most promising and cost-effective solution in security systems. It’s lower cost and accuracy has brought itself in the leading position of all biometric solutions as can be seen from Figure 1.2. Although other biometric technologies are gaining popularity, fingerprint is likely to maintain its leading position in the near future. At present, nearly half of the biometic solutions are being implemented using fingerprint biometrics [1].

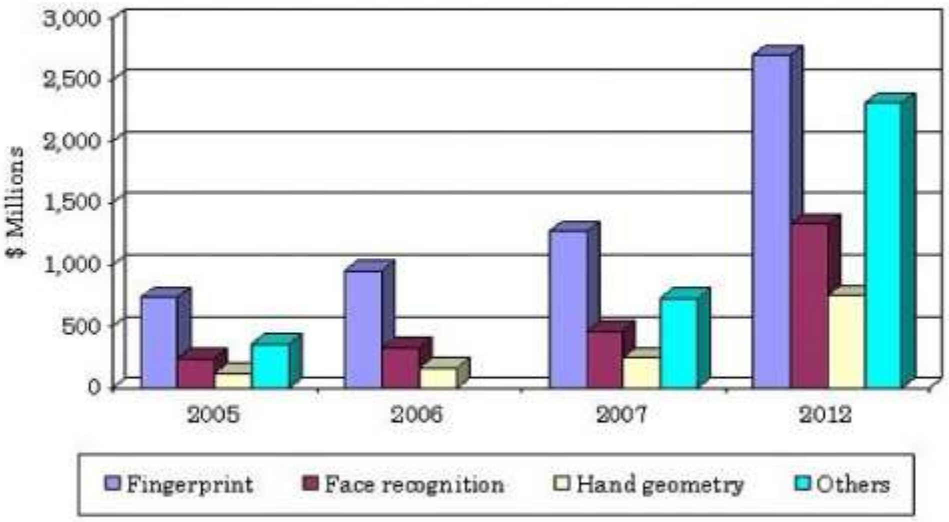

Figure 1.2: Global Biometric Market Projections by Technology, 2005-2012 (BCC Research) [5].

In recent years, government and commercial organisations have substantially increased their own deployment of fingerprint based recognition systems in non forensic applications, including physical and logical access control due to rising concerns about security and fraud. Automatic fingerprint recognition systems performs reliably well as far as recognition is concerned [6].

Over the last two decades, research in fingerprint recognition has seen tremendous growth. Several automatic fingerprint identification systems (AFIS) have been developed for civil, military and forensic applications. FBI-AFIS, US border security and EU passport/ID system are few examples of large scale applications of fingerprint biometrics [1].

The main reasons for the popularity of fingerprint recognition are [1]

- Its success in various applications in the forensic, government, and civilian domains
- The fact that criminals often leave their fingerprint at crime scenes
- The existence of large legacy databases and

- The availability of compact and relatively inexpensive fingerprint readers.

1.3 Challenges in automatic fingerprint recognition

Although significant progress has been made in automatic fingerprint identification in recent years, there are still a number of issues that need to be addressed to improve systems performance and accuracy. Most of the shortcomings in the accuracy of an automatic fingerprint identification system can be attributed to the acquisition process:

1.3.1 Inconsistent contact

Human finger is not a rigid object and if projection of the finger surface onto the image acquisition surface is not precisely controlled, different impressions of a finger can be created by various transformations. Determined by the pressure and contact of the finger on the glass platen, the three-dimensional shape of the finger gets mapped onto the two-dimensional surface of the glass platen. The result of inconsistent contact of finger with the sensor can result in elastic distortion where different portions of the finger are displaced by different magnitudes in different directions.

1.3.2 Non-uniform contact

In an ideal case, only the ridge lines make contact with the sensing surface and valleys remain untouched to make a prefect impression of the fingerprint. However, the dryness of the skin, shallow or worn-out ridges (due to aging or genetics), skin disease, sweat, dirt, and humidity in the air all confound the situation, resulting in a non-ideal contact situation. In the case of inked fingerprints, an additional factor may include inappropriate inking of the finger and may results in noisy, low contrast images, which leads to either spurious or missing minutiae.

1.3.3 Irreproducible contact

Sometimes accidents, manual work, burn etc. inflict injuries to the finger and can permanently damage the ridge structure of the finger. Further, each impression of a finger may possibly depict a different portion of its surface, which may introduce additional spurious minutiae.

1.3.4 Small overlapping area and nonlinear distortion

Fingerprint sensors embedded in consumer electronic devices seem to have small sensing area and the improper placement of user’s finger on the sensor in unsupervised condition may result in a limited overlapping area between two impressions of the same finger. Given that a very small number of minutiae in the overlapping area, it is difficult to determine if two fingerprints are from the same finger.

1.3.5 Latent fingerprint

Latent fingerprints generally suffer from low image quality, small overlapping area, and nonlinear distortion as well as the presence of a complex background. To overcome this problem, current automated system needs extensive manual intervention in latent encoding and in verifying a candidate list returned by the system [1].

1.3.6 Altered/Fake fingerprints

Any unauthorised user may use a fake finger that imitates a legitimate user's fingerprint to access a computer system or pass security checks. Rouges can cover their fingerprints by artificial fingerprints made of glue like substance or they can mutilate their fingers to avoid being identified by automated systems. To identify fake fingerprints, the hardware based liveness detection technique can be adopted by measuring and analysing various vital sign of the live finger such as pulse, perspiration and deformation [1]. To deal with mutilated finger, a mutilation detector can be added, and, when mutilation is detected, effort should be made to identify the subject either by restoring the original fingerprints or using the only unaltered areas of the fingerprint. The use of multibiometrics can be a solution to tackle altered fingerprint [1].

1.3.7 Interoperability

Interoperability is a big issue in a multivendor environment and it can occur in any module of an AFIS: sensor, feature extractor and matcher. Different sensor types such as Optical, Capacitive, RF can produce images that shows variations in resolution, size, distortion, contrast, background noise and so many. The difference in encoding the image into binary may result in varying definition of the same feature. This diversity makes it difficult to build a fingerprint system with principal components sourced from different vendors.

To improve the interoperability among multiple fingerprint systems, international standardisation organisations have established standards for sensors, templates and systems testing- for example, image quality specifications for fingerprint sensors and data exchange formats for minutiae templates [1]. However the superiority in matching accuracy of proprietary templates compared to standard templates in NIST MINEX testing has shown that existing standards must be improved by, for example, including extended features.

1.3.8 Feature extraction artefacts

The feature extraction algorithms are not always perfect and introduce measurement errors as discussed in sensor interoperability. Various image processing operations might introduce inconsistent biases to perturb the location and orientation estimates of the reported fingerprint structures from their gray-scale counterparts.

1.4 Security issues

The security of biometric data is of paramount importance and must be protected from external attacks and tampering as when the biometric data is lost, it is lost forever. We cannot change our face or fingerprint as we can easily change our PIN if our card is lost. Ratha et al. [7] characterize common attacks in biometric systems as coercive attack, impersonation attack, replay attack, and attacks on feature extractor, template database, matcher, and matching results. Some key security issues have also been explored in [8]. Attacks can alter the contents of biometric images or templates and can degrade the performance of a biometric system. It is therefore required to protect the biometric templates (fingerprint template) of individuals at all times.

While system-on-device technology such as built-in sensor, storage and processing modules on a card is a useful measure in verification application, fingerprint ID systems require centralised storage of fingerprint information (template) in large enrolment databases. The unauthorised release of such fingerprint template information from the database poses a serious security and privacy threat. The stolen fingerprint template can be reverse-engineered to construct a fake finger or replayed into the system or it can be used for cross matching across different databases to covertly track people without their consent, thereby compromising their privacy [1].

Two strategies have been proposed in the literature to protect fingerprint templates. One such method is to apply a noninvertible mathematical transformation to the original template to generate a cancellable template and to store the cancellable template only in the database. Therefore, even if the template is lost, the original fingerprint cannot be regenerated. A user can be issued a new cancellable template in case his/her first template is lost or stolen. In the second method, a cryptographic key is generated using the biometric sample such as fingerprint.

The problem with both approaches is that there is some loss of information during the transformation/key generation process that adversely affects the fingerprint recognition system's accuracy [9].

1.5 Research aims and objectives

In this research, an effort will be made to develop and test a novel algorithm for template formation and matching in automatic fingerprint recognition using Level 2 features. The main objectives of this research will be to

- Optimise image enhancement to extract level2 features.
- Optimise the distance between adjacent minutiae using heuristic rules to minimise the number of false or spurious minutiae.
- Develop and test the novel algorithm to create a fingerprint template using multidimentional feature vector.
- Compare and contrast the performance of novel algorithm with other benchmark algorithms such as Cefar, Cept, Utwe, Diti and Ncmi [10].

Some publicly available fingerprint image database in which fingerprints are captured in various environmental conditions using different sensors will be suitable for the evaluation of the novel algorithm in terms of checking its performance and testing sensor interoperability. The performance of any fingerprint matching algorithm is usually determined by two parameters namely False Acceptance Rate (FAR) and False Rejection Rate (FRR). False acceptance occurs when an unregistered finger is falsely matched with a registered finger and false rejection occurs when an already enrolled finger is not recognised by the system. A matching threshold should be carefully chosen to allow the maximum percentage of false minutiae in the match. The optimum threshold of a system is determined by Equal Rate (EER) when FAR and FRR become equal. To calculate FRR, the images from the same finger captured in different times and environmental conditions will be checked against each other and to calculate FAR, different images will be checked against each other to find any false match. The algorithm will be implemented in Matlab as it offers a wide range of image processing tools and a suitable platform for developing and testing algorithm using C programming language.

1.6 Contributions to knowledge

This section provides an overview of the algorithm developed to accomplish the above mentioned research objectives.

Optimising the image enhancement technique to extract level2 features (minutiae).

In a well-defined fingerprint image, the ridge and valley structure stands out in an alternate fashion with their smooth flow lines. This regularity facilitates the detection of ridge endings and bifurcation and consequently, allows minutiae to be precisely extracted from the thinned ridges. However, in practice, a fingerprint image may not always be well defined due to elements of noise that corrupts the clarity of the ridge structures. This corruption may occur due to variations in skin and impression conditions such as scars, humidity, dirt, and non-uniform contact with the fingerprint capturing device [9]. Therefore, image enhancement techniques are often employed to reduce the noise and enhance the definition of ridges against valleys.

To optimise the enhancement process, the methodology proposed by Hong et al. [11] has been applied, which is based on the convolution of the image with Gabor filters [12] tuned to the local ridge orientation and ridge frequency. The enhancement is implemented in several stages namely normalisation, ridge orientation estimation, ridge frequency estimation and filtering.

The normalisation has been implemented by the method proposed by Hong, Wan, and Jain (1998) with zero (0) mean and unit (1) standard deviation to bring all the pixels of the image in the range of 0-255. To identify ridge like regions, the image was segmented in square blocks and a carefully chosen threshold value was used. The region outside the ridge like regions does not contain any feature and should be discarded before the extraction process begins. After optimising the region of interest, an estimation of orientation of the ridge lines was completed by the method proposed by Hong et al. Although pixel wise processing could provide more accurate estimation of the orientation of ridge lines, it demands a lot of computation and therefore a block wise estimation was implemented to reduce the processing time by 36 times (apx) in my 300×300 pixel fingerprint image.

To estimate the ridge frequency across the whole image, the oriented image was passed to the ridge frequency function. Al last, both the ridge oriented image and the ridge frequency image were passed to ridge filter function to smooth the ridge lines. A scale factor of 0.5 for sigma in the x direction and a value of 0.5 for sigma in the y direction have been used to generate the filtered image. The sigma in the x direction which is along the filter controls the bandwidth of the filter and the sigma in the y direction control the orientation selectivity of the filter.

The enhancement with Gabor filtering [12] has made it possible for the algorithm to extract features (valid minutiae) from low quality images.

Optimising the distance between adjacent minutiae using heuristic rules to minimise the number of false or spurious minutiae.

In feature extraction process, the location of valid minutiae should be figured out as accurately as possible. In the feature extraction process of the novel algorithm, only termination and bifurcation were considered as valid minutia points and all other distinguisable features such as crossover, island and spikes generated from image enhancement were discarded.

To achieve this false minutiae rejection technique, a number of trial and error have been implemented and an optimum distance of 6 pixels has been set for removing all invalid minutiae. Therefore, any valid minutie after the image enhacement must be 7 or more pixel away from its neighbour.

Develop and test the novel algorithm to create a fingerprint template using multidimensional feature vector.

The efficiency of many of the commercially established systems heavily relies on the detection of the core and the quality of the image itself. The number of multiple SPs or absence of core on the image can cause some anomalies in the formation of the template and may result in high false acceptance or false rejection. The novel algorithm does not rely on any core or singularity point thus makes the structure invariant to global rotation and translation. Moreover, it does not need orientation of the minutiae points on which most of the established algorithm are based. The matching methodology is based on the local features of each minutiae point such as distances to its nearest neighbours and their internal angle.

The novel algorithm has been tested and evaluated on a publicly available database and has shown some good results with a low FAR and FRR.

1.7 Thesis outline

Chapter 2 discusses in detail the background of template formation and matching in AFRS. The development of the novel algorithm, its performance with results and evaluation are discussed in chapter 3. Finally conclusion and future work are suggested in chapter 4.

Fingerprint Biometrics

2.1 Introduction

Fingerprint of an individual is considered as unique and it remains unchanged over a lifetime if it does not have any severe damage, cut or bruise. Even fingerprints are unique in twins. A fingerprint impression is formed by the ridge and valley structure on a fingertip epidermis. A ridge is defined as a single curved segment, and a valley is the region between two adjacent ridges. The ridge and valley structure on every fingerprint creates some distinguishable features, which are depicted in Figure 2.1.

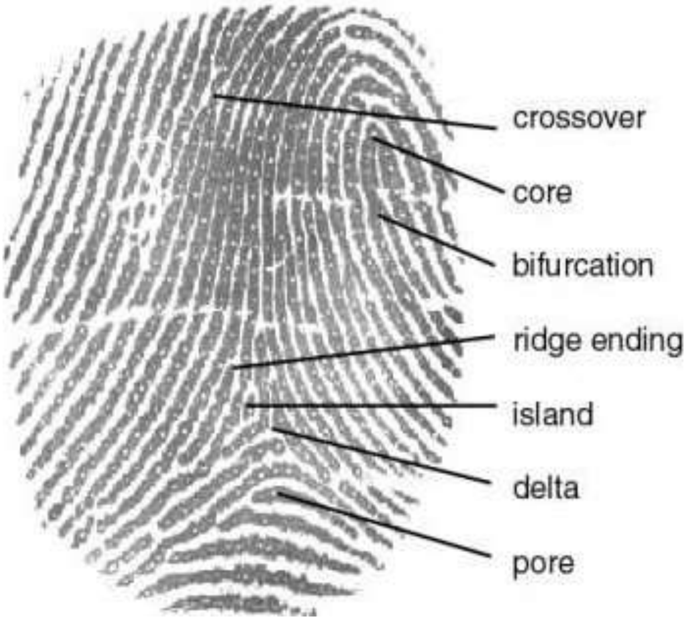

Figure 2.1: A typical fingerprint with its features [13]

A number of features can be extracted from a processed fingerprint image at three different levels [14]. At level1, the whole ridge and valley structure constitutes a global pattern, which can be classified as one of the five major classes as ‘left loop’, ‘right loop’, ‘whorl’, ‘arch’ and ‘tented arch’ (see Figure 2.2).

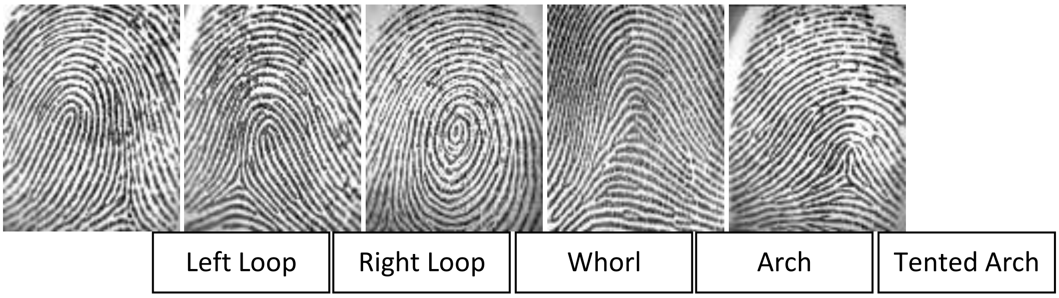

Figure 2.2: Fingerprints of five major classes [14]

At level2, ridge line discontinuities found on any fingerprint are used to construct distinguishable features. The point where the ridge line ends is called a Termination and the point where a ridge line forks out into two lines is called a Bifurcation. Apart from termination and Bifurcation, there are some other features such as island, bridge, lake and crossover, which are considered as level2 features although these features are not very common in every image. The minutiae, which are the local discontinuities in the ridge flow pattern, provide the features that are used for identification. Details such as the type, orientation, and location of minutiae are taken into account when performing minutiae extraction [9].

Level3 features are actually pores, their shape, size, distribution and width of ridges. Pores are very small openings distributed on ridge lines to discharge sweat. While level1 and level2 features are currently used in commercially available automatic fingerprint recognition systems (AFRSs), level3 features are still under research and development stage as they require high resolution image capturing device to extract pores [14]. American National Standard for Information System (ANSI) has defined four different types of features (minutiae) on a fingerprint in its ANSI/NIST-ITL 1-2007 standard [15], which is shown in Table 2.1.

Type	**Description**
A	Ridge ending
B	Bifurcation
C	Compound (trifurcation or crossover)
D	Others/Type undetermined

Table 2.1: Minutiae types at Level2 in ANSI/NIST standard.

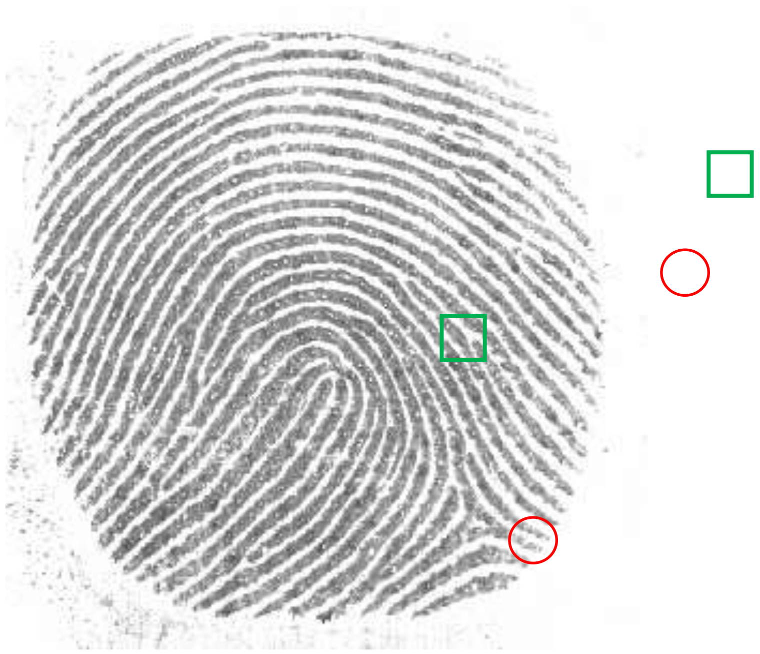

Figure 2.3: Ridge Ending and ○ Bifurcation □ on a fingerprint [16]

In most proprietary AFRS at present, only termination and bifurcation as shown in Figure 2.3 have been recognised as valid minutiae as these two are more than 95% of all level2 features in a typical fingerprint. Such systems first detect the minutiae on a fingerprint image and then match the input minutiae set with minutiae in the stored template [16, 17].

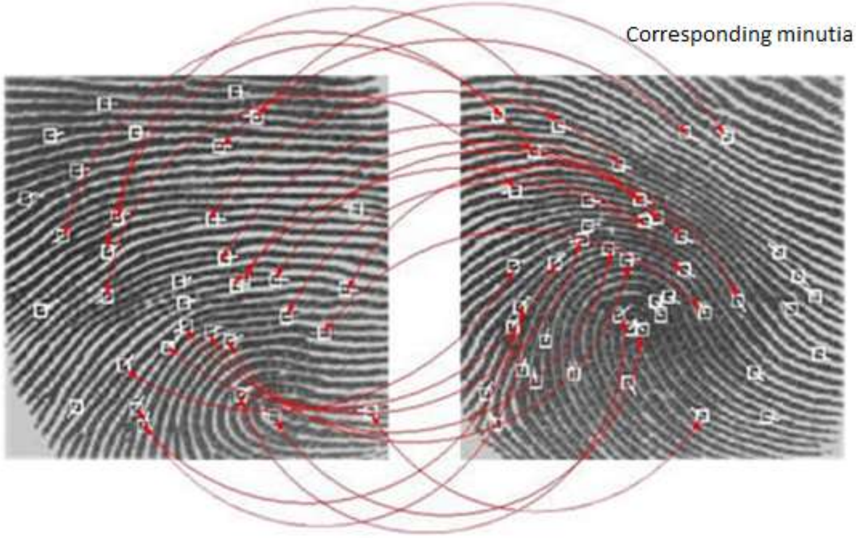

Figure 2.4: Minutiae matching at level2 [16]

Figure 2.4 shows the corresponding minutiae in two impressions from the same fingerprints. Two minutiae are to be matched if they fall within the tolerance with same location and orientation after the alignment. These are called corresponding minutiae on two templates. The process of fingerprint enrolment and matching are implemented in several stages that include post scanned image enhancement, image processing, feature extraction, template formation and matching. The key stages in a typical fingerprint identification or verification process can be realised from Figure 2.5.

As can be seen from Figure 2.5, the matching is performed not on two direct greyscale images but on an intermediary stage called template, which is created using distinctive features at level1, level2 and level3 or combination of these.

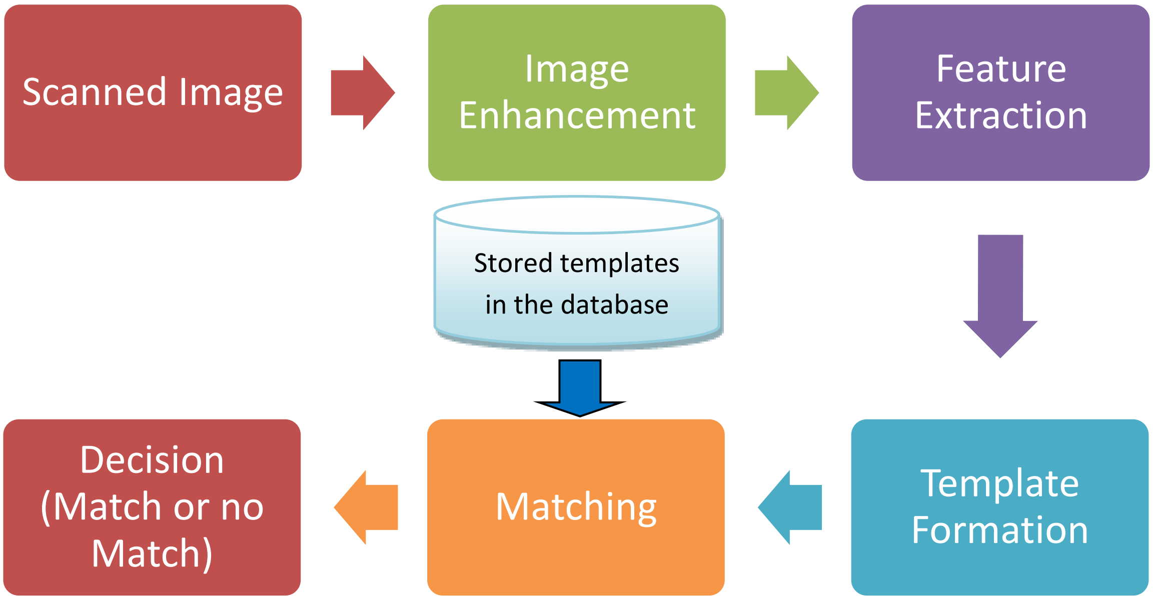

Figure 2.5: A typical fingerprint identification/verification process

Two different scenario can be arised when one fingerprint template is compared with another template in an AFRS. These are verification and identification. Verification is a 1:1 (one to one) matching process where a user provides a token such as ID number or Card and the system checks if the user is genuine that he/she claims to be. On the other hand, in identification process, the user's fingerprint template (query template) is checked against every template stored in the database to identify who the user is. This is a 1:M (one to many) matching process.

Whether it is identification or verification, the image quality is always a major factor in system's reliability. Image quality can vary due to changes in physical and environmental conditions. They may be degraded and corrupted with elements of noise due to many factors including variations in skin and impression conditions. Different types of scanner can also render significantly different impressions based on its resolution and the technology used (such as optical, capacitive or radio frequency (RF)). This degradation can result in a significant number of spurious minutiae being created and genuine minutiae being ignored. A critical step in the process of fingerprint enrolment and matching is to reliably extract minutiae from fingerprint images. Thus, it is necessary to employ image enhancement techniques prior to minutiae extraction to obtain a more reliable estimate of minutiae locations (see Figure 2.5).

Any AFRS's operational performance depends on several factors such as sensor characteristics, the number of demographic distribution of the population enrolled in the system, the type of sensing media and various environmental factors- indoor versus outdoor, temperature, humadity and so many. Also, the quality of an AFRS is measured on how efficiently it can recognise a genuine finger and how good it is rejecting an unauthorised finger. The parameters are quantised as False Acceptance Rate (FAR, the ratio of the number of false match to the total number of comparison when different fingerprint images are checked against each other) and False Rejection Rate (FRR, the ratio of the number of non- match to the total number of comparison when different impression from the same fingerprint are checked against each other).

Depending on the application, the FAR and FRR can be adjusted to suit users' needs [1] - for example, Disney World's fingerprint-based entry system operates on low FRR at the expense of high FAR as they do not want to upset paying customer. On the other hand, an ATM fingerprint verification system may have very low FAR at the expense of higher FRR.

Although the sensing technology has been improved significantly in recent years; in some cases, a fingerprint recognition system may fail to capture the user's fingerprint. Failure to Enrol (FTE) and Failure to Acquire (FTA) [1] refer to the fraction of users who cannot be enrolled or processed by a particular system due to the poor quality of their fingerprints as discussed above. The insufficient number of minutiae present of their finger actually results in the FTA or FTE.

As discussed before, the performance of any AFRS is haviely relied upon the quality of the fingerprint image as well as the efficiency of the feature extraction and matching algorithm. Many commercially available systems use singularity point (SP) or core point for fingerprint indexing and template formation as can be seen from Figure 2.6.

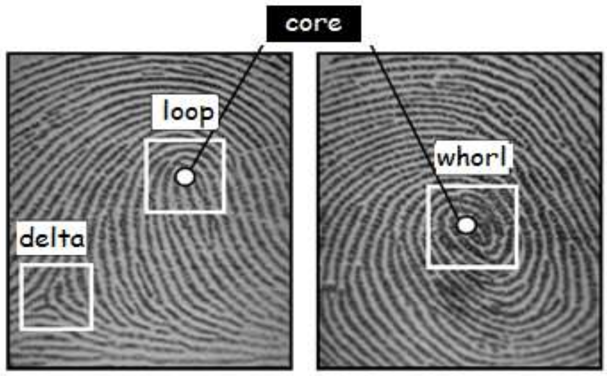

Figure 2.6: Singular regions (white boxes) and core points (small circles) in fingerprint images [9].

These systems use the coordinates and orientation of each minutia on the fingerprint. The accurate detection of the core and the quality of the image itself are critical in these systems' performance. The number of multiple SPs or absence of core on the image can cause real problem in the formation of the template and may result in high FAR and FRR. Also any translation or rotation of the image require an alignment process between the stored template and the query template thus put an overhead on the matching process and the complexity may result in higher FAR or FRR. The absence of real minutiae or presence of spurious or false minutia can also degrade the systems performance. Hence, there is a real case of developing a new algorithm to extract level2 features with minimum error, form a template and match with another template, which is invariant to translation and rotation and can accommodate the loss of real minutiae or occurrence of false or spurious minutiae in the query template.

2.2 Fingerprint template formation and matching

In a well-defined fingerprint image, the ridge and valley structure stands out in an alternate fashion with their smooth flow lines. This regularity facilitates the detection of ridge endings and bifurcation and consequently, allows minutiae to be precisely extracted from the thinned ridges. However, in practice, a fingerprint image may not always be well defined due to elements of noise that corrupts the clarity of the ridge structures. This corruption may occur due to variations in skin and impression conditions such as scars, humidity, dirt, and non-uniform contact with the fingerprint capturing device [9]. Therefore, image enhancement techniques are often employed to reduce the noise and enhance the definition of ridges against valleys.

This chapter provides discussion on the methodology and implementation of a fingerprint image enhancement, image binarisation, thinning or skeleton of the image and finally minutiae extraction. All 1680 images in FVC2006 database had been enhanced utilising all these stages prior to minutiae extraction process. The results of the experiments involving each stage of the fingerprint enhancement algorithm and minutiae extraction are then presented and discussed.

2.3 Image enhancement

One of the most widely cited fingerprint enhancement techniques proposed by Hong et al. [11] is based on the convolution of the image with Gabor filters [12] tuned to the local ridge orientation and ridge frequency. The enhancement is implemented in several stages namely normalisation, ridge orientation estimation, ridge frequency estimation and filtering.

As a result of poor image capture, which may result from non-uniform ink intensity or non-uniform contact with the fingerprint capturing device, a fingerprint image may exhibit distorted levels of variation in gray-level values along the ridges and valleys. To correct this variation, a normalisation is employed to bring the intensity to a pre-specified mean and variance.

The next important step in fingerprint image enhancement is ridge orientation. Orientations are directional vectors representing the ridge flow direction at each location (block) in the image. The most popular gradient-based approach is used to calculate the orientation [18, 19, 20]**,** which makes use of the fact that the orientation vector is orthogonal to the gradient. Firstly, the image is partitioned into square blocks and the gradient is calculated for every pixel, in the x and y directions. Then the orientation vector for each block is derived by performing an averaging operation on all the vectors orthogonal to the gradient pixels in the block. Sometimes noise and corrupted elements in the image may result in incorrect ridge orientation. Assuming that the ridge orientation varies slowly in a local neighbourhood, the orientation image is then smoothed using a low-pass filter to reduce the effect of outliers [21].

After calculating the ridge orientation for each block and smoothing the image with low-pass filter, the image is then processed for frequency estimation. Firstly, the image is divided into square blocks and an oriented window is calculated for each block. For each block, an x-signature signal is constructed using the ridges and valleys in the oriented window. The x-signature is the projection of all the gray level values in the oriented window along a direction orthogonal to the ridge orientation. Consequently, the projection forms a sinusoidal-shape wave in which the centre of a ridge maps itself as a local minimum in the projected wave. The distance between consecutive peaks in the x-signature can then be used to estimate the frequency of the ridges [21]**.**

A well defined ridge orientation and ridge frequency are important characteristic of a fingerprint image, which can be enhanced by a bandpass filter. In recent times, such enhancement is implemented by using a Gabor filter [12]**.** Gabor filters are bandpass filters that have both frequency-selective and orientation-selective properties, which mean the filters can be effectively tuned to specific frequency and orientation values. So far, It has been widely used to facilitate various application in fingerprint matching [22, 23] and fingerprint classification [24]. Based on the local orientation and ridge frequency around each pixel, the Gabor filter is applied to each pixel location in the image. The effect is that the filter enhances the ridges oriented in the direction of the local orientation, and decreases anything oriented differently. Hence, the filter increases the contrast between the foreground ridges and the background, whilst effectively reducing noise.

A different approach to fingerprint image enhancement technique that has been employed by Sherlock [25] is called directional Fourier filtering. The Gabor filter approach that can be computationally expensive involves spatial convolution of the image with filters. Alternatively, operating in the frequency domain allows one to efficiently convolve the fingerprint image with filters of full image size.

In directional Fourier filtering, a set of 16 equispaced directions are used to calculate the orienrtation [21]. An image window is centred at a point in the raw image, which is used to obtain a projection of the local ridge information. The image window is then rotated in each of the 16 equally spaced directions, and in each direction a projection along the window's *y* axis is formed. The projection with the maximum variance is used as the dominant orientation for that point in the image. This process is then repeated for each pixel to form the orientation image.

After the orientation stage computation, the image is passed through a set of bandpass filters tuned to match the ridge orinetation. Fourier transformation is used to convert the image from special domain to frequency domain. Then, it is filtered using a set of 16 Butterworth filters with each filter tuned to a particular orientation. The number of directional filters corresponds to the set of directions used to calculate the orientation image [21]. To get the image back into special domain, an inverse Fourier Transform is used after each directional filter has been independently applied to the image in frequency domain, which produces a set of directionally filtered images called pre-filtered images. These pre-filtered images are used with ridge orientation at each pixel of the original image to construct the final image. Each point in the final image is actually computed by selecting, from the pre-filtered images the pixel value whose filtering direction most closely matches the actual ridge orientation. An enhanced version of the image is obtained from the filtering stage that has been smoothed in the direction of the ridges.

After the directional filtering stage, the image is put for an adaptive thresholding in which each pixel in the gray level image is set as complete black or complete white depending on its gray level intensity above or below the threshold level. Now the gray level image is converted into a binary image where ridge lines are set as black lines whereas valleys are white.

Although both Hong et al [11] and Sherlock's [25] approach take ridge orientation into account, only Hong et al's enhancement method accounts ridge frequency variation whereas Sherlock's method considers ridge frequency as constant. By using both the orientation and ridge frequency information, it allows for accurate tuning of the Gabor filter parameters, which consequently leads to better enhancement results. Therefore, the Gabor filtering approach by Hong et al. has been utilised to perform fingerprint image enhancement.

2.3.1 Methodology

The methodology for fingerprint image enhancement proposed by Hong et al [11], which has been adopted in the experiment, consists of four main stages such as:

- normalisation,
- orientation estimation,
- ridge frequency estimation, and
- Gabor filtering.

In order to detect the minutiae, the enhanced image is processed in three additional stages that include:

- segmentation,
- binarisation, and
- thinning.

In this section, the methodology for each stage of the enhancement algorithm has been discussed, which includes modifications to the original techniques.

2.3.2 Normalisation

It is a process that changes the range of pixel intensity values. The purpose of normalisation is usually to bring the image, or other type of signal, into a range that is more familiar or normal to the senses, hence the term normalization.

Normalization is a linear process. If the intensity range of the image is 50 to 180 and the desired range is 0 to 255, the process entails subtracting 50 from each of pixel intensity, making the range 0 to 130. Then, each pixel intensity is multiplied by 255/130, making the range 0 to 255.

The normalisation approach used by Hong, Wan, and Jain [11] determines the new intensity value $I'[x,y]$ of each pixel in an image as:

$$I'[x,y] = \begin{cases} m_0 + \sqrt{(I[x,y]-m)^2 . {}^{v_0}/_{v}} \; if\ I[x,y] > m \\ m_0 - \sqrt{(I[x,y]-m)^2 . {}^{v_0}/_{v}} \; otherwise \end{cases} \qquad (2.1)$$

where *m* and *v* are the image mean and variance and *m*$_0$ and *v*$_0$ are the desired mean and variance after the normalisation.

As can be seen from Figure 2.7, the pixel intensity of the image in (a) is changed to the desired range (0-255) (image b) that provides a balanced distribution for white and dark pixels hence better output for further processes.

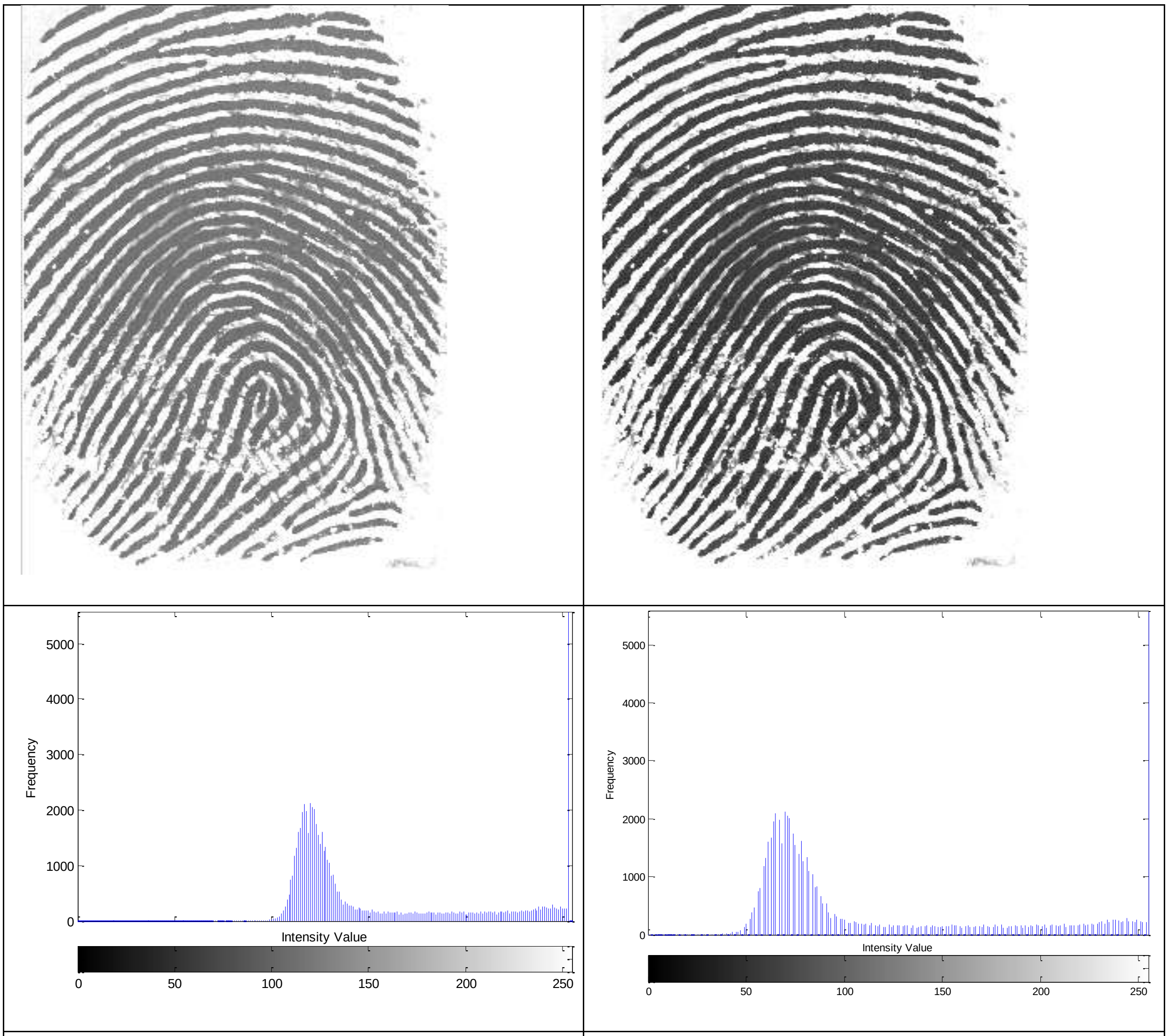

(a) Before normalisation

(b) After normalisation

Figure 2.7: An example of normalisation with zero (0) mean and unit (1) standard deviation. Images before (a) and after (b) normalisation.

2.3.3 Identification of ridge like region

Identifying ridge like regions thus seperating large variating foreground area from the background is an important part in image enhancement. Firstly , the image is broken up into blocks and the standard deviation is calculated for each block. If the standard deviation is above the threshold, it is deemed part of the fingerprint. During the enhancement process, all the images have been normalised to have zero mean, unit standard deviation prior to the identification of ridge like region process so that the threshold specified was relative to a unit standard deviation. A block of 16×16 pixels and a threshold of 0.1 have been used to identify ridge like regions in the enhancement process.

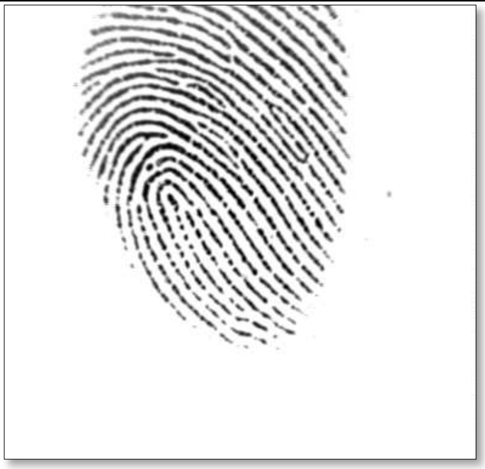	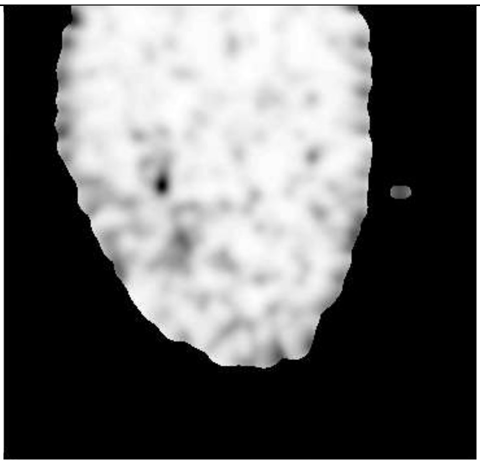
(a) Image with large space that does not contain any information	(b) Area where ridges and valleys are presented

Figure 2.8: Identifying ridge like region with reliability factor of 0.5 in a typical fingerprint.

As can be seen from Figure 2.8 (a) and (b), the region covered by the ridges only has been identified by using a threshold value of 0.1. Any part of the image where the pixel intensity is less than 10% has been considered as the region of no interest.

2.3.4 Orientation estimation

The orientation field actually defines the direction of the ridge lines. Figure 2.9 shows the orientation of a ridge pixel on a fingerprint. The method proposed by Hong et al [11], sometimes called least mean square method is an established method to calculate orientation estimation. In this method, the image can be processed either block wise or pixel wise.

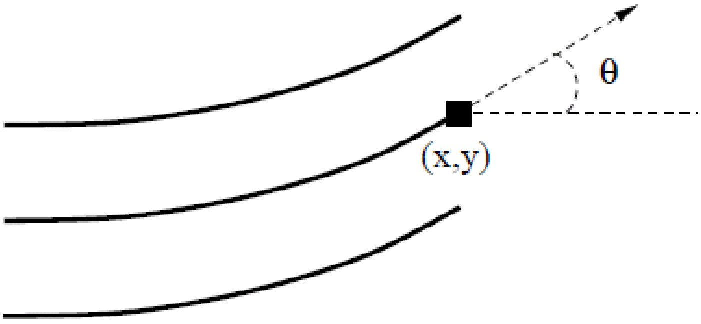

Figure 2.9: Orientation of a ridge pixel.

The steps for calculating the orientation at pixel (i,j) are as follows [21]:

1. Firstly, a block of size $w \times w$ is centred at pixel (i,j) in the normalised fingerprint image.

2. For each pixel in the block, compute the gradients $\partial_x(i,j)$ and $\partial_y(i,j)$, which are the gradient magnitudes in the x and y directions, respectively. The horizontal Sobel operator [26] is used to compute $\partial_x(i,j)$:

$$\begin{pmatrix} 1 & 0 & -1 \\ 2 & 0 & -2 \\ 1 & 0 & -1 \end{pmatrix} \quad (2.2)$$

And the vertical Sobel operator is used to compute $\partial_y(i,j)$:

$$\begin{pmatrix} 1 & 2 & 1 \\ 0 & 0 & 0 \\ -1 & -2 & -1 \end{pmatrix} \qquad (2.3)$$

3. The local orientation at pixel (i,j) can then be estimated using the following equations:

$$V_x(i,j) = \sum_{u=i-\frac{w}{2}}^{i+\frac{w}{2}} \sum_{v=j-\frac{w}{2}}^{j+\frac{w}{2}} 2\partial_x(u,v)\partial_y\,(u,v), \quad (2.4)$$

$$V_y(i,j) = \sum_{u=i-\frac{w}{2}}^{i+\frac{w}{2}} \sum_{v=j-\frac{w}{2}}^{j+\frac{w}{2}} 2\partial_x{}^2(u,v)\partial_y{}^2\,(u,v), \ (2.5)$$

$$\theta(i,j) = \frac{1}{2} tan^{-1}\frac{V_y(i,j)}{V_x(i,j)}, \ (2.6)$$

where $\theta(i,j)$ is the least square estimate of the local orientation at the block centred at pixel (i,j).

4. Smooth the orientation field in a local neighbourhood using a Gaussian filter. The orientation image is firstly converted into a continuous vector field, which is defined as:

$$\Phi_x(i,j) = \cos\big(2\theta(i,j)\big) \qquad (2.7)$$

$$\Phi_y(i,j) = \sin\big(2\theta(i,j)\big) \ (2.8)$$

where Φ_x and Φ_y are the x and y components of the vector field, respectively. After the vector field has been computed, Gaussian smoothing is then performed as follows:

$$\Phi'_x(i,j) = \sum_{u=-\frac{w_\varphi}{2}}^{\frac{w_\varphi}{2}} \sum_{v=-\frac{w_\varphi}{2}}^{\frac{w_\varphi}{2}} G(u,v)\Phi_x\,(i-uw, j-vw), \qquad (2.9)$$

$$\Phi'_y(i,j) = \sum_{u=-\frac{w_\varphi}{2}}^{\frac{w_\varphi}{2}} \sum_{v=-\frac{w_\varphi}{2}}^{\frac{w_\varphi}{2}} G(u,v)\Phi_y\,(i-uw, j-vw) \qquad (2.10)$$

where *G* is a Gaussian low-pass filter of size $w_\varphi \times w_\varphi$.

5. The final smoothed orientation field *O* at pixel (i,j) is defined as:

$$O(i,j) = \frac{1}{2} tan^{-1}\frac{\Phi'_y(i,j)}{\Phi'_x(i,j)}, \qquad (2.11)$$

A 16×16 pixel block wise estimation is done on a finger image that can be seen from Figure 2.10, in which the arrows are pointing to the direction of the ridge flow.

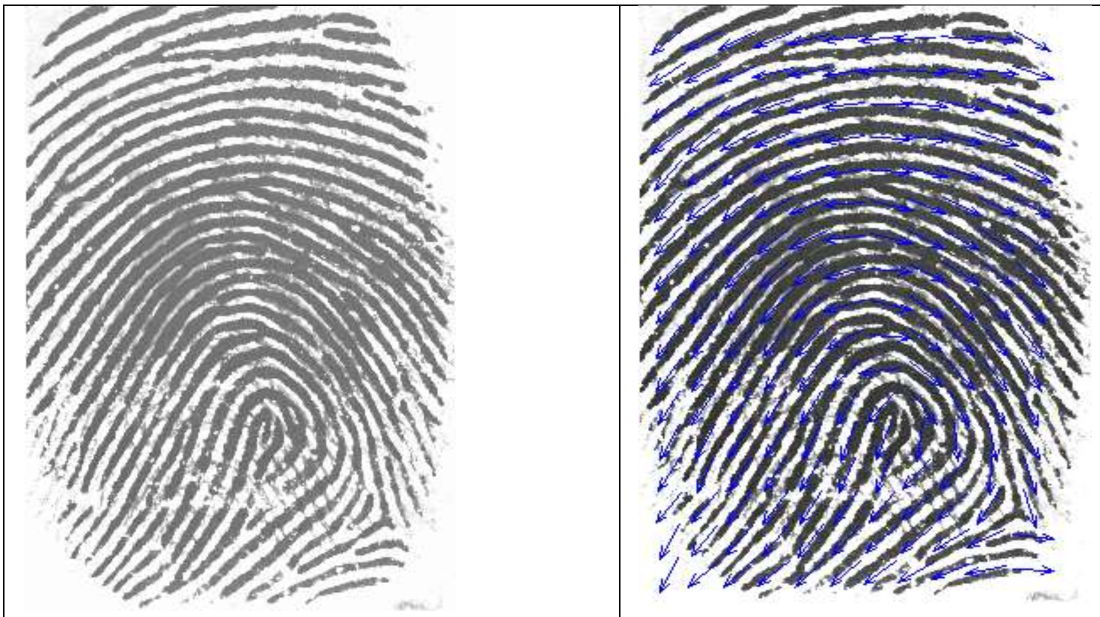

(a) Original Image

(b) Image after normalisation with ridge line orientation

Figure 2.10 Block wise orientation estimation on a typical fingerprint.

2.3.5 Ridge frequency estimation

In the construction of a Gabor filter, local ridge frequency is required in addition to the orientation of the image. The frequency image represents the local frequency of the ridges in a fingerprint. The first step in the frequency estimation stage is to divide the image into blocks of size $W \times W$ pixels. The next step is to project the gray-level values of all the pixels located inside each block along a direction orthogonal to the local ridge orientation [21]. This projection forms an almost sinusoidal-shape wave with the local minimum points corresponding to the ridges in the fingerprint. An example of a projected waveform is shown in Figure 2.11 where intensity varies in a sinusoidal manner and gradually decreases across pixels.

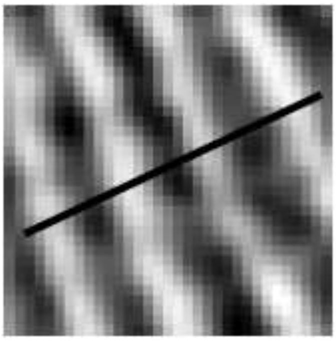

(a)

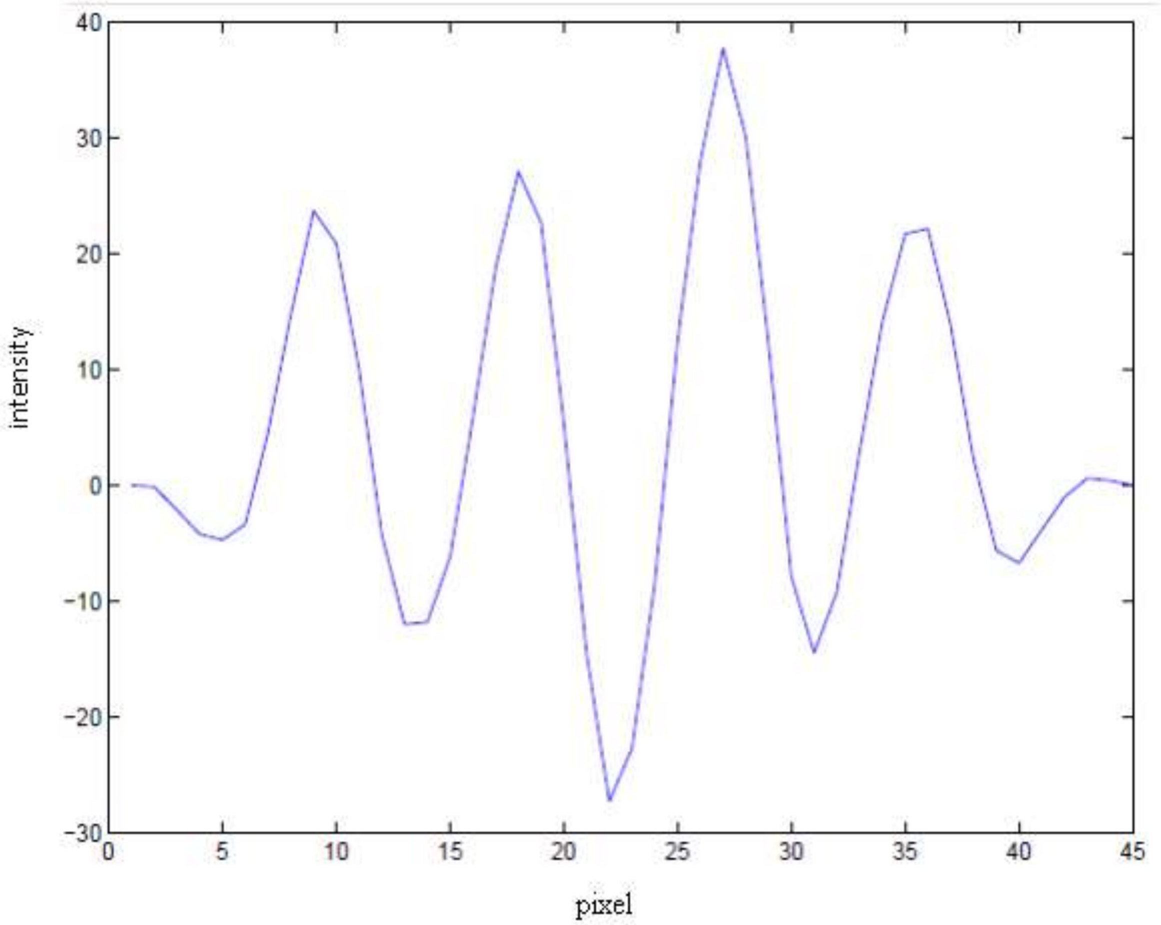

(b)

Figure 2.11: The projection of the intensity values of the pixels along a direction orthogonal to the local ridge orientation. (a) A 32 × 32 block from a fingerprint image. (b) The projected waveform of the block.

The original frequency estimation stage used by Hong et al [11] can be improved by including an additional projection smoothing step prior to computing the ridge spacing [21]. This involves smoothing the projected waveform using a Gaussian lowpass filter of size $W \times W$ to reduce the effect of noise in the projection. The ridge spacing $S(i, j)$ is then computed by counting the median number of pixels between consecutive minima points in the projected waveform. Hence, the ridge frequency $F(i, j)$for a block centred at pixel (i, j) is defined as:

$$F(i,j) = \frac{1}{S(i,j)} \quad (2.12)$$

Ideally the ridge frequency values should fall within a certain range given that the fingerprint is scanned at a fixed resolution. However, there are cases where a valid frequency value cannot be reliably obtained from the projection. Examples are when no consecutive peaks can be detected from the projection, and also when minutiae points appear in the block. For the blocks where minutiae points appear, the projected waveform does not produce a well-defined sinusoidal shape wave, which can lead to an inaccurate estimation of the ridge frequency. Thus, the out of range frequency values are interpolated using values from neighbouring blocks that have a well-defined frequency.

2.3.6 Gabor filtering

Once the ridge orientation and ridge frequency information has been determined, these parameters are used to construct the even-symmetric Gabor filter. A two dimensional Gabor filter consists of a sinusoidal plane wave of a particular orientation and frequency, modulated by a Gaussian envelope [12]. Gabor filters are employed because they have frequency-selective and orientation-selective properties. These properties allow the filter to be tuned to give maximal response to ridges at a specific orientation and frequency in the fingerprint image. Therefore, a properly tuned Gabor filter can be used to effectively preserve the ridge structures while reducing noise. The even-symmetric Gabor filter is the real part of the Gabor function, which is given by a cosine wave modulated by a Gaussian envelop as seen by Figure 2.12.

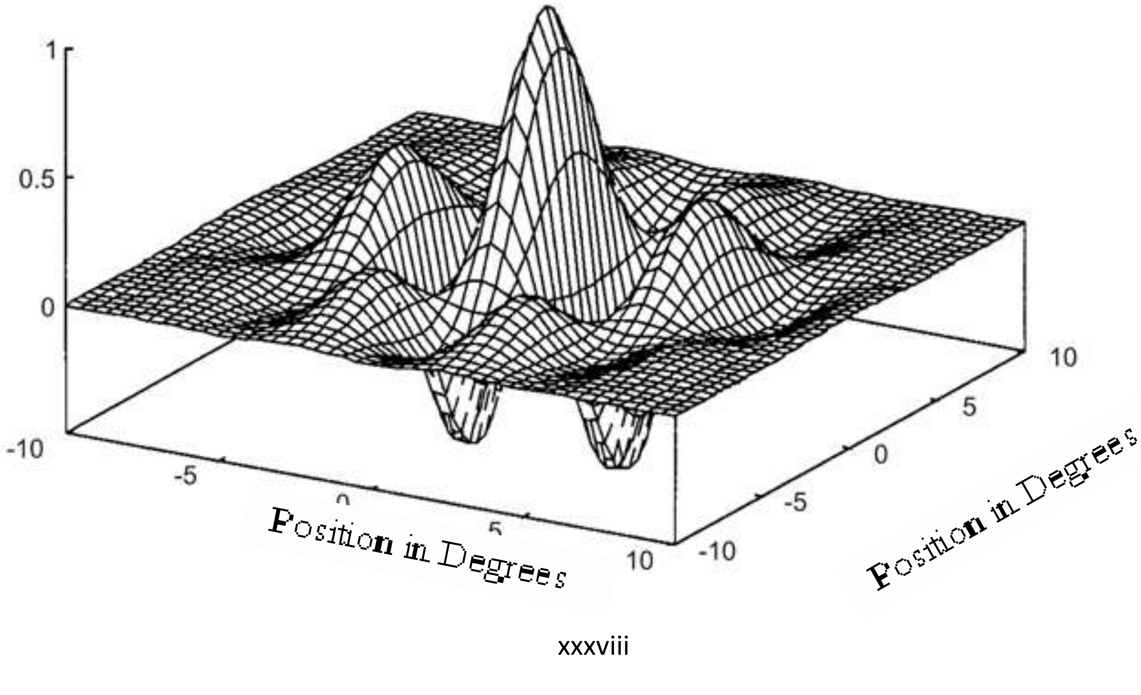

Figure 2.12: An even-symmetric Gabor filter in the spatial domain

An even symmetric Gabor filter in the spatial domain is defined as [27]:

$$G(x,y;\theta,f) = exp\left\{-\frac{1}{2}\left[\frac{x_\theta^2}{\sigma_x^2}+\frac{y_\theta^2}{\sigma_y^2}\right]\right\}\cos(2\pi f x_\theta), \qquad (2.13)$$

$$x_\theta = xcos\theta + ysin\theta \qquad (2.14)$$

$$y_\theta = -xsin\theta + ycos\theta \quad (2.15)$$

where θ is the orientation of the Gabor filter, f is the frequency of the cosine wave, σ_x and σ_y are the standard deviations of the Gaussian envelop along the x and y axes, respectively, and x_θ and y_θ define the x and y axes of the filter coordinate frame, respectively.

The Gabor filter is applied to the fingerprint image by spatially convolving the image with the filter. The convolution of a pixel (i,j) in the image requires the corresponding orientation value $O(i,j)$ and ridge frequency value $F(i,j)$ of that pixel. Hence, the application of the Gabor filter *G* to obtain the enhanced image *E* is performed as follows [21],

$$E(i,j) = \sum_{u=-\frac{w_x}{2}}^{\frac{w_x}{2}} \sum_{v=-\frac{w_y}{2}}^{\frac{w_y}{2}} G\big(u,v;O(i,j),F(i,j)\big)N(i-u,j-v), \qquad (2.16)$$

where O is the orientation image, *F* is the ridge frequency image, *N* is the normalised fingerprint image, and W_x and W_y are the width and height of the Gabor filter mask, respectively.

The filter bandwidth, which specifies the range of frequency the filter responds to, is determined by the standard deviation parameters σ_x and $\sigma_{y.}$ Since the bandwidth of the filter is tuned to match the local ridge frequency, then it can be deduced that the parameter selection of σ_x and σ_y should be related with the ridge frequency. However, in the original algorithm by Hong et al [11], σ_x and σ_y were empirically set to fixed values of 4.0 and 4.0, respectively.

A drawback of using fixed values is that it forces the bandwidth to be constant, which does not take into account the variation that may occur in the values of the ridge frequency. For example, if a filter with a constant bandwidth is applied to a fingerprint image that exhibits significant variation in the frequency values, it could lead to non-uniform enhancement or other enhancement artefacts. Thus, rather than using fixed values of σ_x and $\sigma_{y,}$ these can be a defined as functions of the ridge frequency parameter, which are defined as

$$\sigma_x = k_x F(i,j), \ (2.17)$$

$$\sigma_y = k_y F(i,j), \ (2.18)$$

where F is the ridge frequency image, k_x is a constant variable for σ_x, and k_y is a constant variable for σ_y. This allows a more adaptable approach to be used, as the values of σ_x and $\sigma_y$can now be specified adaptively according to the local ridge frequency of the fingerprint image.

Furthermore, in the original algorithm, the width and height of the filter mask were both set to fixed values of 11. The filter size controls the spatial extent of the filter, which ideally should be able to accommodate the majority of the useful Gabor waveform information. However, a fixed filter size is not optimal in that it does not allow the accommodation of Gabor waveforms of different sized bandwidths. Hence, to allow the filter size to vary according to the bandwidth of the Gabor waveform, the filter size has to be a function of the standard deviation parameters:

$w_x = 6\sigma_x,$ (2.19)

$w_y = 6\sigma_y,$ (2.20)

where w_x and w_y are the width and height of the Gabor filter mask, respectively. In the above equation, the width and height of the filter mask are both specified as 6σ due to most of the Gabor wave information being contained within the region [-3σ, 3σ] away from the *y* axis. Hence, this selection of parameters allows the filter mask to capture the majority of the Gabor waveform information.

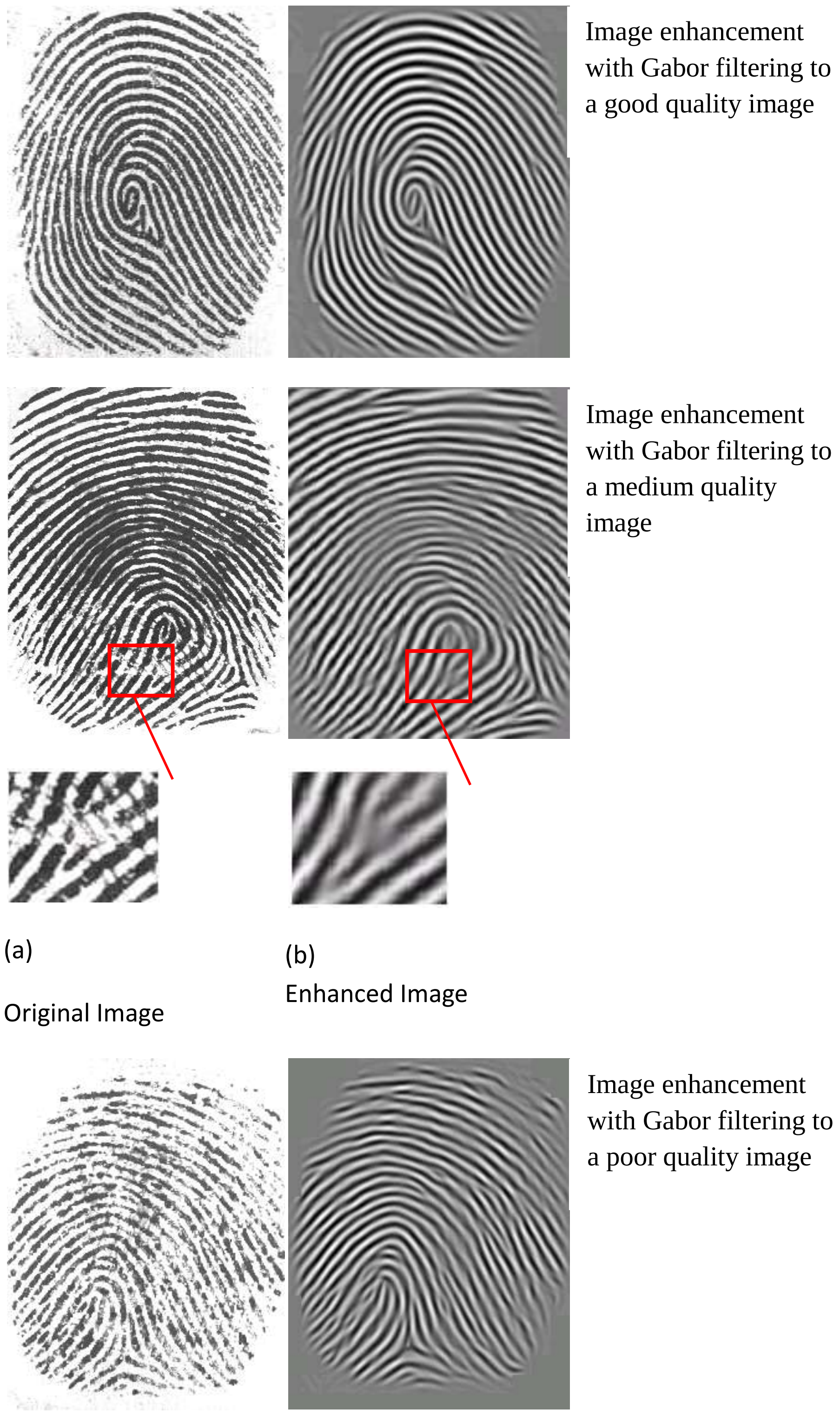
Image enhancement with Gabor filtering to a good quality image
Image enhancement with Gabor filtering to a medium quality image
(a)
Original Image
(b)
Enhanced Image
Image enhancement with Gabor filtering to a poor quality image

Figure 2.13: Results of applying a Gabor filter with $k_x = 0.5$ and $k_y = 0.5$ to a good quality, medium quality and poor quality fingerprint image.

As can be seen from Figure 2.13, the broken ridge lines have been smoothed and some noises have been removed in particular with poor images where ridge and valley structures are not well defined. Although smoothing ridge lines using Gabor Filtering is a great benefit to poor quality images, on some images it can also remove valuable identifying features such as permanent bruise or cut.

2.3.7 Binarisation

Binarisation is the process in which a grayscale image is converted into a pure black and white image. In most minutiae extraction algorithms, there are two levels of interest: the black pixels that represent ridges and the white pixels that represent valleys. This improves the contrast between the ridges and valleys in a fingerprint image, and consequently facilitates the extraction of minutiae.

2.3.8 Thinning

The last stage implemented before the minutiae extraction process is thinning. Thinning is a morphological operation that successively erodes away the foreground pixels until they are one pixel wide resulting in a skeleton image as shown in Figure 2.14. A standard thinning algorithm [28], which performs the thinning operation using two sub-iterations, was implemented in Matlab. The skeleton is the final image in the enhancement process, from which minutiae are extracted.

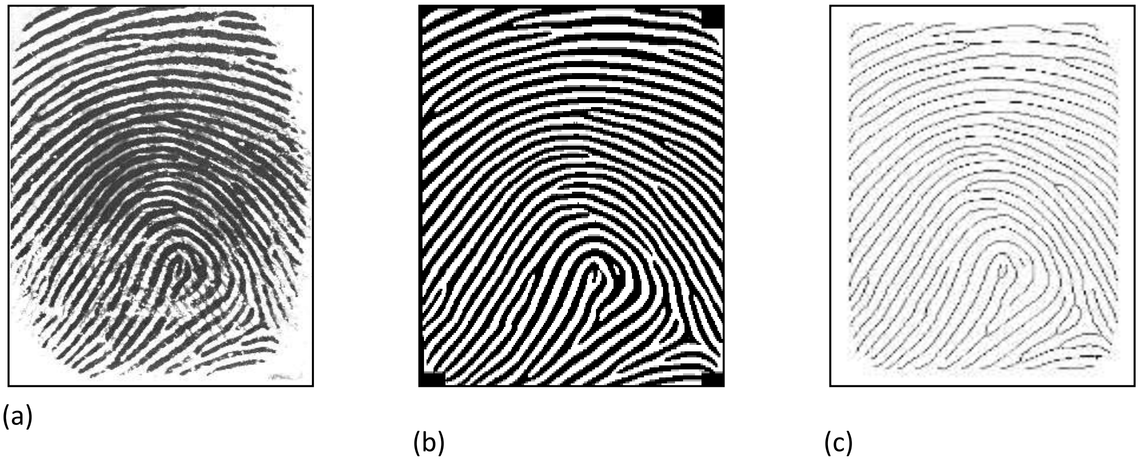

Figure 2.14: (a) A fingerprint gray-scale image; (b) the image obtained after binarisation of the image in (a); (c) skeleton image obtained after a thinning of the image.

2.4 Minutiae extraction

Using the skeleton image, the most commonly employed method that is used for minutiae extraction is the Crossing Number (CN) concept [19, 29, 30]. In this method, a window of 3x3 pixels is used to examine the local neighbourhood of each pixel in the image and the CN value is computed as half the sum of the differences between pairs of adjacent pixels in the eight- neighbourhood. Using the properties of the CN as shown in Table 2.2, the ridge pixel can then be classified as a ridge ending, bifurcation or non-minutiae point [21]. For example, a ridge pixel with a CN of one corresponds to a ridge ending, and a CN of three corresponds to a bifurcation.

CN	Property
0	Isolated Point
1	Ridge Ending Point
2	Continuing Ridge Point

3	Bifurcation Point
4	Crossing Point

Table 2.2: Properties of the Crossing Number (CN).

The CN for a ridge pixel *P* is given by [31]:

$$CN = 0.5\sum_{i=1}^{8}|P_i - P_{i+1}|, \qquad P_9 = P_1 \tag{2.21}$$

where *Pi* is the pixel value in the neighbourhood of *P*. For a pixel *P,* its eight neighbouring pixels are scanned in an anti-clockwise direction as follows:

P_4	P_3	P_2
P_5	P	P_1
P_6	P_7	P_8

Table 2.3: Orientation of neighbouring pixels around the central pixel.

The CN value for a pixel on the ridge is used to identify whether it is a ridge ending or ridge bifurcation. A CN value of 1 can corresponds to a ridge ending or termination and a value of 3 corresponds to a ridge bifurcation as can be seen from Figure 2.15.

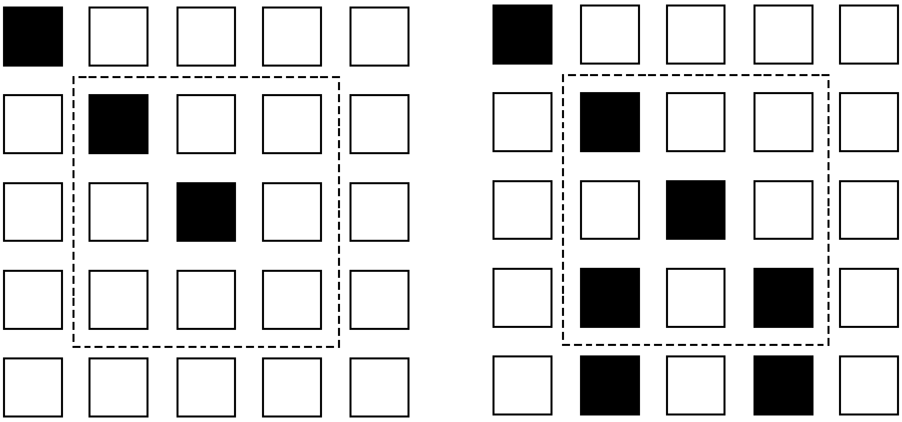

(a) CN=1

(b) CN=3

Figure 2.15: Examples of a ridge ending and bifurcation pixel. (a) A Crossing Number of one corresponds to a ridge ending pixel. (b) A Crossing Number of three corresponds to a bifurcation pixel.

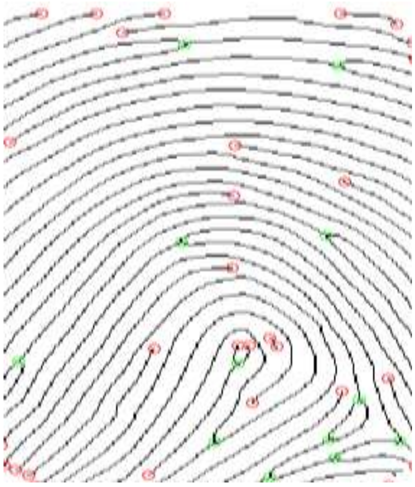

Figure 2.16: Ridge ending and ridge bifurcation on a skeleton image

2.5 Removal of false minutiae

False minutiae on the skeleton may appear due to factors such as noisy images, and image artefacts created by the thinning process. Hence, after the minutiae are extracted, it is necessary to employ a post processing stage in order to validate the minutiae. Figure 2.17 illustrates some examples of false minutiae structures, which include the spur, hole, triangle and spike [32]. It can be seen that the spur structure generates false ridge endings; whereas both the hole and triangle structures generate false bifurcations. The spike structure creates a false bifurcation and a false ridge ending point.

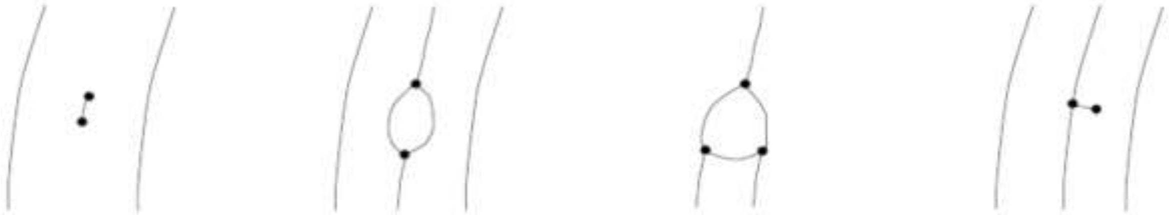

(a) Spur (b) Hole (c) Triangle (d) Spike

Figure 2.17: Examples of typical false minutiae structures.

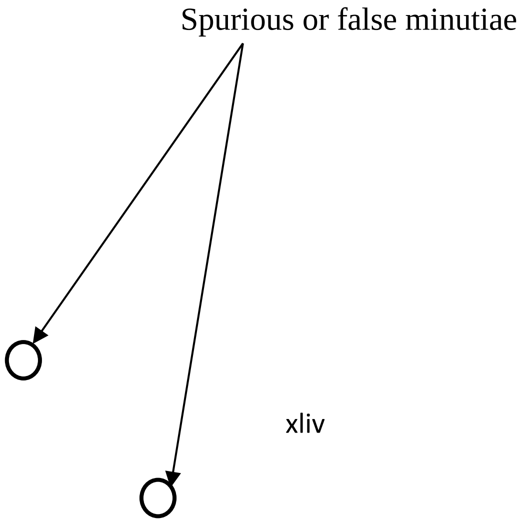

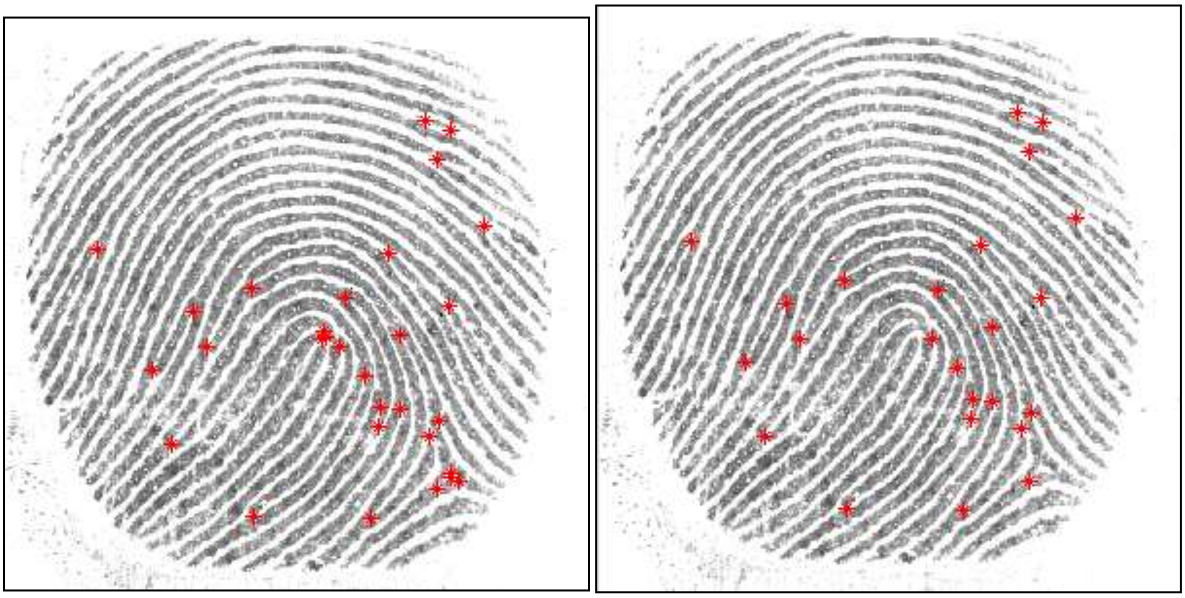

Figure 2. (b)

Figure 2.18 Removal of spurious minutiae. (a) Typical fingerprint with some false or spurious minutiae. (b) Real minutiae after the false or spurious minutiae have been removed.

Most of the proposed method to remove the false or spurious minutiae is based on a series of structural rules [21]. One such approach proposed by Ratha et al. [18], which performs the validation of minutiae based on a set of heuristic rules. For example, a ridge ending point that is connected to a bifurcation point should have a certain distance threshold, below which it is eliminated as an invalid minutia. This heuristic rule corresponds to removal of the spike structure shown in Figure 2.17(d). Additional heuristic rules are then used to eliminate other types of false minutiae. Furthermore, a boundary effect treatment is applied where the minutiae below a certain distance from the boundary of the foreground region are deleted.

A novel approach to the validation of minutiae is the post processing algorithm proposed by Tico and Kuosmanen [33]. Similar to the above techniques, this algorithm operates on the skeleton image. However, rather than employing a different set of heuristics each time to eliminate a specific type of false minutiae, this approach incorporates the validation of different types of minutiae into a single algorithm. It tests the validity of each minutiae point by scanning the skeleton image and examining the local neighbourhood around the minutiae. The algorithm is then able to cancel out false minutiae based on the configuration of the ridge pixels connected to the minutiae point. Rather than using a set of ad hoc techniques to validate the minutiae, the algorithm employed by Tico and Kuosmanen [33] has been used in the experiment. Figure 2.18 shows an example of a typical fingerprint with spurious minutiae before removal and the image with actual minutiae after these have been removed.

2.6 Fingerprint matching

A fingerprint matching algorithm takes two fingerprints as input and returns either a degree of similarity (percentage of match) between them or a binary decision (1 or 0 for matched or non-matched respectively). Instead of direct grayscale matching between two images based on their features, most of the algorithms compare intermediary stage of two fingerprints called template, which is formed through a feature extraction stage as discussed in the previous sections.

Due to the large variability in different impressions of the same finger (i.e., large *intra-class* variations), it is a very complex process to match two fingerprint images. The main factors responsible for intra-class variations are summarized below [16].

Displacement: the same finger may be placed at different locations on a touch sensor during different acquisitions resulting in a (global) translation of the fingerprint area. A finger displacement of just 2 mm (imperceptible to the user) results in a translation of about 40 pixels in a fingerprint image scanned at a resolution of 500 dpi.

Rotation: the same finger may be rotated at different angles with respect to the sensor surface during different acquisitions. In spite of the finger “guide” mounted in certain commercial scanners, involuntary finger rotations of up to ±20° with respect to vertical orientation can be observed in practice.

Partial overlap: finger displacement and rotation often cause part of the fingerprint area to fall outside the sensor’s “field of view,” resulting in a smaller overlap between the foreground areas of the template and the input fingerprints. This problem is particularly serious for small-area touch sensors.

Non-linear distortion: the act of sensing maps the three-dimensional shape of a finger onto the two-dimensional surface of the sensor. This mapping results in a non-linear distortion in successive acquisitions of the same finger due to skin plasticity. Often, fingerprint matching algorithms disregard the characteristic of such a mapping, and consider a fingerprint image as non-distorted by assuming that it was produced by a correct finger placement; a finger placement is correct when: (i) the trajectory of the finger approaching the sensor is orthogonal to the sensor surface; (ii) once the finger touches the sensor surface, the user does not apply traction or torsion. However, due to skin plasticity, the components of the force that are non-orthogonal to the sensor surface produce non-linear distortions (compression or stretching) in the acquired fingerprints. Distortion results in the inability to match fingerprints as rigid patterns.

Pressure and skin condition: the ridge structure of a finger would be accurately captured if ridges of the part of the finger being imaged were in uniform contact with the sensor surface. However, finger pressure, dryness of the skin, skin disease, sweat, dirt, grease, and humidity in the air all confound the situation, resulting in a non-uniform contact. As a consequence, the acquired fingerprint images are very noisy and the noise strongly varies in successive acquisitions of the same finger depending on the magnitude of the above cited causes.

Noise: it is mainly introduced by the fingerprint sensing system; for example, residues are left over on the glass platen from the previous fingerprint capture.

Feature extraction errors: the feature extraction algorithms are imperfect and often introduce measurement errors. Errors may be made during any of the feature extraction stages (e.g., estimation of orientation and frequency images, detection of the number, type, and position of the singularities, segmentation of the fingerprint area from the background, etc.). Aggressive enhancement algorithms may introduce inconsistent biases that perturb the location and orientation of the reported minutiae from their gray-scale counterparts. In low-quality fingerprint images, the minutiae extraction process may introduce a large number of spurious minutiae and may not be able to detect all the true minutiae.

Figure 2.19 shows how different physical and environmental conditions can result in false rejection irrespective of the algorithm used for feature extraction and matching. The pairs of images in each row in Figure 2.19 show the high variability (large *intra-class* variations) between two different impressions of the same finger. On the other hand, the images in each row in Figure 2.20 look very similar in terms of global structure (small *inter-class* variation) and have shown match by many algorithms submitted to FVC 2002 [16]**.** The reason for these false acceptances is certainly indicating the ineffectiveness of the algorithm used for feature extraction and matching.

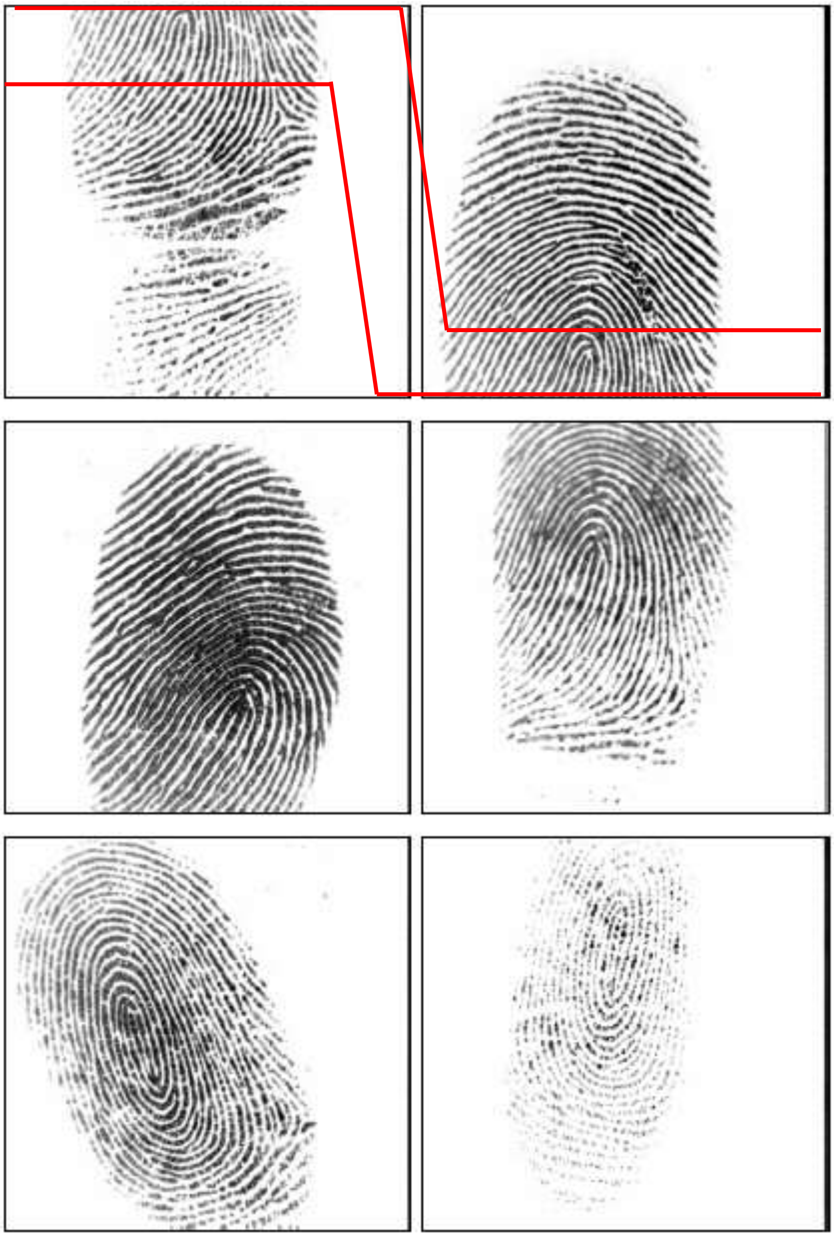

Very small common area between the two impressions which has resulted in false rejection.

The second image is highly distorted from the first one (caused by elastic distortion) and has resulted in false rejection.

The second image from the same finger is of a very poor quality, which is caused by skin condition and resulted in false rejection.

Figure 2.19: Falsely matched fingerprints. Each row shows a pair of impressions of the same finger. The main cause of difficulty is a very small overlap in the first row, high non-linear distortion in the second row, and very different skin conditions in the third row [16].

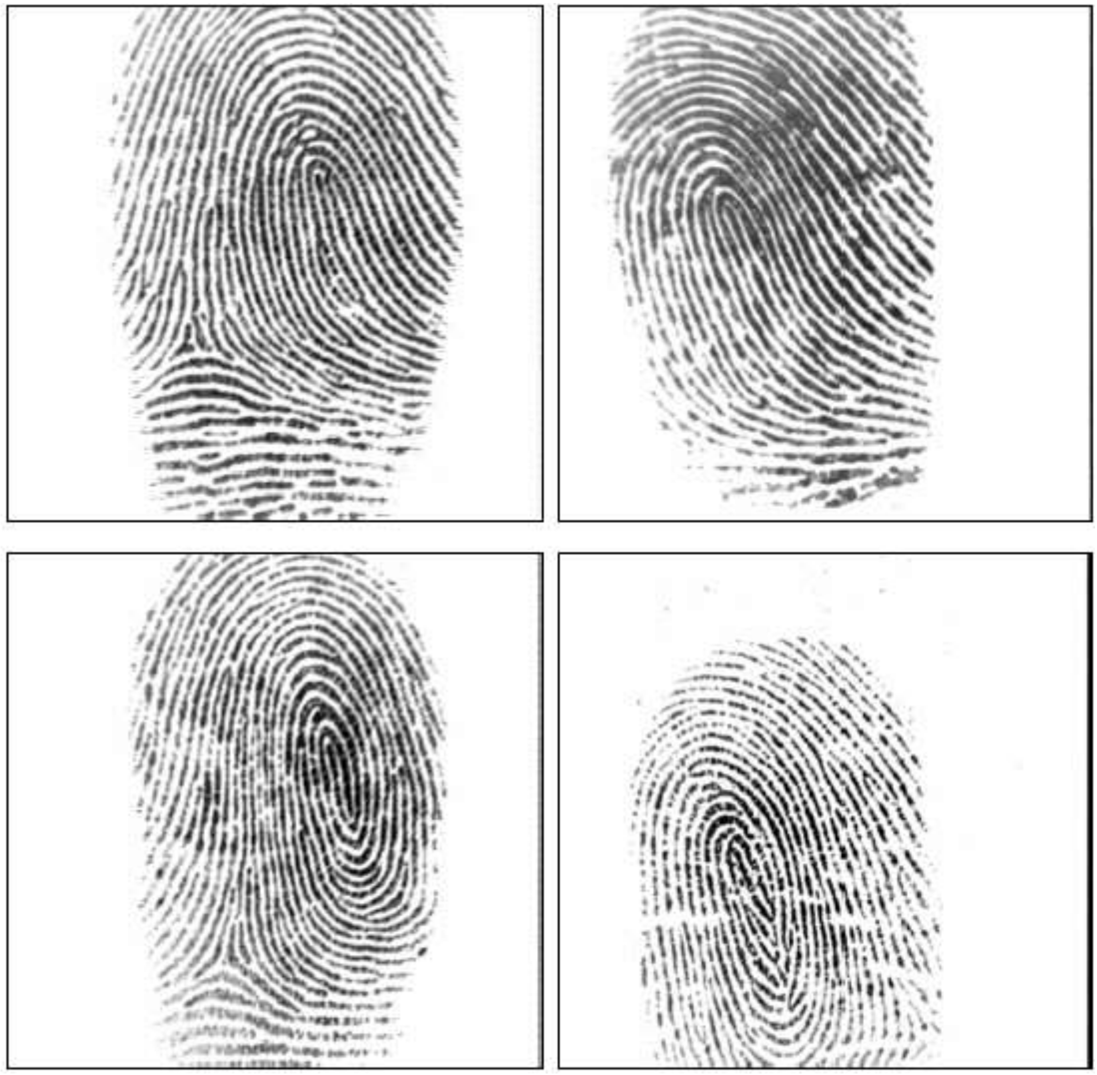

Figure 2.20: Falsely accepted fingerprints. Each pair of impressions in a row is from different fingers, which were falsely matched by some of the algorithms submitted to FVC2002 [16].

Although, many AFIS algorithm performs very well in matching good quality images, it still remains a challenge for any algorithm in matching low-quality and partial latent fingerprints. The quality of the fingerprint can be checked during the enrolment if it is a human-assisted AFIS but human intervention is not feasible in unattended on-line fingerprint recognition systems, which are being increasingly deployed in commercial applications. Moreover, many algorithms require a high level of image processing, which might not be feasible for much smaller stand alone system to accommodate.

The evidence from FVC2000 showed that most errors were made on about 20% poor quality fingerprints [16]. In recent years, the state-of-the-art of fingerprint recognition technology has been perceived throughout different editions of the Fingerprint Verification Competition. Although a direct comparison across different competitions is not possible due to the use of databases of unequal difficulty, the performance of the top algorithms on database DB2 of FVC2006 (which was collected under realistic operating conditions with a large area sensor) are extremely good [16]. However, there is still a need to continually develop more robust systems capable of properly processing and comparing poor quality fingerprint images; this is particularly important when dealing with large scale applications or when small area and relatively inexpensive low quality sensors are employed.

Jain et al have classified fingerprint matching into three families [16].

Correlation-based matching: two fingerprint images are superimposed and the correlation between the corresponding pixels is computed for different alignments (e.g., various displacements and rotations).

Minutiae-based matching: this is the most popular and widely used technique, being the basis of the fingerprint comparison made by fingerprint examiners. Minutiae are extracted from the two fingerprints and stored as sets of points in the two dimensional plane. Minutiae-based matching essentially consists of finding the alignment between the template and the input minutiae feature sets that result in the maximum number of minutiae pairings.

Non-Minutiae feature-based matching: minutiae extraction is difficult in extremely low-quality fingerprint images. While some other features of the fingerprint ridge pattern (e.g., local orientation and frequency, ridge shape, texture information) may be extracted more reliably than minutiae, their distinctiveness as well as persistence is generally lower. The approaches belonging to this family compare fingerprints in terms of features extracted from the ridge pattern. In principle, correlation-based matching could be conceived of as a subfamily of non-minutiae feature-based matching, inasmuch as the pixel intensities are themselves features of the finger pattern.

It has been found that minutiae-based methods perform better than correlation based methods [34]. In the development of the novel algorithm, minutiae-based method in template formation and matching was adopted.

2.7 Minutiae based fingerprint matching

2.7.1 Introduction

Fingerprint features can be analysed at both global and local level. When analyzed at the global level, the fingerprint pattern exhibits one or more regions where the ridge lines assume distinctive shapes (characterized by high curvature, frequent termination, etc.). These regions (called *singularities* or *singular regions*) may be classified into three typologies: *loop*, *delta*, and *whorl* (see Figure 2.2).

Singular regions belonging to loop, delta, and whorl types are typically characterized by ∩, Δ, and O shapes, respectively [35]. Several fingerprint matching algorithms pre align fingerprint images according to a landmark or a centre point, called the *core*. The core corresponds to the centre of the north most loop type singularity. For fingerprints that do not contain loop or whorl singularities i.e., those belonging to the arch class in Figure 2.2, it is difficult to define the core. In these cases, the core is usually associated with the point of maximum ridge line curvature. Unfortunately, due to the high variability of fingerprint patterns, it is difficult to reliably locate a registration (core) point in all the fingerprint images [35].

Minutiae-based matching is basically a point pattern matching problem that is generally intractable because it encounters the minutiae correspondence problem. It can be quite difficult to obtain the minutiae correspondence because the new image can be subject to transformation such as rotation, translation or even deformation. The location and direction errors of the detected minutiae as well as presence of spurious minutiae or absence of genuine minutiae can cause a lot of incongruity in the minutiae correspondence.

2.7.2 Problem formulation

Let **S** and **Q** represent the stored template and the query template respectively in an AFRS. If we consider **S** and **Q** as feature vectors then each minutia is an element of the feature vector. Each minutia can be described by a number of attributes such as its location on the image, orientation and the type. Most common minutiae matching algorithms consider each minutia as a triplet **m** = *{x,y,ϑ}* that indicates the *x,y* minutia location coordinates and the minutiae angle *ϑ* [16]:

$$\mathbf{S} = \{\boldsymbol{m_1}, \boldsymbol{m_{2,}} \dots\dots \boldsymbol{m_m}\}, \quad \boldsymbol{m_i} = \{x_i, y_i, \theta_i\}, \quad i = 1 \dots m \qquad (2.22)$$

$$\mathbf{Q} = \{\boldsymbol{m'_1}, \boldsymbol{m'_2} \dots\dots \boldsymbol{m'_n}\}, \quad \boldsymbol{m'_j} = \{x'_j, y'_j, \theta'_j\}, \quad j = 1 \dots n \qquad (2.23)$$

where *m* and *n* denote the number of minutiae in **S** and **Q** respectively.

A minutia m'_j in **Q** and a minutia m_i in **S** are said to be 'matching' if the *spatial distance (sd)* between between them is smaller than a given tolerance r_0 and the *direction difference (dd)* between them is smaller than an angular tolerance θ_0:

$$sd(\boldsymbol{m'_j}, \boldsymbol{m_i}) = \sqrt{(x'_j - x_i)^2 + (y'_j - y_i)^2} \le r_0, and \qquad (2.24)$$

$$dd(\boldsymbol{m'_j}, \boldsymbol{m_i}) = \boldsymbol{min}(|\theta'_j - \theta_i|, 360^0 - |\theta'_j - \theta_i|) \le \theta_0 \ (2.25)$$

Equation (2.25) takes the minimum of $|\theta'_j - \theta_i|$ and $360^0 - |\theta'_j - \theta_i|$ because of the circulatory nature of the angles. The tolerance boxes (or hyper-spheres) defined by r_0 and θ_0 are required to accommodate the unavoidable errors made by feature extraction algorithms and to count for the small displacement that cause the minutiae position to change.

In many algorithms, alignment of the stored and query templates is mandatory to maximise the number of matching minutiae in terms of their corresponding position and orientation. When two fingerprints are correctly aligned, the displacement (*in x and y*) and rotation (*ϑ*) are recovered and it likely to compensate other geometrical transformations:

- If two fingerprint images have been taken by scanners operating at different resolutions then *scaling* needs to be done.
- Other *distortion-tolerant* geometrical transformations could be useful to match minutiae in case one or both of the fingerprints is affected by severe distortions.

In designing a matching algorithm, the tolerance box should be carefully calculated as adjustment for any other geometrical transformations beyond translation and rotation may results in additional degrees of freedom to the minutiae matcher thus lead to a huge number of new possible alignments which significantly increases the chance of incorrectly matching two fingerprints from different fingers.

If *map*( ) is a function that maps a minutia $\boldsymbol{m}_{\boldsymbol{j}}'$ (from **Q**) into $\boldsymbol{m}_{\boldsymbol{j}}''$ according to a given geometrical transformation; for example, by considering a displacement of [Δ*x*, Δ*y*] and a anticlockwise rotation ϑ around the origin:

$$map_{\Delta x,\Delta y,\theta}\left(\boldsymbol{m}_{\boldsymbol{j}}' = \{x_j', y_j', \theta_j'\},\ \boldsymbol{m}_{\boldsymbol{j}}'' = \{x_j'', y_j'', \theta_j' + \theta\}\right), \quad (2.26)$$

where $\begin{bmatrix} x_j'' \\ y_j'' \end{bmatrix} = \begin{bmatrix} cos\theta - sin\theta \\ sin\theta - cos\theta \end{bmatrix} \begin{bmatrix} x_j' \\ y_j' \end{bmatrix} + \begin{bmatrix} \Delta x \\ \Delta y \end{bmatrix}$ (2.27)

Let *mm( )* is an indicator function that returns 1 in the case where the minutiae $\boldsymbol{m}_{\boldsymbol{j}}''$ and $\boldsymbol{m}_{\boldsymbol{i}}$ match according to equations (2.24) and (2.25)**:**

$$mm\left(\boldsymbol{m}_{\boldsymbol{j}}'', \boldsymbol{m}_{\boldsymbol{i}}\right) = \begin{cases} 1\ sd\left(m_j'', m_i\right) \le r_0\ and\ dd\left(m_j'', m_i\right) \le \theta_0 \\ \qquad 0\ otherwise. \end{cases} \quad (2.28)$$

Then, the matching problem can be formulated as

$$\underset{\Delta x,\Delta y,\theta,P}{maximise} \sum_{i=1}^{m} mm\left(map_{\Delta x,\Delta y,\theta}\left(\boldsymbol{m}_{\boldsymbol{P}(\boldsymbol{i})}'\right), \boldsymbol{m}_{\boldsymbol{i}}\right), \quad (2.29)$$

where *P*(*i*) is an unknown function that determines the *pairing* between Q and S minutiae; in particular, each minutia has either exactly one mate in the other fingerprint or has no mate at all. The constraints are

1. *P(i)=j* indicates that the mate of the $\boldsymbol{m}_{\boldsymbol{i}}$ in **S** is the minutia $\boldsymbol{m}_{\boldsymbol{j}}'$ in **Q.**
2. *P(i)=*null indicates that minutia $\boldsymbol{m}_{\boldsymbol{i}}$ in **S** has no mate in **Q.**
3. A minutia $\boldsymbol{m}_{\boldsymbol{j}}'$ in **Q** has mo mate in **S** if *P(i)≠j* ∀*i*=1.....m.
4. *∀ i=1.....m, k=1.....m, i ≠ k ⇒ P*(*i*) ≠ *P*(*k*) or *P*(*i*) = *P*(*k*) = null (this means that each minutia in Q is associated with a maximum of one minutia in S, that is P is a bijective function).

Note that, in general, *P*(*i*) = *j* does not necessarily mean that minutiae $\boldsymbol{m}_{\boldsymbol{j}}'$ and $\boldsymbol{m}_{\boldsymbol{i}}$ match in the sense of Equations (2.24) and (2.25) but only that they are the most likely pair under the current transformation.

Expression (2.29) requires that the number of minutiae mates be maximized, independently of how strict these mates are; in other words, if two minutiae comply with Equations (2.24) and (2.25), then their contribution to expression (2.29) is made independently of their spatial distance and of their direction difference. Alternatives to expression (2.29) may be introduced where the residual (i.e., the spatial distance and the direction difference between minutiae) for the optimal alignment is also taken into account.

Solving the minutiae matching problem (expression (2.29) is trivial when the correct alignment (Δ*x*, Δ*y*, θ) is known; in fact, the pairing (i.e., the function *P*) can be determined by setting for each *i* = 1...*m*:

- $P(i) = j$ if $\boldsymbol{m}_{\boldsymbol{j}}'' = \ map_{\Delta x,\Delta y,\theta}\left(\boldsymbol{m}_{\boldsymbol{j}}'\right)$ is closest to $\boldsymbol{m}_{\boldsymbol{i}}$ among the minutiae

$\left\{\boldsymbol{m}_{\boldsymbol{k}}'' = \ map_{\Delta x,\Delta y,\theta}(\boldsymbol{m}_{\boldsymbol{k}}') \mid k = 1 \ldots n, \ \ mm(\boldsymbol{m}_{\boldsymbol{k}}'', \boldsymbol{m}_{\boldsymbol{i}}) = 1\right\}$.

- $P(i) = null$ if ∀ *k=1.....n, mm(*$map_{\Delta x,\Delta y,\theta}(\boldsymbol{m}_{\boldsymbol{k}}'), \boldsymbol{m}_{\boldsymbol{i}}$*)* **=** 0.

To comply with constraint (4) above, each minutia $\boldsymbol{m}_{\boldsymbol{j}}''$ already mated has to be marked, to avoid mating it twice or more. Figure 2.21 shows an example of minutiae pairing given a fingerprint alignment.

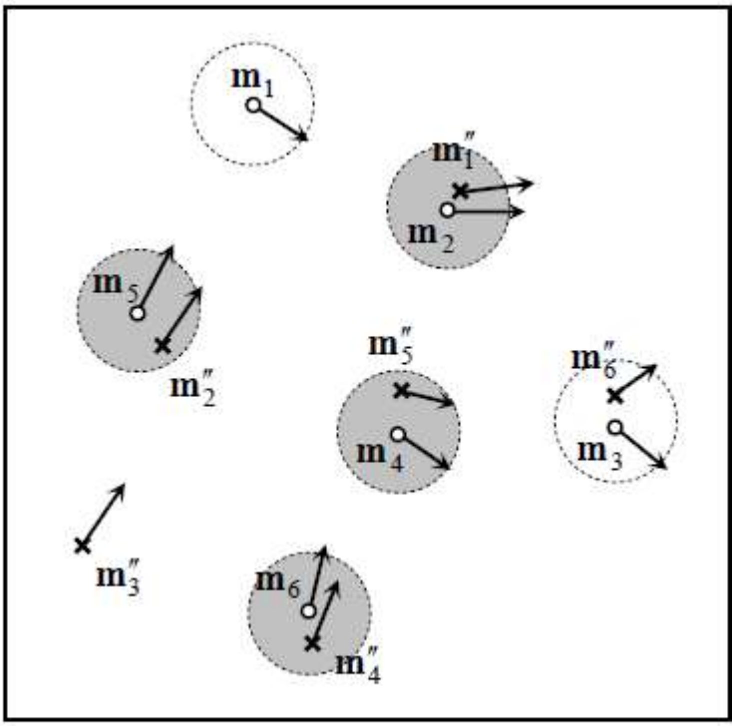

Figure 2.21: Minutiae of Q mapped into S coordinates for a given alignment. Minutiae of S are denoted by o$_s$, whereas minutiae of Q are denoted by x$_s$. Note that Q minutiae are referred to as m'', because what is shown in the figure is their mapping into coordinates of S. Pairing is performed according to the minimum distance. The dashed circles indicate the maximum spatial distance. The gray circles denote successfully mated minutiae; minutiae m_1 of S and minutiae m_3'' of Q have no mates. Minutiae m_3 and m_6'' cannot be mated due to their large orientation difference [36].

To achieve the maximum pairing, a slightly more complicated scheme should be adopted: in fact, in case when a minutia of **Q** falls within the tolerance box of more than one minutia of **S**, the optimum assignment is that which maximises the number of mates (see Figure 2.22). Hungarian assignment algorithm (Ahuja, Mananti and Orlin 1993 [37]) with polynomial time complexity has been used for this purpose (See Jea and Govindraj 2005 [38]; Wang et al 2006b [39]).

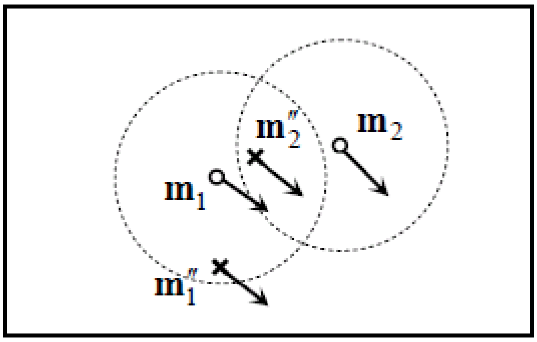

Figure 2.22: In this example, if m_1 was mated with m_2'' (the closest minutiae), m_2 would remain unmated; however, pairing m_1 with m_1'' , allows m_2 to be mated with m_2'', thus maximising equation (2.29) [36].

The maximisation in (2.29) can be easily solved if the function P (minutiae correspondence) is known; in this case, the unknown alignment (Δx, Δy, ϑ) can be determined in the least square sense (Umeyama 1991[40]; Chang et al. 1997 [41]). Unfortunately, in practice, neither the alignment parameters nor the correspondence function P are known in advance and, therefore, solving the matching problem is hard. A brute force approach that is, evaluating all the possible solutions (correspondences and alignments) is prohibitive as the number of possible solutions is exponential in the number of minutiae (the function *P* is more than a permutation due to the possible null values). A few brute force approaches have also been proposed in the literature; for example, Huvanandana, Kim, and Hwang (2000) [42] proposed coarsely quantizing the minutiae locations and performing an exhaustive search to find the optimum alignment. He et al. (2003b) [43] suggested a coarse-to-fine search of the discretized parameter space to determine the alignment, and used Hausdorff distance to evaluate minutiae correspondences.

2.7.3 Similarity score

Unlike in manual matching performed by forensic experts where the number of matching minutiae is itself the main output of the comparison, automatic matching systems must convert this number into a similarity score. This is often performed by simply normalizing the number of matching minutiae (here denoted by *k*) by the average number (*m* + *n*)/2 of minutiae set in **S** and **Q** [36]:

$$score = \frac{2k}{m+n} \quad (2.30)$$

However, further information can be exploited, especially in case of noisy images and limited overlap between **S** and **Q**, to compute a more reliable score; in fact:

- Minutiae quality can be used to weight differently reliable and unreliable minutiae pairs: the contribution from a pair of reliable minutiae should be higher than that from a pair where at least one the two minutiae are of low quality (Chen, Chan, and Moon, 2007 [44]). The quality of a minutia (and of a minutia pair) can be defined according to the fingerprint quality in the region where the minutia lies and/or by keeping into account other local information.

- The normalization in Equation (2.30) tends to excessively penalize fingerprint pairs with partial overlap; a more effective normalization considers the number or minutiae belonging to the intersection of the two fingerprints after the optimal alignment have been determined [38].

In general, the definition of optimal rules for combining various similarity contributions into a single score can be complex; some researchers (Jea and Govindaraju (2005) [38]; Srinivasan et al. (2006) [45]; Jia et al. (2007b) [46]; Feng (2008) [47]; Lumini and Nanni (2008) [48]) propose to apply learning- based techniques where the rule and its parameters are optimized to best separate genuine from impostor scores. Supervised classification is central also in the method proposed by Mansukhani, Tulyakov, and Govindaraju (2007) [49] and by Mansukhani and Govindaraju (2008) [50] where a Support Vector Machine (SVM) is trained to distinguish between genuine and false minutiae pairs. Finally, methods based on the computation of the likelihood ratio to assess the evidential value of comparisons with an arbitrary number of minutiae are quite popular in forensic identification (see Neumann et al. (2006) [51]; Bazen and Veldhuis (2004) [52]).

2.7.4 Point pattern matching

The point pattern matching techniques are well established and can be approached from any of the established classes such as *Algebraic Geometry*, *Hough Transform*, *Relaxation*, *Operations Research Solutions*, *Energy-Minimization* and so on [16].

Algebraic Geometry**:** Several methods have been proposed in the literature for different versions of the problem. Bishnu et al. (2006) [53] proposed an algorithm to perform an inexact partial point pattern matching with O(m^2 × n^2 × *log m*) time complexity. However, this algorithm makes some simplifying assumptions that are not always fulfilled by minutiae points; in fact, the algorithm requires that: (i) all the points in query template **Q** have a mate in stored template **S**, even if some points in **S** can have no mate in **Q**, and (ii) the tolerance boxes around the points do not intersect each other or, equivalently, that the points in **S** are not too close to each other. Since, general purpose algebraic geometry methods do not fit the peculiarity of minutiae matching; some ad-hoc algorithms have been designed for fingerprints such as the algorithm proposed by Udupa, Garg, and Sharma (2001) [54].

Hough Transform: The generalized Hough transform-based approach (Ballard (1981) [55]; Stockman, Kopstein, and Benett (1982) [56]) converts point pattern matching to the problem of detecting peaks in the Hough space of transformation parameters. It discretizes the parameter space and accumulates evidence in the discretized space by deriving transformation parameters that relate two sets of points using a substructure of the feature matching technique. A hierarchical Hough transform-based algorithm may be used to reduce the size of the accumulator array by using a multi-resolution approach. Hough transform-based approaches, also known as “voting-based approaches” are quite popular for minutiae matching. One such method has been proposed by Ratha et al.(1996) [57].

Relaxation: The relaxation approach (e.g., Rosenfeld and Kak (1976) [58]; Ranade and Rosenfeld (1993) [59]) iteratively adjusts the confidence level of each corresponding pair of points based on its consistency with other pairs until a certain criterion is satisfied. At each iteration *r*, the method computes *m* × *n* probabilities p_{ij} (probability that point *i* corresponds to point *j*):

$$p_{ij}^{(r+1)} = \frac{1}{m}\sum_{h-1,k=1\ldots.n}^{m}\left[\max\{c(i,j;h,k).p_{ij}^{(r)}\}\right],\ i = 1\ldots..m,\ \ j = 1\ldots.n, \qquad (2.31)$$

where *c(i,j;h,k)* is a compatibility measure between the pairing *(i,j)* and *(h,k),* which can be defined according to the consistency of the alignments necessary to map point *j* into *i* and point *k* into *h*. Equation (2.22) increases the probability of those pairs that receive substantial support by other pairs, and decreases the probability of the remaining ones. At convergence, each point *i* may be associated with the point *j* such that $p_{ij} = max_s\{p_{is}\}$, where *s* is any other point in the set. Although a number of modified versions of this algorithm have been proposed to reduce the matching complexity (Ton and Jain, 1989) [60], these methods are inherently slow due to their iterative nature.

Operations Research solutions: Tree-pruning approaches attempt to find the correspondence between the two point sets by searching over a tree of possible matches while employing different tree-pruning methods (e.g., branch and bound) to reduce the search space (Baird, 1984) [61]. To prune the tree of possible matches efficiently, this approach tends to impose a number of requirements on the input point sets, such as an equal number of points (n = m) and no outliers (points without correspondence). These requirements are difficult to satisfy in practice, especially in fingerprint minutiae matching. Solutions to point pattern matching may also be derived from some problems which are known in the field of Operations Research as assignment problems, bipartite graph matching (Murty (1992) [62]; Gold and Rangarajan (1996) [63]). A minutiae matching algorithm based on minimum spanning tree matching was proposed by Oh and Ryu (2004) [64].

Energy Minimization: these methods define a function that associates an energy or fitness with each solution of the problem. Optimal solutions are then derived by minimizing the energy function (or maximizing fitness) by using a stochastic algorithm such as the Genetic algorithm (Ansari, Chen, and Hou (1992) [65]; Zhang, Xu, and Chang (2003) [66]) or simulated annealing (Starink and Backer, 1995) [67]. Le, Cheung, and Nguyen (2001) [68] and Tan and Bhanu (2006) [69] provided specific

Genetic algorithm implementations for global minutiae matching. It has been shown that pure Genetic Algorithms are not well suited to fine-tuning the search in complex search spaces, and that hybridization with other local-searches techniques (called Memetic algorithms) can improve their efficiency. A Memetic algorithm for minutiae matching has been recently proposed by Sheng et al. (2007) [70]. In general, the methods belonging to this category tend to be slow and are unsuitable for real-time minutiae matching.

2.8 Minutiae based template formation

There has been proposed several minutiae-based fingerprints matching techniques can be found in the literature. These include methods based on structure matching (Chen and Kuo, 1991 [71]; Hrechak and McHugh, 1990 [72]; Jiang and Yau, 2000 [73]; Wahab et al., 1998 [74]), alignment matching (Jain et al., 1997 [75]; Ratha et al., 1996 [57]; Ross et al., 2003 [23]), non-linear transformation (Almansa and Cohen, 2000 [76]; Bazen and Gerea, 2002 [77]). The principle of all this methods is to obtain the minutiae correspondence accurately. The method proposed by Jain et al., 1997 [75]; Ratha et al., 1996 [57]; Ross et al., 2003 [23] make use of ridges associated with each minutiae to get the correspondence. However, this method may result in inaccurate matching as local ridge information cannot be considered discriminatory feature because the ridges from different fingers or different positions in the same fingerprint may be very similar. The local structure composed of several minutiae close to each other is the basis of the minutiae correspondence in Chen and Kuo, 1991 [71]; Hrechak and McHugh, 1990 [72]; Jiang and Yau, 2000 [73]; Wahab et al., 1998 [74]; Almansa and cohen, 2000 [76]; Bazen and Gerea, 2002 [77]. It is found that the representation of local structure based on a group of minutiae is not very reliable because it relies on the interdependencies between minutiae details, which can be missed or erroneously detected by a minutiae extraction algorithm [34]. Moreover, it is difficult to detect the similarity of local structure because the correspondence between the elements of the local structure cannot be always known.

Dabbah, Woo and Dlay, 2005 [10] have suggested a computationally efficient algorithm in which they formed the template by considering each minutiae as a vector of three elements as distance of each minutia point from the core/SP, orientation with respect to SP and type of minutia point (either Termination or Bifurcation). Each stored template denoted by ***'T'*** is made of a set of minutiae points ***'M'*** such that

$$T = \{m_{1,} m_{2,} m_{3,} \dots \dots m_{M,}\}, \qquad (2.32)$$

$$m_i = \{sd_{i,} od_{i,} type_i\}, i = 1..M \qquad (2.33)$$

And each query template denoted by ***'I'*** can be made of ***'N'*** minutiae points such that

$$I = \{m'_{1,} m'_2, m'_3 \dots \dots m'_N\}, \qquad (2.34)$$

$$m'_j = \{sd_{j,} od_{j,} type_j\}, j = 1..N \qquad (2.35)$$

Where m_i and m_j are minutiae points in '***T***' and '***I***' respectively. For two minutiae to be matched, both minutiae vectors have to be within the same tolerance box (hyper-spheres) defined by r_0 and $\theta_{0,}$which means that

$$De_i - De_j \leq r_0 \quad (2.36)$$

and $\theta e_i - \theta e_j \leq \theta_0$ (2.37)

Where $De_i,\ De_j\ and\ \theta e_i\ ,\ \theta e_i$ are the Euclidean distances and the orientation differences of the minutiae m_i and m_j from the SP respectively.

One of the important aspects in Dabbah et al.'s [10] matching algorithm is the introduction of the type matching of minutiae points from both stored and query templates. By using the type matching as the third element of each vector, they have increased their matching performance, which has resulted in significant improvement in Equal Error Rate (EER) to 4.9% [10].

Although M A Dabbah et al. [10] has shown a better performance compared to some other benchmark algorithm, their algorithm is heavily relying on the accurate detection of the core point or SP. As discussed previously, it is sometimes difficult to detect the SP or core point accurately or even they might be absent on some fingerprint.

Qi, Yang and Wang, 2005 [34] have proposed a matching algorithm where they have embedded global orientation field with each minutiae. They have defined the feature vector *F* of each minutiae *M* that describes its structure characteristics with global fingerprint orientation field as

$$F = \left\{ \left\{ \Psi_m^k \right\}_{i=1}^{N_m} \right\}_{m=1}^{3} \quad (2.38)$$

Where Ψ_m^k is the relative direction between minutiae *M* and the sampling point P_m^k.

They have defined the similarity level $S(i,j)$ between two structure feature vectors $F_i\ and\ F_j$, feature vector from query fingerprint and stored template respectively, as

$$S(i,j) = \begin{cases} \frac{T-|F_i-F_j|}{T}\ if\ |F_i - F_j| < T \\ 0\ otherwise \end{cases} \quad (2.39)$$

Where T is the defined threshold and $|F_i - F_j|$ is the Euclidean distance between these two feature vectors. As the dimensions of the two feature vectors may be different, the Euclidean distance is only computed only using the corresponding components between them. Therefore, if there is no corresponding counterpart of some feature vector, the element will be discarded. As the similarity level $S(i,j),\ (0 \leq S(i,j) \leq 1)$, describes a matching certainty level between two feature vectors instead of simply match or not match, the matching score is highly depending on the threshold level *T.* A not carefully chosen threshold level *T* may result in a higher FRR or FAR.

Another recent template formation technique is proposed by Chengfeng Wang and Marina L. Gavrilova [78], in which they have used Delauney Triangulation structure using minutiae to form Fingerprint Template. The key characteristics of the Delaunay triangulation of a set of points are that it is unique. Also, it can be computed efficiently in *O*(*NlogN*) time [78]. But the real problem with this technique is that it is very vulnerable to distortion and noise. One misplaced minutiae or a new spurious minutia can change all the neighbouring triangles instead of just one triangle. In real life scenario where it is likely to always have some noise and distortion on the scanned image, the efficiency of any algorithm based on Delauney Triangulation will be subject to the ability of the image processing technique to eliminate any false/ spurious minutia and to detect real minutiae.

2.9 Summary

Image enhancement is considered as a pre processing step before feature extraction implemented in most AFIS. A considerable amount of literature has been reviewed in image processing techniques and template formation using level2 features. Minutia based matching technique has also been adapted due to its higher success rate. In the development of the novel algorithm and during the evaluation, all images in the database had been enhanced before passed on to the feature extraction stage. The block sizes have been carefully chosen (16×16 pixels) in identifying ridge like regions and orientation estimation. The technique proposed by Hong et al, [11] which is based on the convolution of the image with Gabor filters tuned to the local ridge orientation has been adopted to enhance images prior to feature extraction stage. The removal of false minutiae was also an important step as it has rendered only the valid termination and bifurcation to the template formation process. Some processed images from the database during the image enhancement and feature extraction process have been presented in previous sections.

Novel Structure for Template Formation and Matching

3.1 Introduction

In general, feature vector of i_{th} detected minutiae from a fingerprint can be described as:

$F_i = (x_i\ y_i\ \omega_i)$, where $(x_i\ y_i)$ is its Cartesian coordinate and ω_i is the local ridge direction (known as orientation).

where $i = \{1,2,3 \dots M\}$ and M is number of minutia points in the fingerprint. Due to translation and rotation, the coordinates and orientation changes and therefore, alignment between the stored template and the query template needs to be performed for calculating the matching score. Instead of using the coordinates and the orientation of the minutia, we use the first N nearest neighbours to form a feature vector; in particular, i_{th} minutiae and its feature vector is defined as:

$$F_i = (D_i, A_i, T_i) \qquad (3.1)$$

where

$$D_i = [d_{i,1} \quad d_{i,2} \quad \cdots\cdots \quad d_{i,(N-1)} \quad d_{i,N}] \qquad (3.2)$$

$$A_i = [a_{i,[1,2]} \quad a_{i,[2,3]} \quad \cdots\cdots \quad a_{i,[(N-1),N]} \quad a_{i,[N,1]}] \qquad (3.3)$$

and $T_i \in \{\, minutia\ type =$
$1\ (ridge\ ending), 2(bifurcation), 3(trifurcation\ or\ crossover), 4\ (other)\}$
(3.4)

$d_{i,N}$ is the Euclidean distance between the i_{th} minutia and its N_{th} nearest neighbour, and $a_{i,[(N-1),N}$ is the angle between lines connecting i_{th} minutia and it's $(N-1)_{th}$ and N_{th} nearest neighbour. This feature vector is illustrated in Figure 3.1.

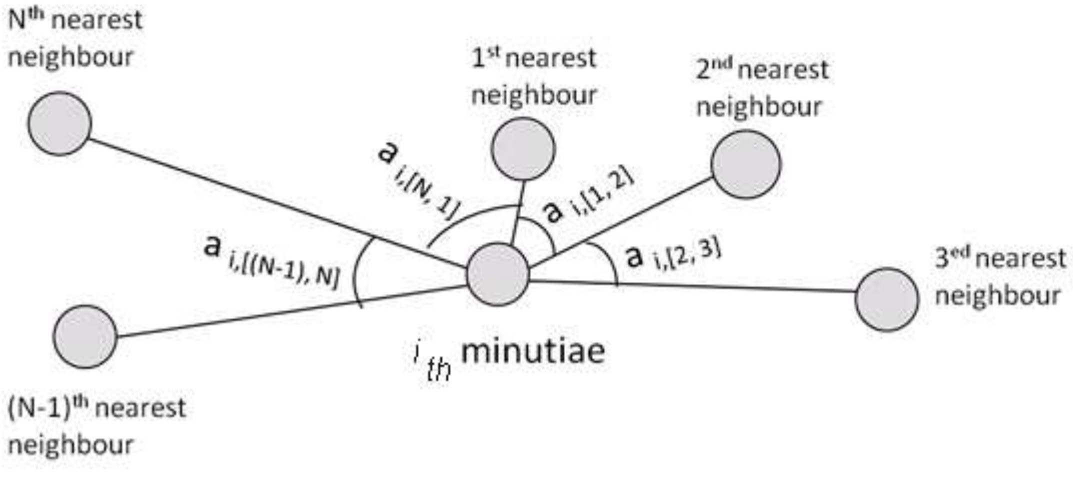

Figure 3.1: Schematic of feature formation of i_{th} minutiae.

Each stored template denoted by $'S'$ is made of a set of minutiae $'M'$ such that

$S = \{F_{1,}F_{2,}F_{3,} \dots \dots F_{M,}\}$ (3.5)

and each query template denoted by $'Q'$ can be made of a set of minutiae such that
Q=$\{F_{1,}F_{2,}F_{3,} \dots \dots F_{N,}\}$, (3.6)
For two minutiae to be matched, both minutiae vectors have to be within the tolerance defined by $type\ T_i$, $distance\ tolerance\ r_0$ and $angle\ tolarence\ \theta_{0,}$which means that

$T_{i=}T_j$ (3.7)

$[\, d_{1(i),}$ - $d_{1(j)}]$ AND $[d_{2(i),}$ - $d_{2(j)}] \dots \dots [\, d_{N(i),}$ - $d_{N(j)}] \leq r_0$ (3.8)
and $[\alpha_{1(i),} - \alpha_{1(j)}]$AND $[\alpha_{1(i),} - \alpha_{1(j)}] \leq \theta_0$ (3.9)

The number of nearest neighbours to construct the feature vector is limited by the total number of minutiae on a fingerprint. Jea and Govindaraju [38] have suggested a five element vector for a minutiae M_i (x_i, y_i, θ) using two of its nearest neighbours N_0 (x_{n0}, y_{n0}, θ_{n0}) and N_1 (x_{n1}, y_{n1}, θ_{n1}) as shown in Figure 3.2. The secondary feature vector S_i (r_{i0}, r_{i1}, φ_{i0}, φ_{i1}, δ_i) in which r_{i0} and r_{i1} are the Euclidean distances between the central minutia M_i and its neighbours N_0 and N_1 respectively. φ_{ik} is the orientation difference between M_i and N_k, where k is 0 or 1. δ_i represents the acute angle between the line segments M_iN_0 and M_iN_1.

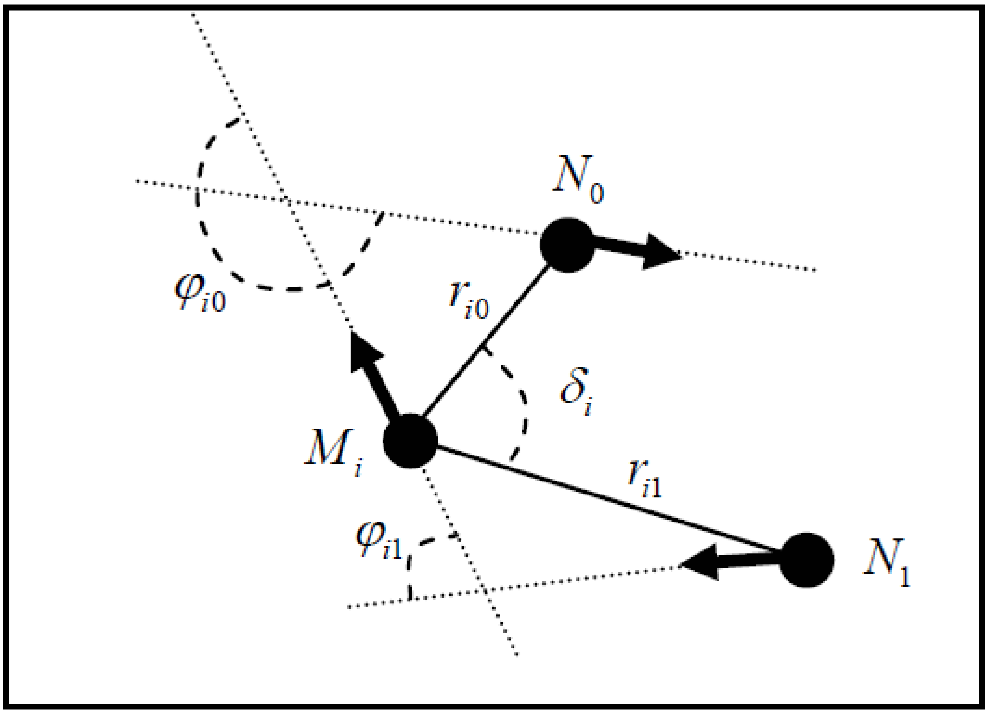

Figure 3.2: Feature vector construction suggested by Jea and Govindaraju [38]. Secondary feature of a minutiae M_i. r_{i0} and r_{i1} are the Euclidean distances between central minutia M_i and its neighbours N_0 and N_1 respectively.

3.2 Tolerance areas

Distortions are inevitable when a 3-dimensional fingertip is mapped onto a 2-dimensional plane. The main causes are vertical pressure, shear forces and varying impression conditions. In Figure 3.2, as the values of r_{i0} and r_{i1} increase, the secondary feature, S_i (r_{i0}, r_{i1}, φ_{i0}, φ_{i1}, δ_i), has larger distortions of φ_{i0}, φ_{i1} and δ_i. Kovács-Vajna [79] has demonstrated that small local deformations can result in a large global distortion. Thus, they have made the assumption that the distortions of distance are less when the values of r_{i0} and r_{i1} are small. However, the distortions of the angle and orientation tend to be larger when r_{i0} and r_{i1} are small.

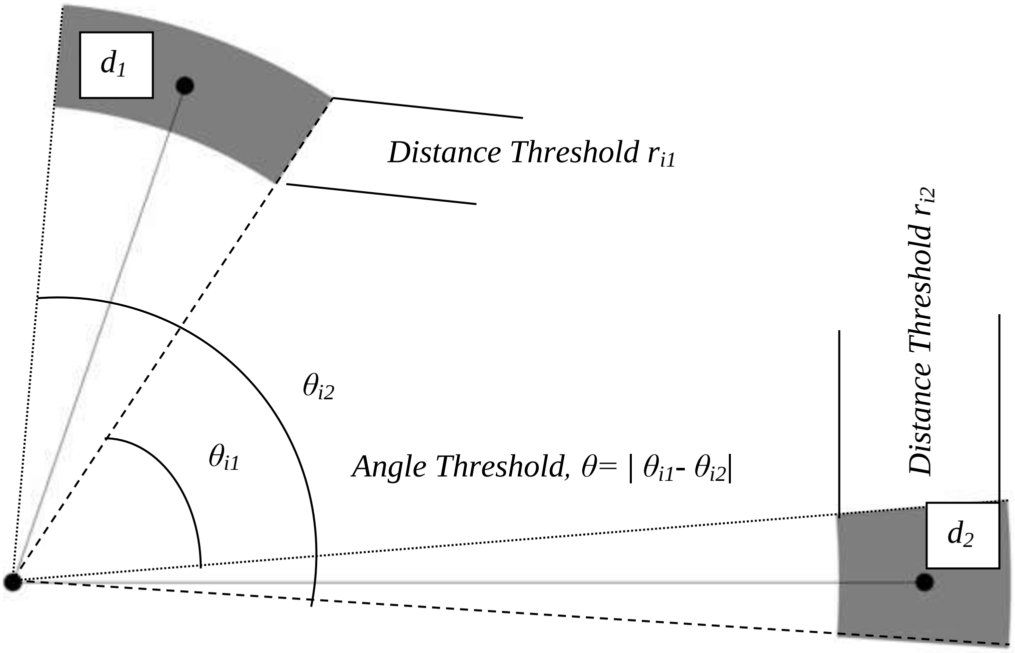

d_1
Distance Threshold r_{i1}
Distance Threshold r_{i2}
θ_{i2}
θ_{i1}
Angle Threshold, $\theta = | \theta_{i1} - \theta_{i2}|$
d_2

Figure 3.3: Dynamic tolerance areas around a minutia for the novel architecture. The gray areas around the two nearest neighbours set the threshold.

Due to these factors, it is reasonable to adjust the tolerance areas according to the values of r_{i0} and r_{i1}. In the novel structure as shown in Figure 3.3 where two nearest neighbour distances and their internal angle have been used, the angle tolerance ϑ_0 is a factor of distance tolerance r_0. The distance thresholds (r_{i1} *and* r_{i2}) should be more restrictive (smaller) when d_1 and d_2 are smaller and more flexible when d_1 and d_2 are larger. On the other hand, the thresholds on angles should be larger in order to allow large distortions when d_1 and d_2 are small, but smaller when d_1 and d_2 are large.

As the novel architecture is constructed by using the two nearest neighbours, their internal angle and the type of minutia, the actual feature for a single minutia is a four element vector such as F_i *(*d_1*,*

d_2, ϑ, τ). Tolerance area is determined by three functions as *Distance Threshold (r_0), Angle Threshold (ϑ_0) and Type (τ)*. In case of match, both the first and second nearest neighbours of corresponding minutiae should fall inside the tolerance box unless there is not much distortion. But if one of the nearest neighbours is missing or if there is any spurious minutia that comes inside the gray box, the algorithm will less likely to consider the corresponding minutiae as a match. Therefore, any loss of actual minutia or appearance of spurious minutia will have an impact on the net matching score between ***Q*** and ***S***.

3.3 Matching score

The matching score can be found by calculating the similarity between two feature vectors in terms of their corresponding nearest neighbour distances and their internal angles. As formulated in equation (3.2, 3.3 and 3.4), the match count is increased by one if all the corresponding distances and their internal angles match on a particular minutia. In real life scenario, it is highly unlikely that for each corresponding minutiae, all the distances and their internal angles will fall inside the tolerance. The percentage matching (*PM*) between two templates ***S*** and ***Q*** can be calculated by the total number of match on their corresponding feature vectors, which is defined as

$$PM = \frac{number\ of\ minutia\ matched}{number\ of\ minutia\ in\ the\ stored\ template} \times 100 \qquad (3.10)$$

The final decision between match or no match between the query template ***Q*** and the stored template ***S*** is determined by *PM* and the threshold, *TH*. As discussed in chapter 1, the threshold *TH* can be set according to the sensitivity of the application. In highly secure applications such as financial transaction, a very low value of FAR is required whereas less secure application such as entry log in a theme park may not require a very low value of FAR. The balance between FAR and FRR can be optimised by statistical observation as these two parameters are inversely proportional to each other. In general, a matching algorithm is evaluated by Error Equal Rate (EER), where FAR and FRR are equal (point of intersection when FRR and FAR are plotted against *PM*).

As can be seen from Figure 3.4, the matching process of the four elements feature vectors starts with reading the templates as (Mx4) and (Nx4) vectors; one from the query template Q and another from the stored template S. The algorithm first compares the size of these two templates and takes size of the smaller template as the outer control for the iteration where each vector of the smaller template is compared with each vector of the bigger template element by element. If the fourth elements (type of minutia) of the corresponding vectors match then only the three remaining elements are checked. To be a full match, the remaining three elements must be within the tolerance. As soon as there is a full match between two vectors, the program control exits the inner loop and takes the next vector from the smaller template and start checking with the vectors in the bigger template. When there is a match found, the vector is marked so it cannot be checked again. The program continues until all the vectors in the smaller template are checked with the vectors in the bigger template.

3.4 Matching of the feature vectors

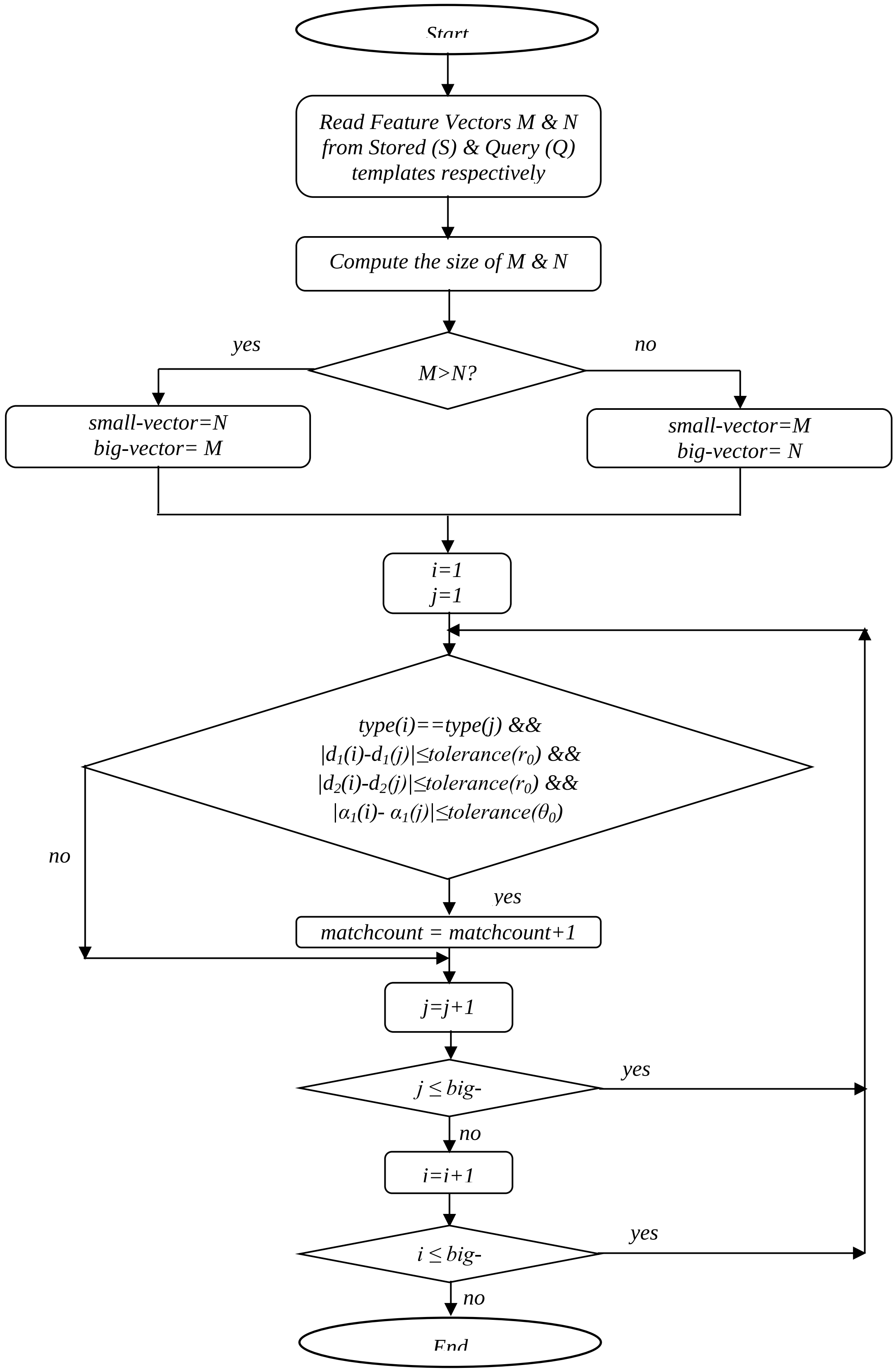
Start
Read Feature Vectors M & N from Stored (S) & Query (Q) templates respectively
Compute the size of M & N
yes
M>N?
no
small-vector=N
big-vector= M
small-vector=M
big-vector= N
i=1
j=1
type(i)==type(j) &&
$|d_1(i)-d_1(j)|\leq tolerance(r_0)$ &&
$|d_2(i)-d_2(j)|\leq tolerance(r_0)$ &&
$|\alpha_1(i)- \alpha_1(j)|\leq tolerance(\theta_0)$
no
yes
matchcount = matchcount+1
j=j+1
$j \leq$ big-
yes
no
i=i+1
$i \leq$ big-
yes
no
End

Figure 3.4: Matching algorithm of two feature vectors in the novel architecture.

Although it is highly unlikely, in some cases there can be multiple matches between the vectors from query and stored templates. The algorithm takes this into account and it considers the match as a true match in its first instance and rejects the rest.

3.5 Research methodology

The novel algorithm for the formation of fingerprint template and matching using minutiae at level2 has been developed and tested on publicly available fingerprint database FVC- 2006. A total of 1680 fingerprints (140 fingers with 12 impressions per finger, many of which are of a poor quality) have been used to evaluate the algorithm. The performance of any fingerprint matching algorithm is normally determined by Error Equal Rate (EER) when FAR and FRR are equal. To evaluate the FRR, the images from the same finger were matched against each other and a total of 9,240 checks (66 checks on 12 images from the same finger from 140 users) were performed. The FAR was calculated on cross match result, i.e., a total of 9,730 matching was performed among different finger images where the first sample from each set was taken and checked with others. The algorithm was implemented with Matlab 7.11.0.

Some of the limitations in already established minutiae-based algorithms, which requires accurate detection of singularity region or core on a fingerprint has been overcome as the novel algorithm does not rely on any singularity region or core. Also the alignment between the query template and the stored template is not required during the matching process thus made the novel algorithm more efficient and eliminates lots of computation overhead and saves time.

3.6 Evaluation of the novel algorithm

In previous chapters, automatic fingerprint identification systems have been discussed in detail. Also formation of the template and matching using level2 features has been defined in the novel algorithm. The novel algorithm is defined as Transformation Invariant Algorithm for Automatic Fingerprint Recognition (**TIAAFR**). In this chapter the performance evaluation of the developed system described in detail and obtained results are presented. The algorithm has been implemented in Matlab 7.11.0.

The publicly available database FVC 2006 (DB2) has been used to evaluate the novel algorithm. The reason for choosing this database is its diversity of enrolled users and wider acceptability among developers. This database has been used in the Fourth International Fingerprint Verification Competition where 53 (27 industrial, 13 academic, and 13 independent developers) participants tested and evaluated their algorithms [80]. The full database also includes images scanned by capacitive and thermal sensors, which creates an opportunity to test any algorithm across platforms and check their interoperability. FVC 2006 (DB2) comes with 1680 images in which 140 fingers have been scanned with 12 impressions per finger. The images were scanned by an optical sensor with the resolution of 400x560 pixels at 569 dpi. Each image is available in BMP, 256 grey level formats. A heterogeneous population including manual workers and elderly people has been used to create the database. There was no constraint such as minimum quality of the image on the users during the enrolment. Figure 3.5 shows some sample images from the database. It can be clearly seen from these images that their orientation, type and quality varies significantly and these variations are necessary to rigorously test the efficiency of any fingerprint matching algorithm.

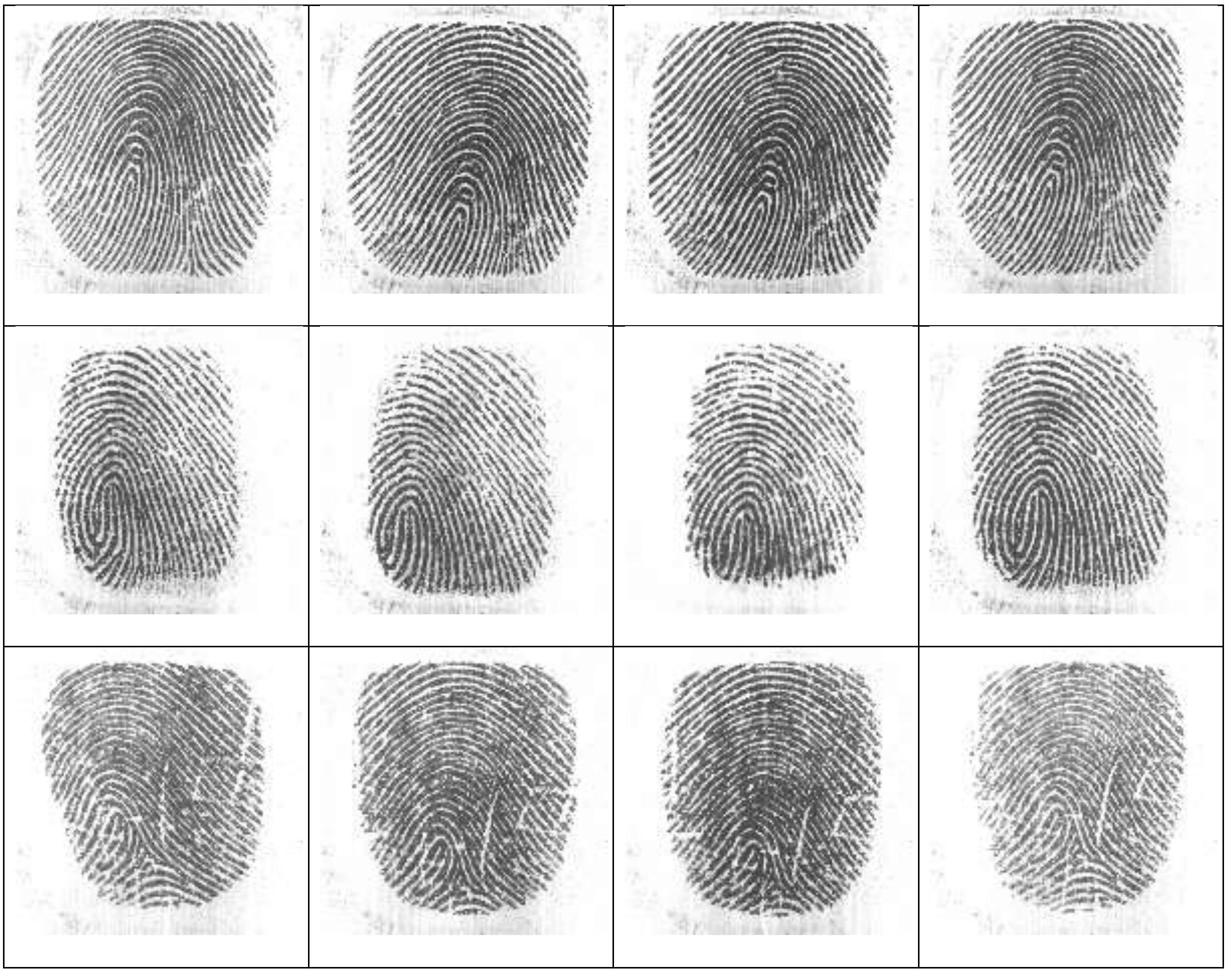

Figure 3.5: Some images from FVC 2006 (DB2). Each row corresponds to the impressions from same finger [16].

3.7 Minutiae extraction process

The images from the database were of varying quality as can be seen from Figure 3.5. The first row shows a set of good quality images whereas the last row shows the images with lots of cuts and scars. Each image has been enhanced before it was forwarded to the feature (minutiae) extraction process. Figure 3.6 is showing all the steps through which a sample image is processed.

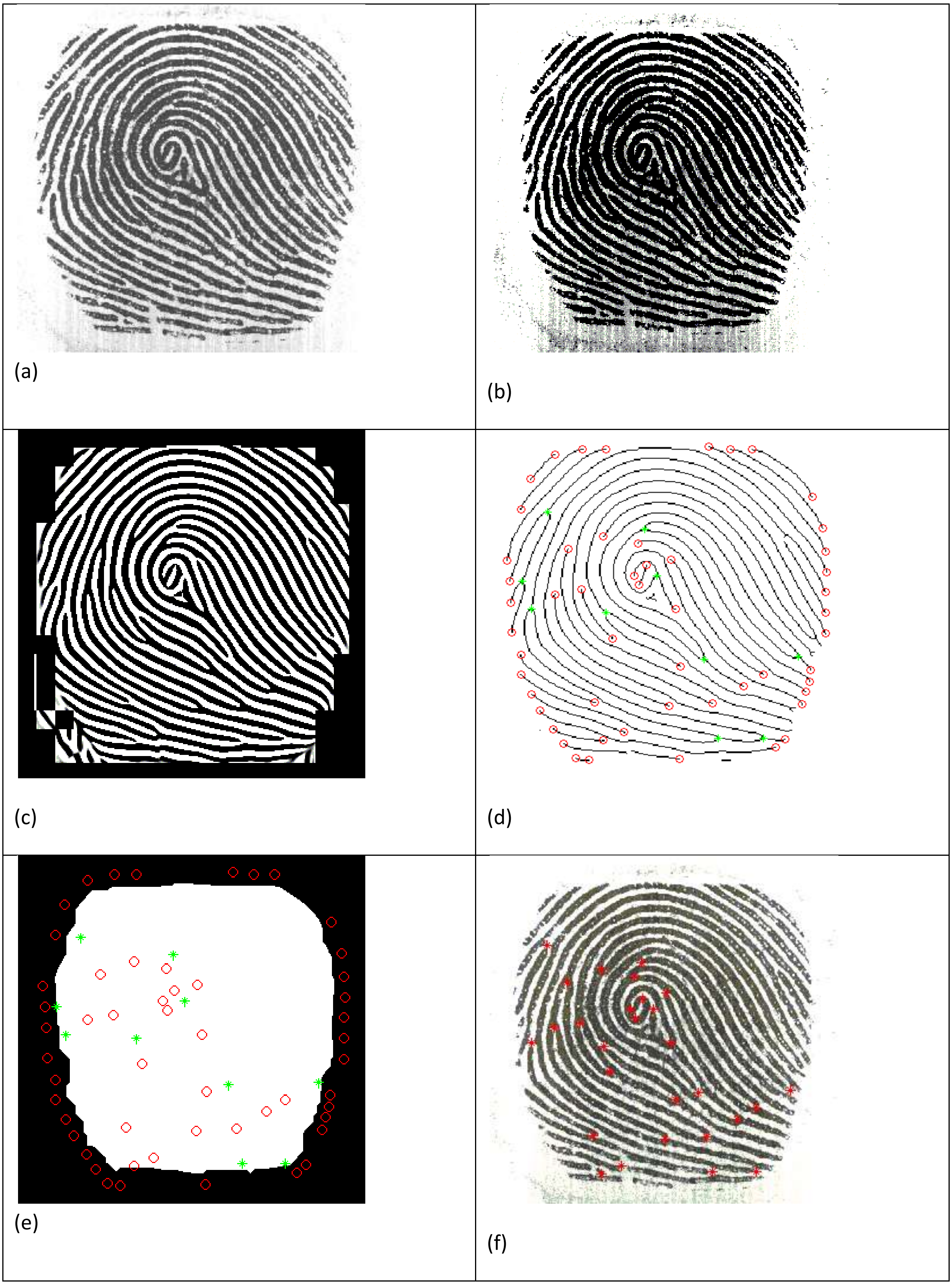

Figure 3.6: Stages of extracting minutiae at Level2, (a) Original fingerprint, (b) Normalised image, (c) Binarised image, (d) Thinned binary image with minutiae (termination and bifurcation) , (e)

Extracting actual minutiae after applying ROI (region of interest), (f) Original image with actual minutiae at level2.

Impression	Number of Termination	Number of Bifurcation	Total number of Minutiae
1 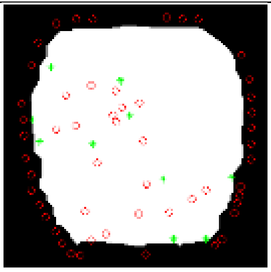	10	19	29
2 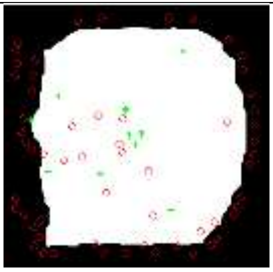	10	14	24
3 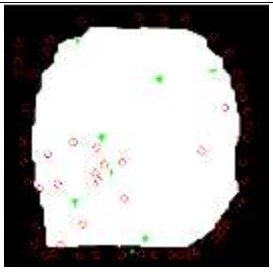	7	14	21
4 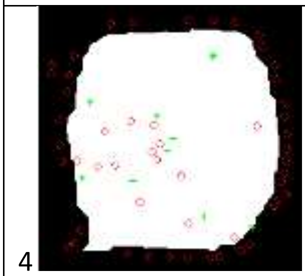	9	14	23

Figure 3.7: Varying number of minutia in different impression from the same finger, which differ in orientation and position.

As can be seen from Figure 3.7 the number of valid minutiae from the same finger is varying on numbers and types for different impressions. Any difference in the total number of extracted minutiae results in non match between the corresponding minutiae of the query and stored template. When the difference between the total number of extracted minutiae in query and stored template is higher, the percentage match (*PM*) is likely to be lower as the distribution of the minutiae in a fingerprint is considered uniform. Figure 3.8 is showing the normal distribution of minutiae in the FVC 2006 (DB2) extracted by the novel algorithm in which 140 optically scanned fingerprints have been used.

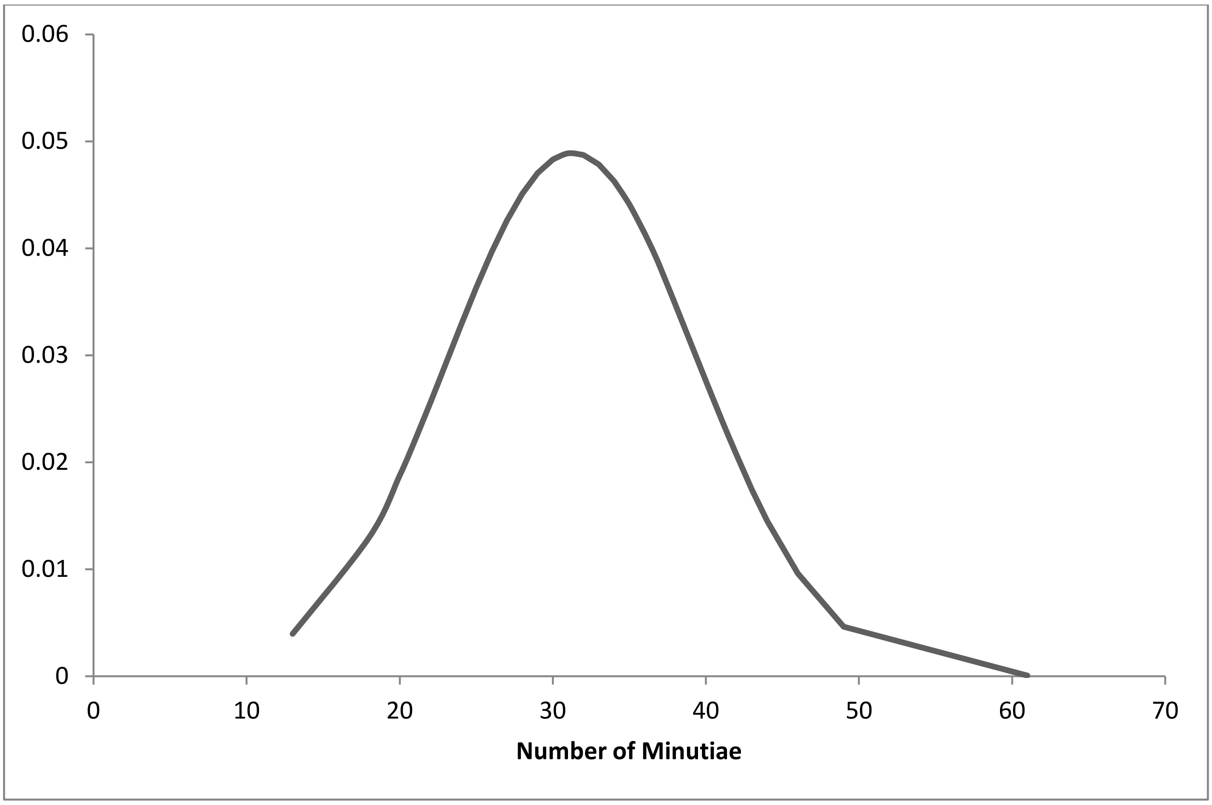

Figure 3.8: Normal distribution of extracted minutiae in finger images from FVC 2006(DB2).

3.8 Performance evaluation

The performance of the novel algorithm has been evaluated by calculating FRR and FAR. The FRR is the fraction of genuine fingerprints which are rejected and is calculated as follows

$$FRR = \frac{Number\ of\ genuine\ fingerprints\ rejected}{Total\ number\ of\ checks} \quad (3.11)$$

To calculate FRR, each image is checked against different impressions from the same finger. A total of 9,240 checks have been made for FRR. If a fingerprint '*x*' was checked against another fingerprint '*y*', the symmetric check, i.e., '*y*' against '*x*' was not executed to avoid correlation in the score.

The FAR is the fraction of imposter or false fingerprint match out of total number of checks and is defined as

$$FAR = \frac{Number\ of\ imposter\ fingerprints\ accepted}{Total\ number\ of\ checks} \quad (3.12)$$

Figure 3.9 shows a snapshot of the Matlab function used to calculate FAR and FRR in evaluation of the algorithm.

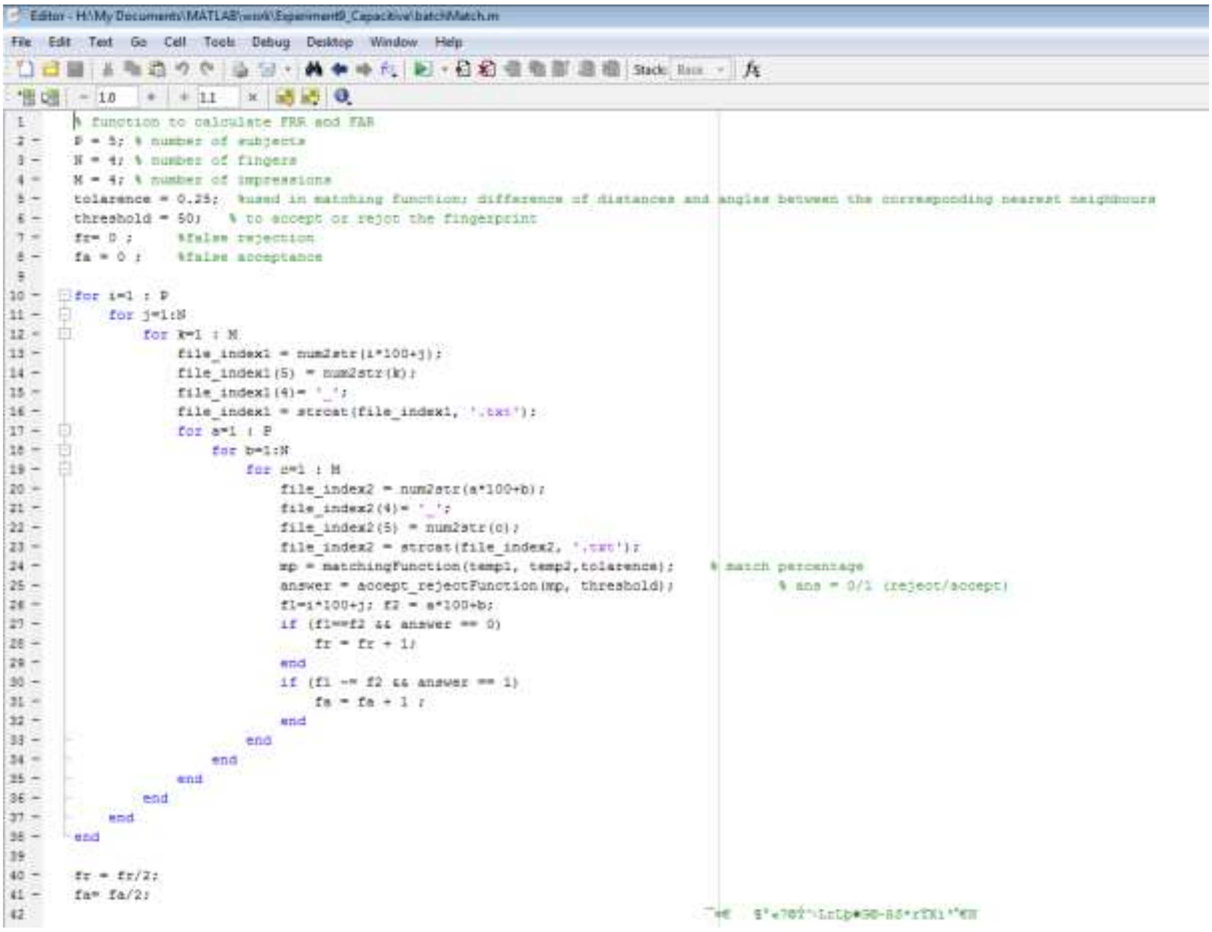
Editor - H:\My Documents\MATLAB\work\Experiment9_Capacitive\batchMatch.m
File Edit Text Go Cell Tools Debug Desktop Window Help
Stack: Base
1.0
1.1

```
% function to calculate FRR and FAR
P = 5; % number of subjects
N = 4; % number of fingers
M = 4; % number of impressions
tolarence = 0.25;  %used in matching function; difference of distances and angles between the corresponding nearest neighbours
threshold = 50;    % to accept or rejct the fingerprint
fr= 0 ;       %false rejection
fa = 0 ;      %false acceptance

for i=1 : P
    for j=1:N
        for k=1 : M
            file_index1 = num2str(i*100+j);
            file_index1(5) = num2str(k);
            file_index1(4)= '_';
            file_index1 = strcat(file_index1, '.txt');
            for a=1 : P
                for b=1:N
                    for c=1 : M
                        file_index2 = num2str(a*100+b);
                        file_index2(4)= '_';
                        file_index2(5) = num2str(c);
                        file_index2 = strcat(file_index2, '.txt');
                        mp = matchingFunction(temp1, temp2,tolarence);    % match percentage
                        answer = accept_rejectFunction(mp, threshold);          % ans = 0/1 (reject/accept)
                        f1=i*100+j; f2 = a*100+b;
                        if (f1==f2 && answer == 0)
                            fr = fr + 1;
                        end
                        if (f1 ~= f2 && answer == 1)
                            fa = fa + 1 ;
                        end
                    end
                end
            end
        end
    end
end

fr = fr/2;
fa= fa/2;
```

Figure 3.9: Matlab function to calculate FAR and FRR

To calculate FAR, the first sample from each finger was checked against the first sample of remaining fingerprint images in the database and a total of 9,730 checks (fingerprint images) were made. Again the symmetric match was not executed to avoided correlation in the matching score.

A range of tolerances have been used to observe the performance of the algorithm against difference thresholds. Table 3.1 summarises the result for EER (%) on different tolerances (*α*). It can be seen that the tolerance of 0.15 offers the optimum performance of the novel algorithm with the minimum EER.

Tolerance, *α* (%)	5.0	10.0	15.0	20.0
EER (%)	18.2	4.0	3.5	4.6
Threshold (%)	4.8	10.0	25.0	41.0

Table 3.1: EER for a range of tolerances.

If the tolerance is decreased to make the matching more accurate, the number of false rejection increases. On the other hand, a higher value of tolerance increases the number of false match. As can be seen from Figure 3.10, the **TIAAFR** has performed best at α =15% with an EER of 3.5%.

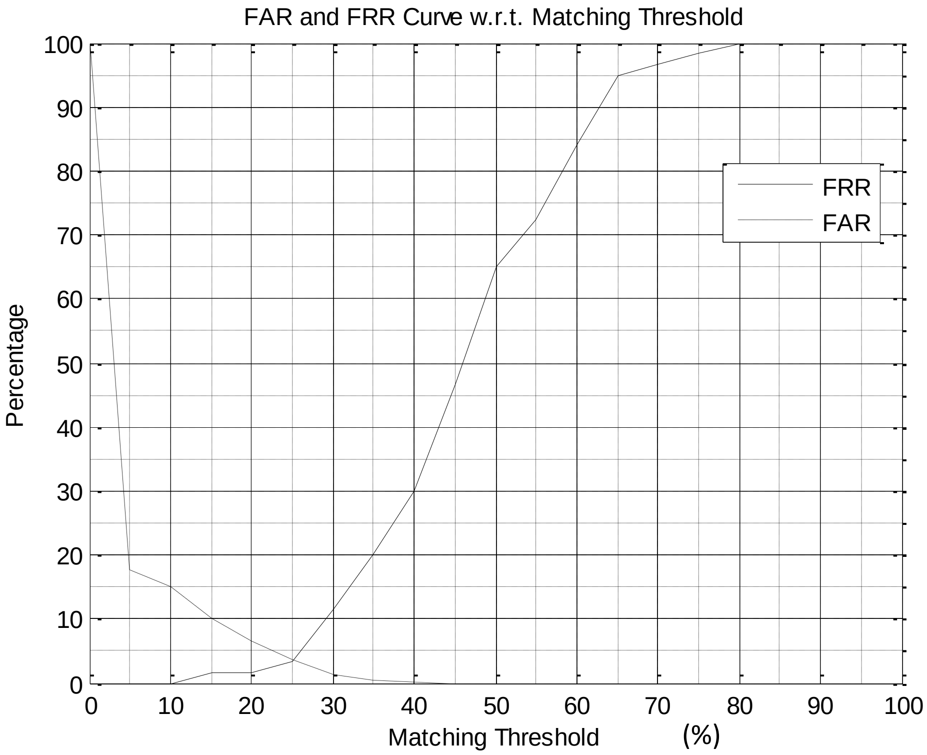

Figure 3.10: Performance of **TIAAFR**.

Algorithm	**TIAAFR**	Cefar	Cetp	Utwe	Diti	Ncmi
EER(%)	3.50	4.90	5.06	7.98	23.64	49.11

Table 3.2: Comparison of **TIAAFR** with other benchmark algorithms [10].

Table 3.2 shows a comparison of the novel algorithm to other benchmark algorithms. It performs better than other algorithms and further research is underway to improve EER.

3.9 Performance evaluation of TIAAFR across images from different sensors

In order to evaluate the performance of TIAAFR in terms of sensor interoperability, another publicly available fingerprint database, **ATVS-FFp DB [79],** has been used. This database contains fingerprint samples of the index and middle fingers of both hands of 17 users. Four samples of each fingerprint have been captured by optical using Biometrica Fx2000 @ 512 dpi, capacitive using Precise 100SC @ 500 dpi and thermal using Yubee with Atmel's Fingerchip @ 500 dpi sensors. This way the dataset comprises a total of 816 real images (68 fingers x 4 samples/finger x 3 sensors).

Figure 3.11 shows a comparison of images and their extracted minutiae scanned by three different scanners (capacitive, optical and thermal). As can be seen from this figure, there is a clear difference between the finger impressions and the number of minutiae. A comparative analysis is also done by measuring the processing time for minutiae extraction and template formation for each type of sensor image that can be seen in Table 3.3.

Sensor Type	Average time for minutiae extraction from an image	Average time for template formation of an image
Capacitive	1.79 sec	08.56 msec
Optical	3.67 sec	40.59 msec
Thermal	3.03 sec	19.72 msec

Table 3.3: Comparison of processing times in TIAAFR for images scanned by different sensors (Capacitive, Optical and Thermal)

	Original Image	Skeleton image with extracted minutiae (real and false)	Minutiae (real and false) within ROI	Orginal image with real minutiuae
Capacitive	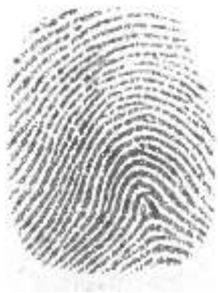	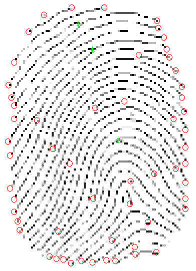	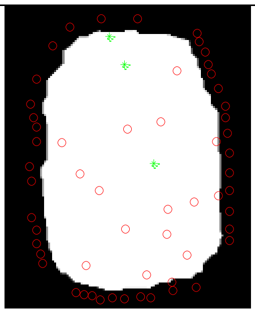	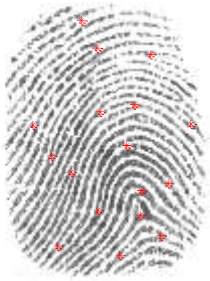
Optical	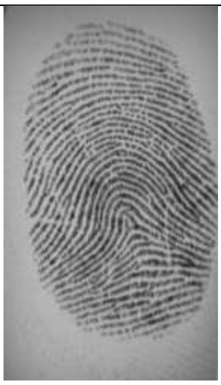	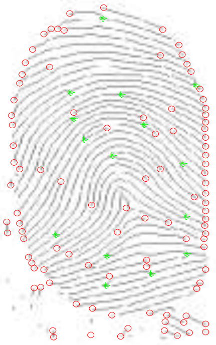	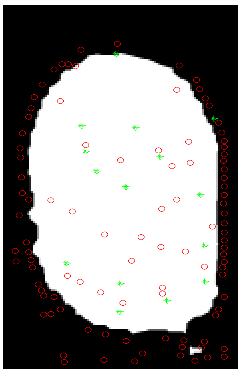	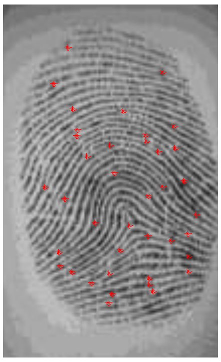
Thermal	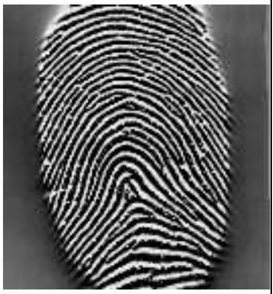	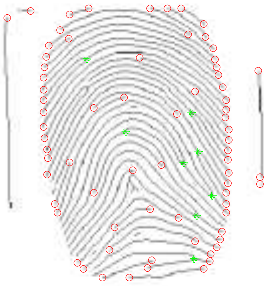	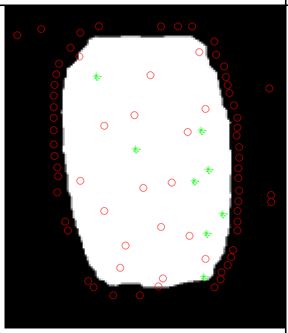	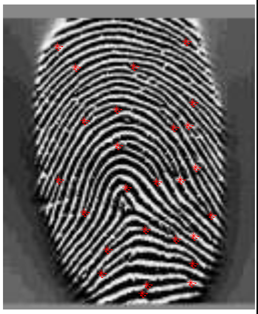

Figure 3.11: Comparison of images scanned by different sensors with their processed versions and extracted minutiae.

As can be seen from Table 3.3 and Figure 3.12, the TIAAFR has performed best on images scanned by optical sensor and worst on images scanned by thermal sensors. The image quality and the number of extracted minutiae are the key factors in template formation and matching. A substantial difference in extracted minutiae, their numbers and corresponding positions can be realised from Figure 3.12.

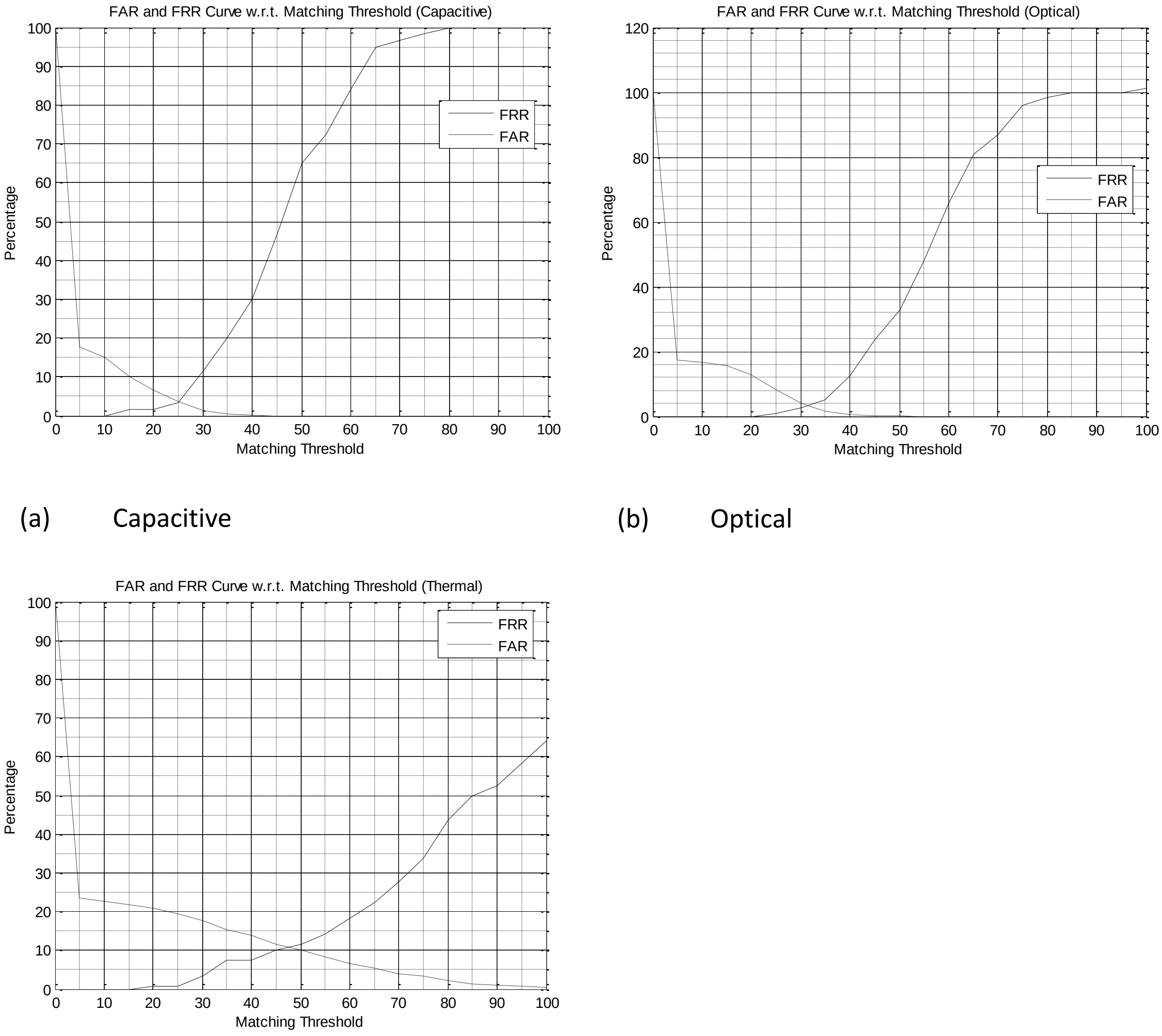

(a) Capacitive

(b) Optical

(c) Thermal

Figure 3.12: Comparison of matching performance of TIAAFR across images scanned by different sensors.

Although TIAAFR has performed very well with equal to or less than 3.5% EER on optical and capacitive images, a result of 10% EER on thermal images is likely to make TIAAFR unacceptable for thermally scanned images. The poor quality of the thermal images and the presence of lots of noises have contributed to the higher EER.

Original Image		Processed image with extracted minutiae	Number of Termination	Number of Bifurcation	Total number of Minutiae
Capacitive	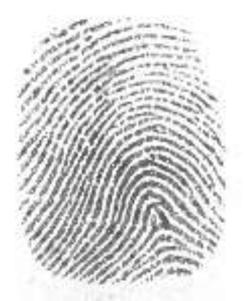	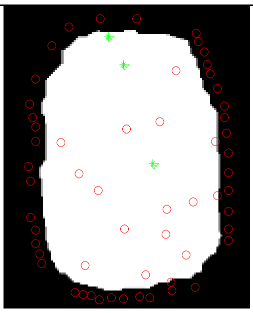	3	15	18
Optical	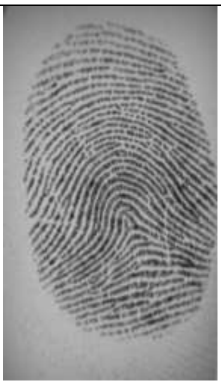	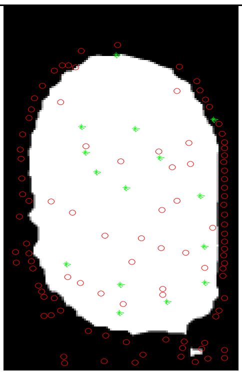	13	25	38
Thermal	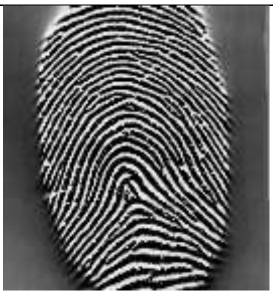	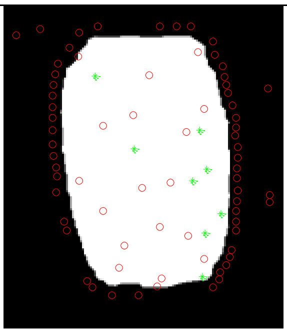	8	17	25

Figure 3.13: Difference in image quality and the number of extracted minutiae on images from the same finger scanned by capacitive, optical and thermal sensors.

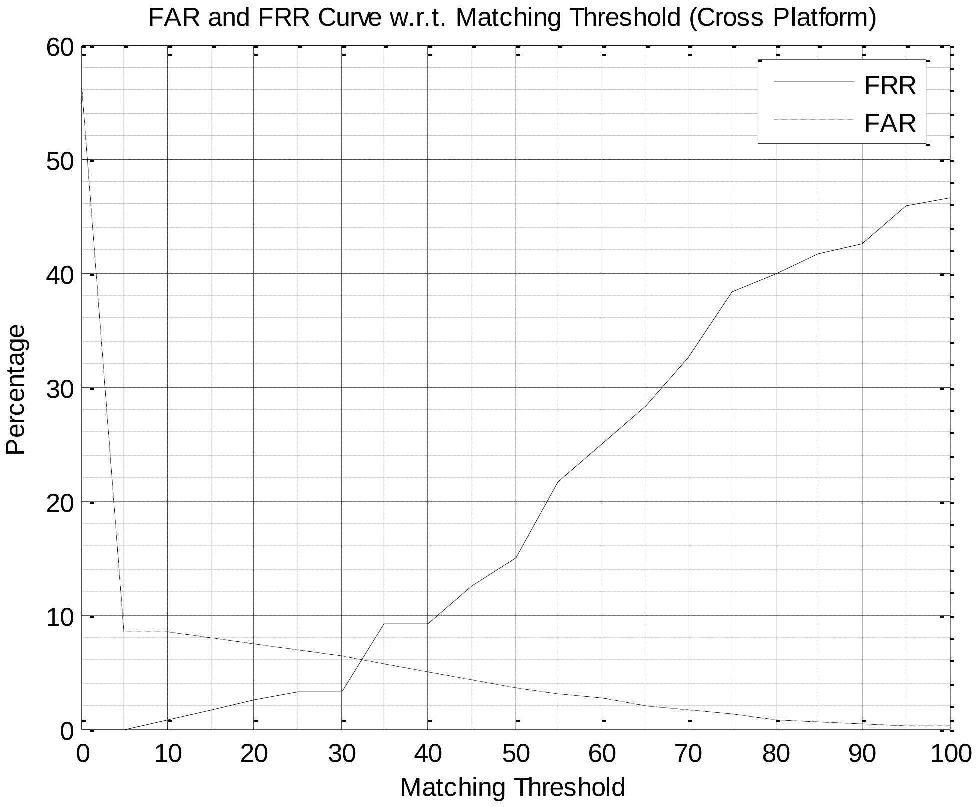

Figure 3.14: Performance of TIAFFR in sensor interoperability (capacitive, optical and thermal).

Another performance check of TIAAFR has also been carried out to see the sensor interoperability performance of the algorithm. From ATVS-FFp database, 45 images (15 different images with 3 impressions per image (1 optical, 1 capacitive and 1 thermal)) has been randomly picked to form a small database and matching has been performed across images**.** Figure 3.14 shows the result of FAR and FRR in cross platforms in which the EER has resulted at 8%, which is reasonably high. As can be seen from some good quality sample images in Figure 3.13, there are huge differences in common areas and the number of valid minutiae across the images. Any appearance of new minutiae or loss of real minutiae contributes to the low matching scores that are discussed in section 3.8. The difference between the numbers of minutiae on the same finger has also contributed to the lower matching score in the calculation of FAR and FRR.

3.10 Summary

The novel algorithm has been designed and tested with publicly available databases to evaluate its performance. The four element feature vector for each minutia in a fingerprint is constructed using the attributes of the minutiae and its neighbours. Only the first two nearest neighbour distances and their internal angle have been taken into consideration as higher number of neighbouring distances and their internal angles will result into to a higher degree of uncertainty (mismatch) if any of the higher order distances or angles does not fall in the tolerance box. The other local attributes such as number of ridge lines between its neighbours as suggested by Jiang and Yau, 2000 [73] have not been taken into consideration because any false or spurious minutia will result in an incorrect number of ridge lines between two real minutiae. As this novel algorithm is taking only the first two nearest neighbour distances into account, it is not affected by the distant neighbours and even if there is a false or missing minutia in any part of the image, it will only affect the limited locality which is a greater advantage over other algorithm based on structural matching such as template formed by Delauney Triangulation or the template which uses the core as a reference. In case of non linear or elastic distortion, the internal angle is likely to be unaffected when the neighbouring distances are not very small. If the first two nearest neighbours are at the same distance then the neighbour with the smaller '*x*' coordinate is considered as the first nearest neighbour.

It has been found that the algorithm has reduced the computation time significantly as it does not align the query and stored template during the matching process. Any translation or rotation also does not have any impact on its performance unless the scanned image is unevenly distorted due to inconsistent contact. Although the simple structure of the novel algorithm saves a lot of computation time by avoiding image processing overhead, the accuracy might be affected by the quality of the image where the relative positions of minutiae are severely altered. Also the big difference in minutiae numbers between the stored and the query template may result in false match. A number of distance and angle tolerances have been set to optimise the threshold at which it performs best.

Although this algorithm has performed very well with a 3.5% or less EER on optical and capacitive images, the performance of the algorithm is not satisfactory on thermal image due to the poor quality and presence of noise in images. It has also not given a satisfactory result when images on cross platform have been used to check its interoperability performance. Possible reasons are big differences in image quality, presence or noise and disparity in image resolution.

However, the usefulness of the algorithm on optical and capacitive images is confirmed in the tests conducted, which shows a very good performance. The image quality plays an important part in the quality of the template formation and therefore consistency in fingerprint enrolment, image resolution and other environmental conditions are suggested for better performance.

Conclusion and Recommendation for Future Work

4.1 Conclusion

The main focus of this work has been to develop and test an automated fingerprint recognition algorithm based on level2 features (minutiae), which can address some issues in some existing algorithms. As a pre processing step, image enhancement has been performed on all images before they are passed onto feature extraction stage. The most popular Gabor Filtering technique has been used in the enhancement process with optimised block size for image orientation and ridge frequency estimation. The invalid or false minutiae have been removed using some heuristic rules before the template has been formed.

The test run on 1680 images have shown that the Gabor filter has been able to effectively enhance the clarity of the ridge structures while reducing noise when accurate estimation of ridge orientation is combined with ridge frequency. However, for low quality images that exhibit high intensities of noise, the filter was less effective in smoothing ridge lines due to inaccurate estimation of the orientation and ridge frequency parameters. Overall, the results have shown that the implemented enhancement algorithm is a useful step to employ prior to minutiae extraction.

To extract minutiae at level2, the Crossing Number method has been implemented on the skeleton image. Tests have shown that this method is able to accurately detect all valid bifurcations and ridge endings from the thinned image. However, there were cases where the extracted minutiae did not correspond to valid minutia points. Hence, image post processing stage was implemented to validate the minutiae. The test results from the minutiae validation algorithm indicate that this additional post processing stage has been effective in eliminating various types of false minutiae structures.

In this novel algorithm the template has been formed using the local attributes of each minutia. The tolerance for both the distance and the angle has been optimised to address non linear and elastic distortion. The avoidance of some other local characteristics such as ridge numbers between adjacent minutiae has made the structure more robust against any spurious minutia that may arise from noise. Also the computation requirement is reduced significantly as the matching process does not require any pre alignment between the stored and the query template.

Unlike other geometry based template, this novel structure does not store the actual coordinates and the orientation of the minutiae, which may pose a threat to identity loss if the template is lost or stolen. The multidimensional feature vector completely based on local attributes has made the template cancellable, which is another key advantage of this algorithm in security enhancement.

In cross platform environment, this algorithm has performed well, in particular for optical and capacitive scanned images. However, the performance on thermal scanned images was not satisfactory due to poor image qualities and disparity in image resolution. Also the difference in threshold for optical and capacitive scanned images indicates that its effectiveness can be affected by the number of valid minutiae on the image itself.

4.2 Recommendation for future work

In order to enhance the efficiency of the novel algorithm for more accurate fingerprint identification, further work needs to be carried out as follows:

Although the Gabor filter has been successfully used to enhance all the images, in particular, it has been very useful in enhancing poor quality images, but any error in local frequency estimation or ridge orientation will result in false or spurious minutiae and consequently results in high FAR and FRR. Therefore, an investigation is required into a filter whose primary aim is to specifically enhance the minutiae along with the ridge structure.

In the design of the novel algorithm, the global feature such as finger type has not been taken into consideration. Global pattern such as loop, whorl, arch etc are used for fingerprint indexing and they can reduce the search time substantially during identification process. A number of established algorithms have embedded the global feature in the matching process to improve their matching score. It would have given a better matching score and significantly reduced the false matching (FAR) had the global features embedded into the feature vector to categorise the template.

The elastic or non linear distortion can always affect the performance of any algorithm so it has done on the novel algorithm. Inconsistent pressure on the scanner by the user can result in incoherent stretching or contraction, which may cause uneven scaling on neighbouring distances and their internal angles. Further work needs to be done to accommodate the non linear and elastic distortion in the formation of the feature vector.

The algorithm has been tested on the images scanned by optical sensors but to evaluate its performance more it can be tested on images scanned by other types of sensors such as capacitive, thermal or radio frequency sensors. Images taken at different resolution and different size can also be an issue for this algorithm. Therefore, more research needs to be done if the novel algorithm is to work across multi vendor platforms where images are taken using different sensors with different image resolution.

References

[1] A. K. Jain; F. Jianjiang and K. Nandakumar, "Fingerprint Matching," *Computer Vision and Pattern Recognition , IEEE Computer Society* , vol.43, no.2, pp.36-44, Feb. 2010, doi: 10.1109/MC.2010.38

[2] http://www.globalsecurity.org/security/systems/biometrics.htm accessed on 03 November 2011

[3] http://biometrics.pbworks.com accessed on 10 February 2012

[4] http://www.biometrics.gov accessed on 21 January 2011

[5] http://www.bccresearch.com/report/biometrics-global-market-ift042b.html accessed on 09 December 2011.

[6] S. Memon; N. Manivannan; A. Noor and C. Tigli, "Fingerprint Biometrics for Identity management," *International Journal of Industrial Engineering and Management (IJIEM),* vol2, no 2, pp 39-44, 2011.

[7] N. K. Ratha; J. H. Connell and R. M. Bolle, "Enhancing security and privacy in biometrics-based authentication systems", *IBM Systems Journal*, vol. 40, no. 3, pp. 614-634, 2001.

[8] S. Memon; N. Manivannan; A. Noor and C. Tigli,*"Automatic detection of Active Sweat Pores of fingerprint using high-pass and correlation filtering",* Electronic Letters, Vol. 46, No 18, pp. 1268-1269, 2010.

[9] A. K. Jain; L Hong; S. Pankanti and R. Bolle, "An identity authentication system using fingerprints," *Proceedings of the IEEE*, vol. 85, no. 9, pp.1365-1388, 1997.

[10] M. A. Dabbah; W. L. Woo and S. S. Dlay, "Computationally Efficient Fingerprint Algorithm for Automatic Recognition," *Proceedings of the 5th WSEAS Int. Conf. on SIGNAL, SPEECH and IMAGE PROCESSING*, Corfu, Greece, pp. 90-95, Aug 17-19, 2005.

[11] L. Hong; Y. Wan and A. K. Jain, "Fingerprint image enhancement: Algorithm and performance evaluation"*, IEEE Transactions on Pattern Analysis and Machine Intelligence,* vol. 20, no. 8, pp. 777–789, 1998.

[12] D. Gabor, "Theory of communication," *Journal of the Institute of Electrical Engineers*, vol. 93, pp. 429–457, 1946

[13] Jean-François Mainguet, Fingerprint Biometrics (2009, 02 October) [online], Available: http://fingerchip.pagesperso-orange.fr/biometrics/types/fingerprint.htm

[14] A. K. Jain; Y. Chen and M. Demirkus, "Pores and Ridges: Fingerprint Matching Using Level 3 Features", *Pattern recognition,* 18th International Conference on Pattern Recognition (ICPR), vol. 4, pp, 477-480. ICPR 2006.

[15] NIST Special Publication 500-271, ANSI/NIST-ITL 1-2007 (2008, 17 March), [online] Available: http://www.nist.gov/itl/ansi/upload/Approved-Std-20070427-2.pdf

[16] D. Maltoni; D. Maio; A. K. Jain and S. Prabhakar, *"Handbook of Fingerprint Recognition"*, Springer-Verlag London Limited 2009.

[17] D. Maio and D. Maltoni, "Direct gray-scale minutiae detection in fingerprints*," IEEE Trans. Pattern Analysis Machine Intelligence*, vol. 19, no 1, pp 27-40, 1997.

[18] N. Ratha; S. Chen and A. K. Jain, *"Adaptive flow orientation based feature extraction in fingerprint image,"* Pattern Recognition vol. 28, no. 11, pp. 1657–1672, 1995.

[19] S. Kasaei and B. Boashash, "Fingerprint feature extraction using block-direction on reconstructed images," *In IEEE region TEN Conf. digital signal Processing applications,* TENCON, pp. 303–306, Dec 1997.

[20] D. Simon-Zorita; J. Ortega-Garcia; S. Cruz-Llanas and J. Gonzalez-Rodriguez, "Minutiae extraction scheme for fingerprint recognition systems," *In Proceedings of the International Conference on Image Processing,* vol. 3, pp. 254–257, Oct 2001.

[21] R. Thai, "Fingerprint Image Enhancement and Minutiae Extraction", BSc (Honours) Project, University of Western Australia, Australia, 2003.

[22] S. Prabhakar; J. Wang; A. K. Jain; S. Pankanti and R. Bolle., "Minutiae verification and classification for fingerprint matching," *In Proc. 15th International Conference Pattern Recognition (ICPR),* vol. 1, pp. 25–29, Sep 2000.

[23] A. Ross; A. K. Jain and J. Reisman, "A hybrid fingerprint matcher," *Pattern Recognition,* vol. 36, no 7, pp.1661–1673, Jul 2003.

[24] A. K. Jain; S. Prabhakar and L. Hong, "A multichannel approach to fingerprint classification," *IEEE Transactions on Pattern Analysis and Machine Intelligence,* vol. 21, no. 4, pp. 348–359, 1999.

[25] D. B. G. Sherlock; D. M. Monro and K. Millard, "Fingerprint enhancement by directional Fourier filtering," *In IEE Proc. Vis. Image Signal Processing,* vol. 141, pp. 87–9, 1994.

[26] I. Sobel, "An Isotropic 3×3 Gradient Operator, Machine Vision for Three – Dimensional Scenes," *Freeman, H.*, Academic Pres, NY, 376-379, 1990.

[27] A. K. Jain, and F. Farrokhnia, "Unsupervised texture segmentation using Gabor filters," *IEEE Pattern Recognition,* vol24, no. 12, pp. 167–186, 1991.

[28] Z. Guo and R. W. Hall, "Parallel thinning with two-subiteration algorithms," *Communications of the ACM 32*, vol. 3, pp. 359–373, Mar 1989.

[29] J. C. Amengual; A. Juan; J. C. Prez; F. Prat; S. Sez and J. M. Vilar, "Real-time minutiae extraction in fingerprint images". *In Proc. of the 6th Int. Conf. on Image Processing and its Applications,* pp. 871–875, Jul 1997.

[30] B. M. Mehtre, "Fingerprint image analysis for automatic identification," *Machine Vision and Applications vol. 6*, no. 2 pp. 124–139, 1993.

[31] H Tamura, “A comparison of line thinning algorithms from digital geometry viewpoint”, *Proc. of the 4th Int. Conf. on Pattern Recognition*, pp. 715–719, 1978.

[32] Q. Xiao and H. Raafat, “Fingerprint image post processing: a combined statistical and structural approach,” *Pattern Recognition,* vol. 24, no. 10, pp. 985–992, 1991.

[33] M. Tico, and P. Kuosmanen, “An algorithm for fingerprint image post processing,” *In Proceedings of the Thirty-Fourth Asilomar Conference on Signals, Systems and Computers*, vol. 2, pp. 1735–1739, Nov 2000.

[34] J. Qi; S. Yang and Y. Wang, “Fingerprint matching combining the global orientation field with minutia”, *Pattern Recognition Letters,* vol. 26, pp. 2424-2430, 2005

[35] D. Maltoni, “A Tutorial on Fingerprint Recognition”, *Biometric Systems Laboratory - DEIS* - University of Bologna, via Sacchi 3, 47023, Cesena (FC) – Italy.

[36] K.M. Kryszczuk; P. Morier and A. Drygajlo, “Study of the Distinctiveness of Level 2 and Level 3 Features in Fragmentary Fingerprint Comparison,” in *Proc. Workshop on Biometric Authentication (in ECCV* 2004*)*, LNCS 3087, pp. 124–133, 2004.

[37] R. Ahuja; T. Magnanti and J Orlin, “*Network Flows*,” Prentice-Hall, Upper Saddle River, NJ, 1993.

[38] T. Y. Jea and V. Govindaraju, “A minutia-based partial fingerprint recognition system,” *Pattern Recognition*, vol. 38, no. 10, pp. 1672–1684, 2005.

[39] C. Wang; M. Gavrilova; Y. Luo and J. Rokne, “An Efficient Algorithm for Fingerprint Matching,” in *Proc. Int. Conf. On Pattern Recognition (*18*th)*, vol. 1, pp. 1034–1037, 2006.

[40] S. Umeyama, “Least-square estimation of transformation parameters between two point patterns,” *IEEE Transactions on Pattern Analysis Machine Intelligence*, vol. 13, no. 4, pp. 76–380, 1991.

[41] S. H. Chang; F. H. Cheng; W. H. Hsu and G. Z. Wu, “Fast algorithm for point pattern matching: Invariant to translations, rotations and scale changes,” *Pattern Recognition*, vol. 30, pp. 311–320, 1997.

[42] S. Huvanandana; C. Kim and J. N. Hwang, “Reliable and Fast Fingerprint Identification for Security Applications,” in *Proc. Int. Conf. on Image Processing*, 2000.

[43] Y. He; J. Tian; Q. Ren and X. Yang, “Maximum-Likelihood Deformation Analysis of Different-Sized Fingerprints,” in *Proc. Int. Conf. on Audio- and Video-Based Biometric Person Authentication (*4*th)*, pp. 421–428, 2003b.

[44] J. Chen; F. Chan and Y. S. Moon, “Fingerprint Matching with Minutiae Quality Score,” in *Proc. Int. Conf. on Biometrics*, LNCS 4642, pp. 663–672, 2007

[45] H. Srinivasan; S. N. Srihari; M. J. Beal; P. Phatak and G. Fang, “Comparison of ROC-Based and Likelihood Methods for Fingerprint Verification,” in *Proc. SPIE Conf. On Biometric Technology for Human Identification III*, 2006.

[46] J. Jia , L. Cai; P. Lu and X. Lu, “Fingerprint matching based on weighting method and the SVM,” *Neurocomputing*, vol. 70, no. 4–6, pp. 849–858, 2007b.

[47] J. Feng, “Combining minutiae descriptors for fingerprint matching,” *Pattern Recognition*, vol. 41, no. 1, pp. 342–352, 2008.

[48] A. Lumini A. and L. Nanni, “Advanced methods for two-class pattern recognition problem formulation for minutiae-based fingerprint verification,” *Pattern Recognition Letters*, vol. 29, no. 2, pp. 142–148, 2008.

[49] P. Mansukhani; S. Tulyakov and V. Govindaraju, “Using Support Vector Machines to Eliminate False Minutiae Matches During Fingerprint Verification,” in *Proc. SPIE Conf. on Biometric Technology for Human Identification IV*, 2007.

[50] P. Mansukhani and V. Govindaraju, “Selecting Optimal Classification Features for SVM-Based Elimination of Incorrectly Matched Minutiae,” in *Proc. SPIE Conf. on Biometric Technology for Human Identification V*, 2008.

[51] C. Neumann; C. Champod; R. Puch-Solis; N. Egli; A. Anthonioz; D. Meuwly and A. Bromage-Griffiths, “Computation of Likelihood Ratios in Fingerprint Identification for Configurations of Three Minutiae,” in *Proc. Journal of Forensic Sciences*, vol. 51, no. 6, pp. 1255–1266, 2006.

[52] A. M. Bazen and R. N. J. Veldhuis, “Likelihood-ratio-based biometric verification,” *IEEE Transaction on Circuits and Systems for Video Technology*, vol. 14, no. 1, pp. 86–94, 2004.

[53] A. Bishnu; S. Das; S. C. Nandy and B. B. Bhattacharya, “Simple algorithms for partial point set pattern matching under rigid motion,” *Pattern Recognition*, vol. 39, no. 9, pp. 1662–1671, 2006.

[54] R. Udupa; G. Garg and P. Sharma, “Fast and Accurate Fingerprint Verification,” in *Proc. Int. Conf. on Audio- and Video-Based Biometric Person Authentication (*3*rd)*, pp. 192–197, 2001

[55] D. H. Ballard, “Generalizing the Hough transform to detect arbitrary shapes,” *Pattern Recognition*, vol. 3, no. 2, pp. 110–122, 1981

[56] G. Stockman; S. Kopstein and S. Benett, “Matching images to models for registration of and object detection via clustering,” *IEEE Transactions on Pattern Analysis Machine Intelligence*, vol. 4, no. 3, pp. 229–241, 1982.

[57] N. K. Ratha; K. Karu; S. Chen and A. K. Jain, “A real-time matching system for large fingerprint databases,” *IEEE Transactions on Pattern Analysis Machine Intelligence*, vol. 18, no. 8, pp. 799–813, 1996.

[58] A. Rosenfeld and A. Kak, “*Digital Picture Processing*,” Academic, New York, 1976

[59] A. Ranade and A. Rosenfeld, “Point pattern matching by relaxation,” *Pattern Recognition*, vol. 12, no. 2, pp. 269–275, 1993.

[60] J. Ton and A. K. Jain, “Registering landsat images by point matching,” *IEEE Transaction Geoscience Remote Sensing,* vol. 27, no. 5, pp. 642–651, 1989.

[61] H. Baird, "Model Based Image Matching Using Location," MIT Press, Cambridge, MA, 1984.

[62] K. G. Murty, Network programming, Prentice-Hall, Englewood Cliffs, NJ, 1992.

[63] S. Gold and A. Rangarajan, "A graduated assignement algorithm for graph matching," IEEE Transactions on Pattern Analysis Machine Intelligence, vol. 18, no. 4, pp. 377– 388, 1996.

[64] C. Oh and Y. K. Ryu, "Study on the center of rotation method based on minimum spanning tree matching algorithm for fingerprint recognition," Optical Engineering, vol. 43, no. 4, pp. 822–829, 2004.

[65] N. Ansari; M. H. Chen and E. S. H. Hou, "A genetic algorithm for point pattern matching," in *Dynamic Genetic and Chaotic Programming*, B. Souckec and IRIS group (Eds.), Wiley, New York, 1992.

[66] L. H. Zhang; W. L. Xu and C. Chang, "Genetic algorithm for affine point pattern matching," Pattern Recognition Letters, vol. 24, no. 3, pp. 9–19, 2003.

[67] J. P. P. Starink and E. Backer, "Finding point correspondence using simulated annealing," Pattern Recognition, vol. 28, no. 2, pp. 231–240, 1995.

[68] T. V. Le; K. Y. Cheung and M. H. Nguyen, "A Fingerprint Recognizer Using Fuzzy Evolutionary Programming," in Proc. Int. Conf. on System Sciences, 2001.

[69] X. Tan and B. Bhanu, "Fingerprint matching by genetic algorithms," Pattern Recognition, vol. 39, no. 3, pp. 465–477, 2006.

[70] W. Sheng; G. Howells; M. C. Fairhurst and F. Deravi, "A memetic fingerprint matching algorithm," IEEE Transactions on Information Forensics and Security, vol. 2, no. 3, pp. 402–412, 2007.

[71] Z Chen and C. H. Kuo, "A Topology-Based Matching Algorithm for Fingerprint Authentication," in *Proc. Int. Carnahan Conf. on Security Technology (*25*th)*, pp. 84–87, 1991

[72] A. Hrechak and J. McHugh, "Automated fingerprint recognition using structural matching," *Pattern Recognition*, vol. 23, no. 8, pp. 893–904, 1990

[73] X. Jiang and W. Y. Yau, "Fingerprint Minutiae Matching Based on the Local and Global Structures," in *Proc. Int. Conf. on Pattern Recognition (*15*th)*, vol. 2, pp. 1042–1045, 2000

[74] A. Wahab; S. H. Chin and E. C. Tan, "Novel approach to automated fingerprint recognition," *IEE Proceedings Vision Image and Signal Processing*, vol. 145, no. 3, pp. 160–166, 1998.

[75] A. K. Jain; L. Hong and R. Bolle, "On-line fingerprint verification," *IEEE Transactions on Pattern Analysis Machine Intelligence*, vol. 19, no. 4, pp. 302–313, 1997.

[76] A. Almansa and L. Cohen, "Fingerprint Image Matching by Minimization of a Thin-Plate Energy Using a Two-Step Iterative Algorithm with Auxiliary Variables," in *Proc. Workshop on Applications of Computer Vision*, pp. 35–40, 2000.

[77] A. M. Bazen and S. H. Gerez, “Systematic methods for the computation of the directional fields and singular points of fingerprints,” *IEEE Transactions on Pattern Analysis Machine Intelligence*, vol. 24, no. 7, pp. 905–919, 2002.

[78] C. Wang and M. L. Gavrilova, *“Delaunay Triangulation Algorithm for Fingerprint Matching”,* Proceedings of the 3rd International Symposium on Voronoi Diagrams in Science and Engineering, IEEE Computer Society Washington, DC, USA ©2006 (ISVD’06).

[79] Z. M. Kov´acs-Vajna. A fingerprint verification system based on triangular matching and dynamic time warping. IEEE Trans. on PAMI, 22(11):1266–1276, 2000.

[80] http://bias.csr.unibo.it/fvc2006/databases.asp accessed in March 2012

Appendix A

List of publications

1. Noor A., Manivanan N., Balachandran W, *“Transformation invariant algorithm for automatic fingerprint recognition (TIAAFR)”,* Electronic Letters, the IET (submitted for publication).

2. Memon S., Manivannan N., Noor A., Tigli C., *“Security Issues in Automated Fingerprint Identification Systems”,* Bahria University Journal of Information & Technology, Vol 4, Issue 1, August 2011.

3. Manivannan N., Noor A., Tigli C., Memon Shahzad., *“Fingerprint Biometrics for Identity management”,* International Journal of Industrial Engineering and Management (IJIEM), Vol2, No 2, pp 39-44, 2011.

4. Memon S., Manivannan N., Noor A., Balachadran W., Boulgouris N. V., *“Fingerprint Sensors: Liveness Detection Issue and Hardware based Solutions”,* Vol 136, Issue 1 , pp 35-49. January 2012.